Multi-Stage Model for Predicting the Mechanical and Durability Characteristics of Cement-Based Material

マルチステージモデルによるセメント系材料の力学特性及び耐久性予測

by

Siventhirarajah Krishnya
B.Sc. Eng. *(Hons.)* (2015), M.Sc. Eng. (2018)

DISSERTATION

Presented in Partial Fulfillment of the Requirements for the Degree of

DOCTOR OF PHILOSOPHY

in

Division of Sustainable Resources Engineering
Graduate School of Engineering

of the

HOKKAIDO
UNIVERSITY

Japan

Approved by the committee in charge,

Associate Prof. Yogarajah Elakneswaran, *Chair*
Prof. Tsutomu Sato
Prof. Ryoma Kitagaki
Prof. Takafumi Sugiyama

March 2022

ABSTRACT

Cement based materials such as mortar and concrete are the most widely used building materials in the global construction industry. Owing to the diverse components such as hydration products, aggregates and cement-aggregate interfacial zone, they highly reveal a complicated microstructure. Different varieties of hydration products such as calcium silicate hydrate (C-S-H), calcium hydroxide, ettringite, hydrotalcite, and AFm phases are formed depending on the binder composition. The main hydration product, the C-S-H, has a complex pore structure with high specific area. It is also well-known that C-S-H in hydrated matrix exists in two different forms namely low-density C-S-H (LD C-S-H) and high-density C-S-H (HD C-S-H). Moreover, the occurrence of cement-aggregate interface (interfacial transition zone) is related to the wall-effect initiated by the aggregate surface that disturbs the normal packing of cement particles. Due to its higher porosity, the interfacial transition zone (ITZ) in cementitious composite is considered as a weaker phase compared to aggregate and hydrated matrix in concrete and mortar. The aforementioned microstructure of the cementitious materials are the utmost significant factors that govern the progress of mechanical and ionic transport properties.

Predicting the mechanical and transport properties of hydrated matrix are no doubt the most complicated processes. In most of the previously proposed models, the prediction relies on number of assumptions and simplifications which limit the application range and further developments of the models. Needless to say, to realistically simulate the responses of binder, the model should integrate all the constituents of hydration. Therefore, the purpose of this research work was to develop a model for reliably predicting the mechanical and transport

properties from the detailed microstructure.

In the first part of the research work, a two-stage model, called **HyMeC** (**Hy**dration and **Me**chanical properties of **C**ement-based material), is proposed to predict the mechanical properties of the cement paste from the micro-structure. Firstly, relative humidity, thermodynamic, cement hydration and model for volumetric prediction are integrated to accurately predict the volume fraction of hydration products. Subsequently, a multi-scale model is developed in three hierarchical levels, that initiates from C–S–H matrix considering the formation of two types of C–S–H (low- and high-density C−S–H) to cement paste for the computation of the mechanical properties of cement paste. As the volume fraction of C–S–H and capillary porosity are the most significant components which determines the mechanical properties of cement paste, prime consideration herein is given to C–S–H space ratio. The proposed model is well verified at the predictions of relative humidity, chemical shrinkage and capillary porosity, compressive strength, Young's modulus and Poisson's ratio with independent sets of experimental results.

In the next part, the mechanical properties such as Young's modulus and Poisson's ratio of mortar and concrete are evaluated using a multi-scale model developed in five hierarchical levels: from nano-scale cement hydrates to the scale of concrete. In the proposed model, the microstructure of mortar/ concrete is considered as a three-phase material: fine/ coarse aggregates, ITZ of aggregates and bulk paste/ mortar. The primary input is the microstructure of cement paste and ITZ, which are predicted as the function of curing time using coupled cement hydration-thermodynamic model. The ITZ volume fraction is analytically computed based on aggregate particle size distribution. Multi-level homogenization methods (based on

three-phase sphere model for two-phase composite material) are finally implemented to predict the effective properties of mortar and concrete. Here, the equivalent matrix consisted of fine/ coarse aggregate, bulk paste/ mortar and ITZ are obtained with the first and second levels homogenization procedures for mortar/ concrete. To validate the predictability of the models for mortar and concrete, predicted values are compared with independent experimental data sets. The influences of ITZ on properties of mortar and concrete are also discussed based on the outcomes.

The diffusion of both carbon dioxide and chlorides, in the hydrated cement paste is carried out in the latter part of the research work. A COMSOL-IPHREEQC interface based on MATLAB language is developed to simulate a multi-dimensional and multi-species ionic transport for cement-based materials. The COMSOL Multiphysics is used to perform the ionic transport calculations, and IPHREEQC carries out the chemical reactions using thermodynamic database. Based on the thermodynamic insight, the phase-equilibrium model and the surface complexation model are used to express the physical and chemical interactions. More importantly, the proposed transport model (COMSOL-IPHREEQC) is coupled with cement hydration model (HyMeC-COMSOL- IPHREEQC) to continue the hydration reaction while doing the transport reaction. The transport of carbon dioxide and chloride are influenced by saturation degree, concentration of exposure solution (chloride ion and CO_2 gas in the atmosphere), and porosity of the cement matrix. The proposed model is verified with different set of experimental results as well as with previously developed model in order to confirm the predictability of this proposed model.

概要

モルタルやコンクリートなどのセメント系材料は世界の建設業界で最も広く使用されている建設材料である。セメント系材料は水和物、骨材、遷移帯などの多様なコンポーネントにより複雑な微細構造を形成している。セメントの組成に応じて、カルシウムシリケート水和物（C-S-H)、水酸化カルシウム、エトリンガイト、ハイドロタルサイト、AFm 相などのさまざまな種類の水和生成物が形成される。主な水和生成物である C-S-H は、比表面積が大きく複雑な細孔構造を有し、さらに C-S-H は低密度 C-S-H（LD C-S-H）と高密度 C-S-H（HD C-S-H）の 2 つの異なる形態で存在することがよく知られている。また、セメント-骨材界面（遷移帯）は、セメント粒子による通常の充填が妨げられるため骨材表面における壁効果によって形成され、遷移帯は、高い空隙率によりコンクリートやモルタル中の骨材やセメントマトリックスに比べて脆弱相と見なされる。前述のようにセメント系材料の微細構造は、機械的およびイオン拡散を支配する最も重要な要因です。また、セメント系材料の力学特性及び拡散性を予測することは非常に複雑なプロセスを伴っている。そのため、これまでに提案されているモデルの多くは、いくつかの仮定と簡略化を行っており、モデルの適用範囲やさらなる開発が制限されている。したがって、セメントの反応を現実に即してシミュレートするためには、水和反応のすべての構成要素を統合したモデルが必要である。そこで、本研究の目的は、微細構造からセメント系材料の機械的特性と拡散性能を予測するモデルを開発することである。

第 1 章では、本研究の背景と目的及び論文の構成・位置づけを示した。

第 2 章では、本研究に関連する既往の研究をレビューし、問題点を明らかにした。本章では、セメント、コンクリート、微細構造、ITZ および水和物の基礎について詳細に説明した。また、さまざまな環境条件におけるイオン（海水からの塩化物イオンと大気からの CO_2 ガス）拡散後の水和生成物と細孔溶液中のイオン濃度の変化について詳しく説明した。さらに、セメント系材料の力学特性及び拡散性を予測する先行研究モデルの説明とその限界について述べた。

第 3 章では、HyMeC (Hydration and Mechanical properties of Cement-based material)と呼ばれる 2 ステージモデルを提案し、微細構造からセメントペーストの力学特性を予測した。まず、相対湿度、熱力学相平衡、セメント水和および体積変化のモデルを統合して水和生成物の体積分率を正確に予測した。続いて、セメントペーストの機械的特性を計算するために、C-S-H マトリックスから始まり、2 種類の C-S-H（低密度および高密度 C-S-H）の形成を考慮してセメントペーストに至るまで、3 つの階層レベルによってマルチスケールモデルを開発した。C-S-H の体積分率と毛細管空隙による空隙率は、セメントペーストの機械的特性を決定する最も重要な要素であるため、ここでは C-S-H の空間比率を考慮した。提案したモデルによって予測した、

相対湿度、化学収縮率、毛細管空隙率、圧縮強度、ヤング率、ポアソン比は、既往の実験結果とよく一致することを確認した。

第 4 章では、モルタルやコンクリートのヤング率およびポアソン比などの力学特性をナノスケールからコンクリートまでの拡張マルチスケールモデルによって評価した。提案したマルチスケールモデルでは、モルタル・コンクリートの微細構造は、骨材相（細骨材および粗骨材)、骨材界面にある ITZ 相、ペースト・モルタル相の 3 相と見なされる。主な入力項目は、セメントペーストと ITZ の微細構造であり、セメント水和-熱力学連成モデルを用いて養生時間の関数として予測され、ITZ の体積分率は、骨材の粒度分布に基づいて解析的に算出される。モルタルとコンクリートの力学特性を予測するためにマルチレベル均質化法（2 相複合材料の 3 相球モデルに基づく）を実装した。ここでは、モルタル・コンクリートの第 1 レベルおよび第 2 レベルの均質化法によりペースト･モルタルおよび ITZ で構成される等価マトリックスが得られる。モルタルとコンクリートのモデルの予測を検証するため、予測値を既往の実験結果と比較した。また、モルタルとコンクリートの特性に ITZ が及ばす影響についても検討を行った。

第 5 章では、セメントペースト中の塩化物イオンと二酸化炭素の拡散について検討を行った。セメント系材料の多次元・多種イオン輸送をシミュレートするために、MATLAB 言語をベースとした COMSOL-IPHREEQC インターフェースを開発した。イオン輸送計算には COMSOL Multiphysics を使用し、熱力学データベースを用いて IPHREEQC によって化学反応をシミュレートした。熱力学的な知見に基づき、物理的・化学的な相互作用を表現するために、相平衡モデルと表面錯形成モデルを用いた。提案したイオン輸送モデル（COMSOL-IPHREEQC）はセメント水和モデル（HyMeC-COMSOL-IPHREEQC）と統合され、輸送反応を伴いながら水和反応をシミュレートすることを可能とした。炭酸ガスと塩化物イオンの拡散は、飽和度、曝露溶液（塩化物イオンと大気中の炭酸ガス）の濃度、セメントマトリックスの空隙率に影響される。提案したモデルの妥当性を確認するために、過去に開発されたモデルと同様に、異なる実験結果を用いて検証を行った。

第 6 章では、本研究の成果を総括し、今後の課題について述べた。提案した HyMeC モデルと HyMeC—COMSOL モデルによって予測した計算結果は実験結果とよく一致すること示し、実現象をよくシミュレートできることを示した。さらに、モルタルとコンクリートの圧縮強度予測、モルタルとコンクリートの多種イオン拡散予測、混和材の影響などのモデル拡張を今後の研究課題として示した。

ACKNOWLEDGEMENTS

I am extremely grateful to Prof. Yogarajah ELAKNESWARAN. He has always been a great supervisor during my three years graduate career at Hokkaido University, and his continuous encouragement, guidance and mentorship have been instrumental to the success of this research journey. He has greatly impacted my professional and personal growth; his expertise and his emphasis on quality and dedication in works had been my inspirations, which also had let me realize the true academic passion. I really would hope to persevere the lessons I have learned from him throughout my academic career and would like to covey them to my future students.

I am thankful to have Professors Tsutomu SATO, Ryoma KITAGAKI and Takafumi SUGIYAMA as members of the dissertation evaluation committee. Their vast knowledge and experience in their respective areas could be undoubtedly helpful to improve my research work and dissertation. I am extremely appreciative for all their time and thoughtful comments throughout.

I would also like to express the sincere appreciation to the Shimizu Institute of Technology, Center for Construction Engineering, Japan, for providing the research opportunity and supporting in funding (full-funded). The appreciation would also go to D-DRIVE for partially supporting in funding.

I would also like to acknowledge the laboratory research team; it was really a wonderful company and had been interactive and supportive throughout the three years.

Finally, I would like to thank my great family. My husband, whose love and care have kept

me always strong and inspired, and whose encouragements have kept me always motivated. I am so blessed to have wonderful parents and lovely sister and brother; they have always emphasized strong educational goals since my childhood, encouraged to follow my academic passion. I am eternally grateful and thank you all for your love and support.

CONTENTS

LIST OF FIGURES

LIST OF TABLES

CHAPTER 1

INTRODUCTION OF DISSERTATION

1.1 General background

Cement composites are the utmost popular and extensively used construction materials all over the world, particularly due to their desirable mechanical characteristics. Their applicability in the field of Civil Engineering is diverse including the construction of buildings, roads, dams, harbors, airports, and so on (Wriggers and Moftah, 2006; Krishnya, Elakneswaran and Yoda, 2021; Sun et al., 2021). However, these cement based materials always reveal a complex behavior with varying properties that are controlled by the characteristics of components, their microstructure and their interfaces (Bernard and Kamali-Bernard, 2015). In the exposure to water, the cement is hydrated into calcium silicate hydrate (C−S−H) and other hydration products (Elakneswaran et al., 2016). The C−S−H typically forms to around 50–70% of the hydrated cement paste (Krishnya, Yoda and Elakneswaran, 2021; Sun et al., 2021). As the most important binding phase, formation of C-S-H gel determines the final properties of cement-based materials. In addition, it tends to bind the steel reinforcements, aggregates, sand and other hydration products with each other in hydrated cement/concrete. Initially, the porosity of the cement matrix is apparently high, and when hydration is taken place, the development of hydration products continues to fill the existing voids system, leading to a denser microstructure with decreasing porosity (Sant, Bentz and Weiss, 2011; Krishnya, Yoda and Elakneswaran, 2021). This porosity network is known as one of the weakest zones in the hydrated matrix.

At the macroscale, the cementitious composites (concrete and mortar) are often viewed as three phase material, i.e., having bulk paste (or cement paste), aggregate and interfacial transition zone (ITZ) (Sharma and Bishnoi, 2020a; Krishnya, Elakneswaran and Yoda, 2021). The formation of ITZ around the aggregate is due to size discrepancy between cement grains and aggregates (Gao et al., 2014). When the cement is mixed with aggregates, the normal packing of cement grains disrupts due to the geometrical wall effect (i.e., small cement grains pack more easily in the vicinity of aggregate compared to large ones). Consequently, within the zone close to the aggregate surface, the volume fraction of cement grain is lower compared to zones further out (Jiang et al., 2016; Sharma and Bishnoi, 2020). The porosity of the ITZ is therefore approximately 1.2-2.5 times higher than that of bulk paste. In fact, ITZ is not a definite zone, but a region of transition, and a thickness ranging between 10 and 50 μm is known for typical mortars and concrete (Nadeau, 2002; Sharma and Bishnoi, 2020). Because of its high porosity compared to bulk paste matrix, ITZ is considered to reveal adverse effects on the performance of mortars and concretes.

It is admitted that the microstructure determines the progression of mechanical and transport properties. The abovementioned microstructure of the cement-based materials (i.e., C-S-H, porosity, other hydration products, aggregate and ITZ) depends mainly on clinker composition, water to cement ratio (w/c), aggregate properties and its content, curing condition (temperature and curing method) and hydration periods. The mechanical properties are important for the structures which are subjected to the boundary conditions of restrained displacements, particularly when the deformation is restrained from a very young age on pavements, dams, concrete slabs of composite structures, massive parts poured in successive layers, etc. The evolution of intrinsic properties in time is one of the most critical material-

to-structural mechanical design parameters (Bernard, Ulm and Lemarchand, 2003). Furthermore, many deterioration processes of concrete structures are reported to be related with transport processes in material such as moisture transfer, diffusion of carbon dioxide, and penetration of chloride into the material (Jiang et al., 2016). The transport of ions, moisture and gas causes adverse effects on the concrete structure such as reinforcement corrosion, leaching of calcium ions, dissolution of C-S-H and other hydration products, thus increasing the porosity of the cement matrix (Sugiyama, Ritthichauy and Tsuji, 2003). The mechanical properties are also affected by the transport process due to the changes in the hydration products and porosity of the matrix.

Owing to the significant use of cement-based material and constantly increasing expectations of the users, an enormous effort, both experimentally and numerically, has been undertaken to study the progression of mechanical and transport properties of cementitious materials. Specifying material properties and model parameters is crucial for the structural analysis. Particularly, this is very important, if the influence of mix composition, processing steps and environmental conditions during the construction stage on the long-term durability of the structure needs to be evaluated. The parameters of concrete can possibly be determined by experiments; however, this is a time-consuming and tedious process that can considerably hold up the design work (Vorel, Šmilauer and Bittnar, 2012). Therefore, developing a virtual testing tool, i.e., integrated set of models, algorithms and procedures for predicting the mechanical and durability characteristics of materials, can be a better alternative. However, the scientific understanding and predicting the mechanical and transport properties of concrete is no doubt the most complicated processes, as the microstructure of the concrete falls across nano-scale (C-S-H) to macro-scale (aggregate). In most of the previously

proposed models, the progression of microstructure could be predicted with certain assumptions and simplifications (van Breugel, 1995a; Bentz, 1999; Koichi Maekawa, Ishida and Kishi, 2009; Stefan et al., 2010). There is still a great need to develop novel model with reduced assumption and simplification to predict the concrete properties in a reliable manner.

1.2 Scope and objective of the research

The objective of the research presented in this dissertation is to develop a new model, capable of determining the mechanical and transport properties of cementitious material from its evolution of microstructure with less assumption. From the perspective of Material Engineering, yet significant effort has been given on understanding microstructural responses, mechanical responses and durability responses by considering different factors such as different type of cement (clinker composition), w/c, aggregate content, hydration, exposure period and etc.

Firstly, the microstructure of the cement paste is determined using thermodynamic calculation, and by considering the microstructure of the cement paste in multi-scales, the mechanical properties are predicted using the three hierarchical levels of multi-scale model. These three levels of multi-scale model are then extended up to the concrete (i.e., five levels) to simulate the mechanical properties of mortar and concrete. In the subsequent part, by coupling the microstructure of cement paste with COMSOL-Multiphysics, the ions concentration in the pore solutions and hydration products after the transport are precisely predicted. The scope of the research work is summarized in **Figure 1.1.**

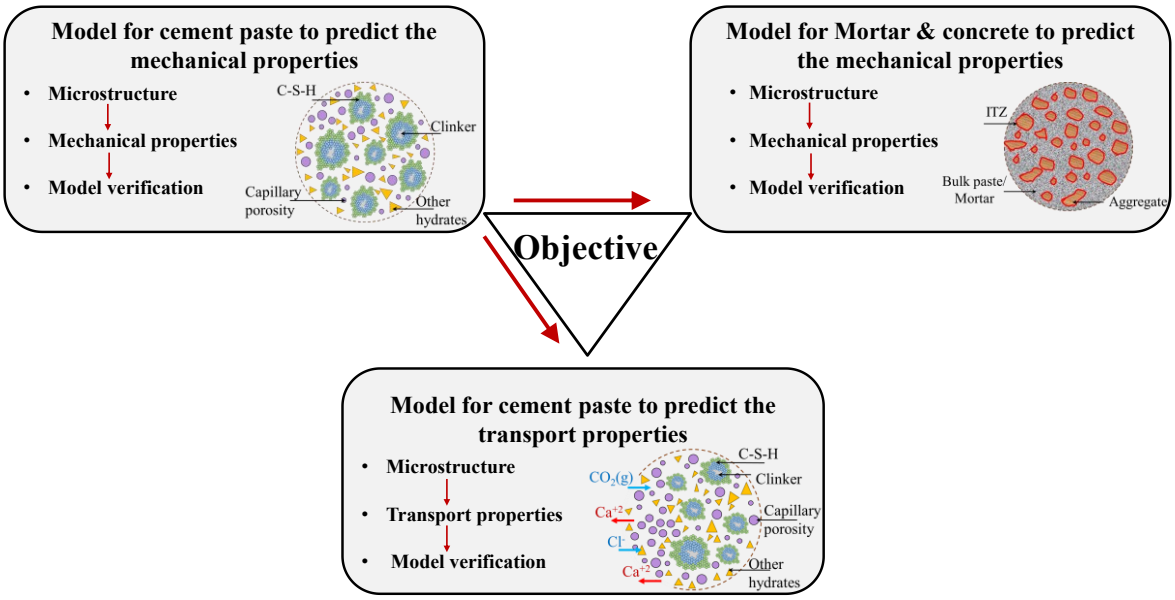

Figure 1.1: Outline of the scope of the research work

1.3 Originality and significance of the work

Currently, increased attention is paid on the prediction behavior of cement-based materials due to high demand in construction industry. This research work focuses on introducing a novel model for the prediction of mechanical and transport behavior of cementitious materials.

Most of the previous model for cement paste were developed based on certain assumptions such as (i) assuming cement paste as three phase material consisted of only the unhydrated clinker, hydration products and porosity; (ii) ignoring the volume of C–S–H, but alternatively, considered only capillary porosity or gel space ratio to predict the mechanical properties; (iii) only employing the C–S–H and portlandite as hydration products in the cement matrix; (iv) assuming C–S–H as a single matrix with constant gel porosity, ignored the two types of C–S–H formation. The proposed model addresses the limitations found in the currently available models and tends to predict the mechanical properties of cement paste realistically by

considering the detail microstructure of the hardened matrix (two types of C-S-H, portlandite, ettringite, monosulfate, hydrotalcite, Fe-siliceous hydrogarnet, capillary pores and chemical shrinkage which are depending on the clinker composition and w/c).

As the ITZ is the weakest zone in mortar and concrete, the prime consideration needs to be given on it when predicting the mechanical properties of mortar and concrete. In the proposed model, mortar and concrete are represented as three phase materials (aggregate, ITZ and bulk paste/ mortar). Unlike most of the previously proposed models (wherein constant properties of ITZ and bulk paste were used), the computations of mechanical properties of ITZ and bulk paste are herein based on the detailed microstructure of hydrated cement paste including two types of C-S-H, capillary porosity, chemical shrinkage and other hydration products. Since the microstructure of cement matrix varies depending on curing time, chemical composition of clinker, w/c and curing temperature, the realistic computations of ITZ and bulk paste are emphasized in this proposed framework.

Moreover, as the transport of ions, moisture and gas cause adverse effects on the concrete structure, a new model is developed to predict the ion concentration, hydration products and mechanical properties during the exposure conditions. The proposed transport model (COMSOL-IPHREEQC) is coupled with cement hydration model to continue the hydration reaction while doing the transport reaction, while the ion concentration in the pore solution and hydration products after 28 days of hydration are involved as additional input parameters to the previously developed transport model.

1.4 Organization of Dissertation

This dissertation is organized into a total of seven chapters.

Chapter 1 describes the objective, scope and significance of this study.

Chapter 2 presents a review of relevant literature on various aspects. Early sections of this chapter discuss the fundamentals of cement and concrete, microstructure, ITZ and hydration products for the basic understanding. Latter sections discuss the details and limitation of the previously developed models to predict the mechanical properties of cementitious materials. Finally, the changes in the hydration products and ion concentration in the pore solution after the transport of ions from different environment (chloride ion from the sea water and CO_2 from the atmosphere) are discussed.

Chapter 3 details all procedures adopted in the proposed model to predict the mechanical properties such as compressive strength, Young's modulus and Poisson's ratio of cement paste from its microstructure. In addition, the predictability of the proposed model is verified with different set of experimental results as well as previously developed model. Moreover, the newly proposed relative humidity model to predict the relative humidity with hydration period insight the cement paste is discussed by using the predicted compressive strength.

Chapter 4 describes the method to determine the volume fraction of ITZ, and hence predict the mechanical properties of mortar and concrete using the homogenization method and multi-scale model of the cement paste. In addition, the capability of the proposed model for mortar and concrete is verified with different set of experimental results reported in the previous work. Finally, the effect of ITZ on the mechanical properties of mortar and concrete

is discussed.

Chapter 5 presents model description for the ion transport and gas transport using coupled MATLAB and COMSOL Multiphysics. Also, the proposed model for the transport of ions and gas is validated with previously developed model and experimental results reported in the literatures.

Chapter 6 presents the overview of the findings and conclusions drawn in this work, along with the recommendations for the future works.

CHAPTER 2

LITERATURE REVIEW

2.1 Introduction

Concrete is the utmost consumed material in the world due to its low cost and growing demand for infrastructure, in which cement is the active ingredient (Bauchy et al., 2015). This cement commodity is manufactured by the mixture of pure limestone (60-75 %) and clay (25-40 %) at the temperature approximately 1450 °C for between 8 and 20 hours which chemically transforms the mixture into hard nodules called clinker (Varas, De Buergo and Fort, 2005). During the clinker making process, alite (C_3S or $3CaO.SiO_2$), belite (C_2S or $2CaO.SiO_2$), aluminate (C_3A or $3CaO.Al2O_3$) and alumina ferrite (C_4AF or $4CaO.(Al, Fe)_2O_3$) form at different temperature. Finally, the clinker is mixed with gypsum and ground to make final cement product (Varas, De Buergo and Fort, 2005).

In the presence of water (known as hydration reaction), immediately after the mixing, the microstructure of cement-based material undergoes a marked transformation from a viscous suspension into a solid skeleton due to variety of complex chemical reactions and physical changes in the matrix. The early reaction of the cement is rapid, and the initial progression of stiffness is crucial for constructability. It is also known that the reactions may gradually continue for years, and the evolving microstructure determines the long-term mechanical and transport properties that govern the durability responses of the material. Within several hours after setting, however, the rate of hydration reaches the peak, begins to decrease, and continues to decrease with time. It should be noted that most of the hydration solid products

that exist in mature cement paste have nucleated already, presenting in considerable contents by the time the maximum rate is achieved. In latter stage, the dissolution rates of initially-formed cement phases tent to decrease significantly due to less surface area for dissolution (as that would be covered partly by hydration products). (Bullard et al., 2017).

2.2 Microstructure

2.2.1 Hydration products

During the hydration process, number of products would form depending on the clinker composition and mixing condition. Calcium silica hydrate (C-S-H), portlandite (CH), ettringite, monosulfate, hydrogarnet and hydrotalcite are constitutive phases existing in the Ordinary Portland Cement (OPC) (Krishnya, Yoda and Elakneswaran, 2021). The simple stoichiometric reactions for the hydration of four phases in clinker are detailed in Eq. (2.1) - Eq. (2.6). Alite and belite mainly produce C-S-H and CH (Eq. 2.1 and 2.2), while ettringite form due to reaction of aluminate and gypsum ($C\bar{S}H_2$) as shown in Eq. (2.3). Besides, additional aluminate reacts with ettringite to produce monosulfoaluminate (see Eq. 2.4). Eq. (2.5) presents the continued hydration of aluminate after the consumption by monosulfoaluminate, and the formation of hydrogarnet from the reaction of alumina ferrite is shown in Eq. (2.6).

$$C_3S + H \rightarrow C-S-H + CH \quad (2.1)$$

$$C_2S + H \rightarrow C-S-H + CH \quad (2.2)$$

$$C_3A + C\bar{S}H_2 + H \rightarrow C_6A\bar{S}_3H_{32} \quad (2.3)$$

$$C_3A + C_6A\bar{S}_3H_{32} + H \rightarrow C_4A\bar{S}H_{12} \quad (2.4)$$

$$C_3A + CH + H \rightarrow C_4AH_{13} \quad (2.5)$$

$$C_4AF + CH + H \rightarrow C_3(A,F)H_6 \quad (2.6)$$

Among these hydration products, C-S-H phase (the prime bonding agent and having high specific area with internal pore structure) governs the mechanical properties (Jennings et al., 2005; Thomas, Jennings and Allen, 2010) The molar ratio of calcium to silica (Ca/Si) is one of the important parameters for the structure of C–S–H, and that ranges approximately between 0.7– 2.(Thomas, Jennings and Allen, 2010; Papatzani, Paine and Calabria-Holley, 2015). The higher values may be obtained under extreme hydration or curing conditions, while the lower values can be obtained in the presence of supplementary cementitious materials. The Ca/Si ratio of 1.6 is typically considered for the OPC hydration reaction (Tennis and Jennings, 2000).

Many previous studies have confirmed that the formation of C–S–H in the cement matrix occurs in two stages with different intrinsic characteristics (Tennis and Jennings, 2000; Jennings et al., 2005). At the early stage of the hydration process, the progression of C–S–H occurs on the surface of cement particles, and with the time, the cement particles are partially/ fully covered by C–S–H layer as shown in Figure 2.1. Subsequently, the formation of new C–S–H is induced within the space confined by the existing C–S–H, as the diffusion process continues to be occurred through the previously formed C–S–H layer (refer **Figure 2.1**). The C–S–H formed under the confinement has higher density (hereafter referred to be HD C–S–H) compared to the C–S–H formed at the early stage as the outer product (hereafter referred to be LD C–S–H). Each of them forms not only with different densities, but also forms with

different volume fractions and gel porosity (Tennis and Jennings, 2000; Thomas and Jennings, 2006). The LD C-S-H is formed as a stable structure with 36 % of porosity, while HD C-S-H are formed with 26 % of porosity (Jennings et al., 2007).

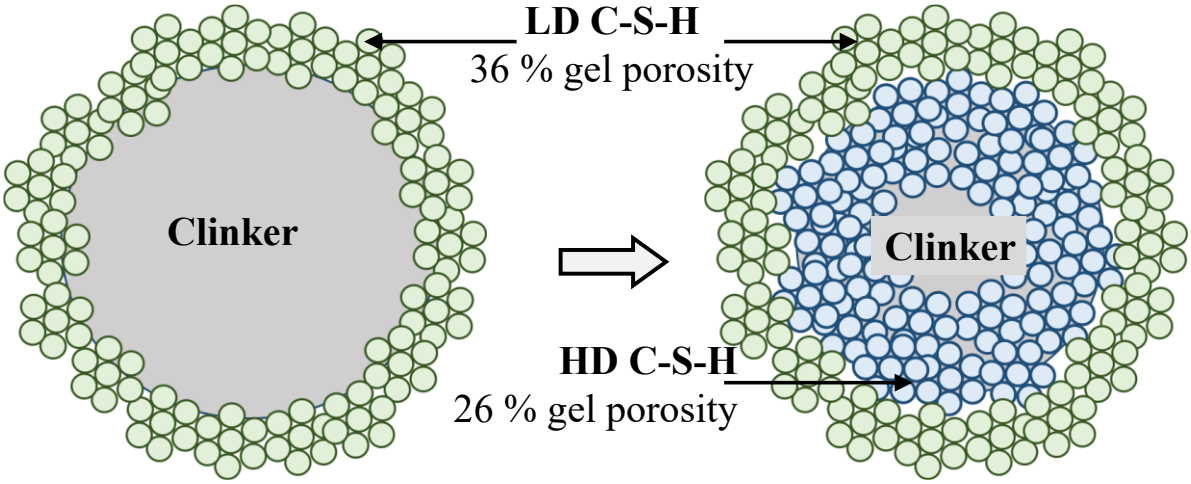

Figure 2.1: Formation of two types of C-S-H

The porosity of the hydrated matrix is also one of the significant microstructures, which establishes at different scales. This porosity network (and its connectivity) is the governing factor for the development of mechanical and durability properties of hardened matrix. In particular, capillary porosity is known as the weakest part in the hydrated matrix. The hydration products themselves have to tolerate most of the applied load, whereas the neighboring capillary porosity remains almost unstressed (Pichler et al., 2013). As well established, the porosity of the hardened matrix reduces with increasing hydration time due to the formation of hydration products. It should be highlighted that the matrix becomes more susceptible when the capillary pores are evolved to be connected compared to that progress separately (Krishnya, Yoda and Elakneswaran, 2021).

2.2.2 Interfacial Transition Zone (ITZ)

The aggregate-cement interface, so called the interfacial transition zone (ITZ) in the previous studies, is considered as the third phase introduced by the presence of aggregates in mortar and concrete. The ITZ is often referred to be the most mysterious region and critical in progressing material properties (Gao et al., 2014; Jebli et al., 2018; Krishnya, Elakneswaran and Yoda, 2021). Nevertheless, the microstructure and thickness of ITZ are still not fully understood that how far it differs from the bulk paste. One of the major reasons can be that the ITZ is not a definite phase within cementitious composite, as no clear discrete boundary exists between the ITZ and the bulk paste (Scrivener, Lyon and Laugesen, 2004). Typically, it has been studied as a specific property profile (for instance, ITZ was defined as the zone with an excess of porosity) (Gao et al., 2014). The ITZ thickness ranging between 10 and 50 μm is documented for mortars and concrete (Crumbie, 1994; Krishnya, Elakneswaran and Yoda, 2021). However, the thickness is found to be influenced by various casting factors such as curing age, w/c ratio, aggregates properties (type, roughness, shape and size), aggregate content and supplementary cementitious materials (Nadeau, 2002; Scrivener, Lyon and Laugesen, 2004; Gao et al., 2013).

Various mechanisms such as wall effect, formation of water film around the particles, micro bleeding, filtration effect etc. have been reported for the formation of ITZ (Sharma and Bishnoi, 2020). A general viewpoint in the concrete research is that ITZ is formed due to the size discrepancy between cement particles and aggregates (Li, Zhao and Pang, 1999), as the diameter of aggregates is considerably larger than that of cement grains. While cement mix with aggregates, due to the geometrical wall effect, the regular packing of cement grains can be dislocated, i.e., small cement grains pack more easily near to the aggregate surface

compared to large ones. Thus, inside the region adjacent to the aggregate surface, the volume fraction of cement is lower compared to zones further out as illustrated in **Figure 2.2.** As the result, the excess amount porosity exist in the ITZ layer compared to that of bulk paste.

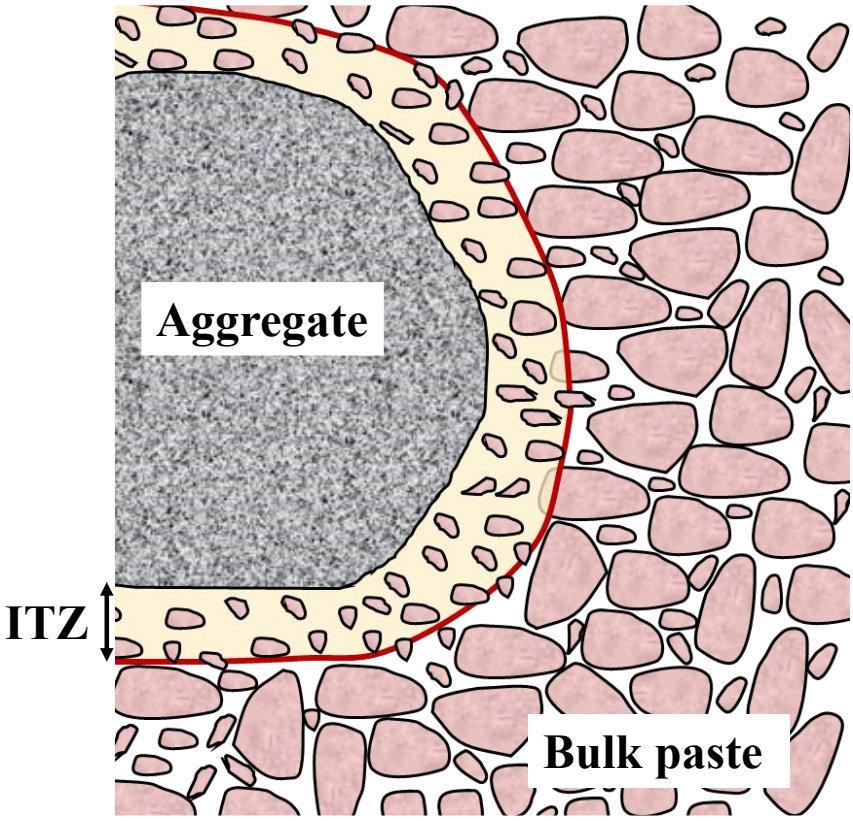

Figure 2.2: Illustration of formation of ITZ within concrete/ mortar

The microstructure of hydrated matrix in the ITZ also considerably vary with distance from aggregate due to bleeding and segregation effects during the setting of concrete/ mortar (Crumbie, 1994). The microstructure of the ITZ generally can be described in terms of hydration reaction and porosity. Hydration reaction adjacent to the aggregate surface varies from the reaction which takes place in the bulk paste due to excess amount water in ITZ. In the past, Nadeau (2002) proposed a model to predict the clinker content in the ITZ and bulk paste based on experimental results of Scrivener and Pratt (1996). **Figure 2.3** shows the

variation of clinker content and effective w/c with the distance from aggregate surface based on the proposed model by Nadeau (2002). Similar tendency of experiment results were also observed by Crumbie (1994). As explained above, the clinker content is low near to the aggregate surface, while the effective w/c is high due to wall effect. This tendency is clearly captured by the proposed model for unreacted clinker and effective w/c as revealed in **Figure 2.3.**

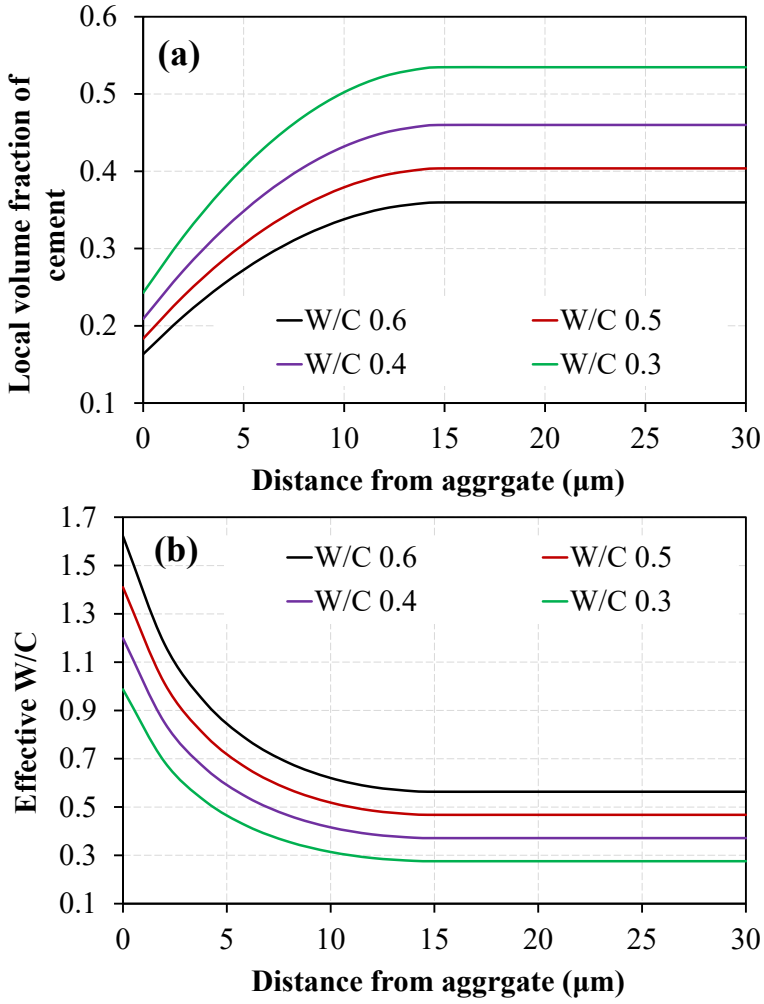

Figure 2.3: Variation of (a) clinker content and (b) effective w/c with distance from aggregate surface

The reaction degree of clinker is high at the zone closer to the aggregate surface due to the higher w/c compared to bulk paste (**Figure 2.4**). As depicted in **Figure 2.4**, cement particles adjacent to aggregates (first 15 µm distance) reacts rapidly and shows approximately 20 % higher degree of hydration than that of cement particles at the distance further away about 20 µm after one day of hydration. However, the variation between the degree of reaction of both clinkers (i.e., near to aggregate and away from aggregate) decrease with hydration period. The variation after 1 year is only around 5 % (refer **Figure 2.4**). This is because, after 28 days of hydration, larger cement particles which are away from the aggregates remain dominant, while smaller size particles located near to the aggregate surface had already reacted during earlier hydration (Crumbie, 1994).

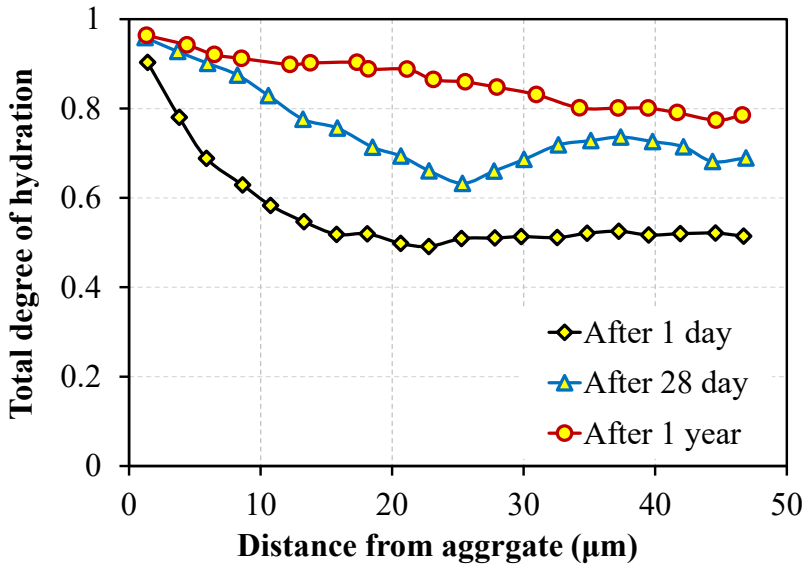

Figure 2.4: Variation of hydration degree with distance from aggregate surface (modified from Crumbie, 1994)

The variations of the microstructure in terms of (a) porosity, (b) formation of portlandite and (c) other hydration products with the distance from aggregate surface are illustrated in **Figure**

2.5, which are based on the experimental results of Scrivener, Lyon and Laugesen (2004). Porosity, which is the volume that does not consist of solid skeleton in the hydrated matrix, is much higher close to aggregates compared to the bulk paste due to the excess amount of water and low amount of clinker. After the first day of hydration, the porosity adjacent to the aggregate is approximately 20 % higher than that of bulk paste (away from the aggregate). However, with increasing hydration periods (i.e., after 28 days and 1 year), the porosity in ITZ decreases by approximately an equivalent amount that reduced in the bulk paste. This could be attributed to the hydration reaction in the ITZ as well as in the bulk paste (refer **Figure 2.5(a)**).

The formation main hydration products such as portlandite and C-S-H also shows different behavior due to the inclusion of aggregates. During the hydration process, silica concentration is very low, as clinker consists of low amount of silica (mainly consumed by C-S-H around the cement grains). On the other hand, the concentration of calcium is much higher in the pore solution. Due to the high mobility of calcium ion and silica prevents the nucleation of calcium hydroxide around cement grain, calcium hydroxide (portlandite) forms far away from the cement grains which is close to the aggregate surface (more porous zone) (Scrivener, Lyon and Laugesen, 2004b). Therefore, high amount of portlandite precipitates in the zone close to aggregate surface as shown in **Figure 2.5(b)**. However, a little amount of clinker exists in the ITZ, and high amount of portlandite forms in the ITZ due to the calcium ions coming from the reaction of clinker away from aggregate. The variation in the formation of other hydration products (mainly C-S-H) with distance from aggregate is depicted in **Figure 2.5(c)**. It can be seen that considerably low amount of C-S-H precipitates near to the aggregate surface because of low amount of clinker and low mobility of silica. The formation of hydration

products increases with the time due to the hydration reaction in the ITZ and bulk paste.

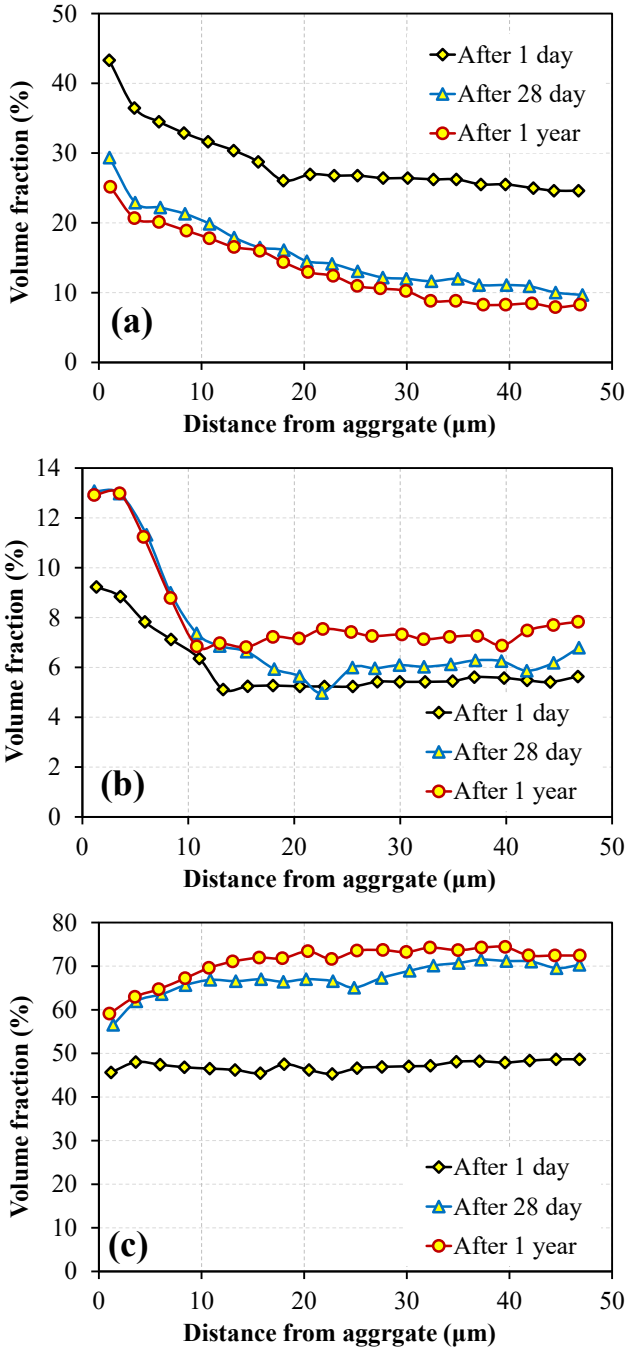

Figure 2.5: Variations of the volume fraction of (a) porosity, (b) portlandite and (c) other hydration products (modified from Scrivener, Lyon and Laugesen, 2004)

During the application of loads, the adhesive bonds (ITZ) between the aggregate and hydrated matrix are damaged and leads to the weakening of the concrete structure, and eventually the cracks develop and propagate either through the particles or around them (Erdem, Dawson and Thom, 2012). Due to the excess porosity, the ITZ behaves as preferential pathway for the ingression and diffusion of ions, liquids and gases and leaching of ions from the hydrated matrix (Crumbie, 1994). Therefore, a clear understanding on the relationship between the microstructure of cement-based material and their properties is required to allow the design and analysis of the systems with improved accuracy.

2.3 Existing models for cementitious materials

As mentioned earlier, the understanding and predicting the microstructure of cement paste are no doubt the most complicated processes. However, with the aid of newly developed computer-based packages/models, the prediction of microstructure of hydrated cement could be reasonably achievable in the recent decades. CEMHYD3D model (Bentz, 1999), HYMOSTRUC model (van Breugel, 1995b) and DuCOM model (Koichi Maekawa, Ishida and Kishi, 2009) are the well-known models proposed for the prediction of microstructure and intrinsic properties of cementitious materials. And also, several simplified empirical and analytical models have also been proposed for the predictions of volume of phases, hence linked to the mechanical properties of cement-based (Constantinides and Ulm, 2004; Haecker et al., 2005; Stefan et al., 2010; Zheng et al., 2010; Wu et al., 2012; Duplan et al., 2014; Aouissi et al., 2016; Chen et al., 2016; Das, Maroli and Neithalath, 2016; Hlobil, Šmilauer and Chanvillard, 2016; Bahafid et al., 2018; Lavergne et al., 2018; Mazaheripour et al., 2018).

2.3.1 CEMHYD3D

CEMHYD3D is one of the utmost extensively-used package for the prediction of the microstructure of cementitious material. The mechanism is based on the voxel approach which is similar to the finite element method (Bentz, 1999). In this approach, the whole volume of the hydrated matrix is filled with smaller elements (referred as voxel), positioned with their faces in contact, whereas every individual element can be separately assigned shape, size and material properties. The selection of the size of this voxel needs to be adequate to capture the important fundamental processes such as reaction, transport, dissolution, and diffusion. The main factors involving in hydration process such as particle size distribution of cement grain, chemical composition, temperature and curing conditions are considered in this model. Initially, random 3D microstructure which mainly consists of four phases of clinker and gypsum, is built using the autocorrelation functions. The hydrates are precipitated around the cement particles which are exposed to water contact. Based on the predicted hydration products and porosity, the compressive strength is estimated using the gel space ratio theory as detailed in Eq. (2.7) and (2.8).

$$\sigma_c = \sigma_0 X^n \tag{2.7}$$

where, σ_c is compressive strength, X is gel-space ratio, σ_0 is intrinsic strength which depends on the chemical composition of the cement and particle size distribution, and n is commonly an assumed value between 2.6 and 3.

$$X = \frac{0.68\alpha}{0.32\alpha + \frac{w}{c}} \tag{2.8}$$

where, α is the hydration degree and $\frac{w}{c}$ is water to cement ratio.

2.3.2 HYMOSTRUC

The HYMOSTRUC model was developed by van Breugel in 1995 to simulate the growth of hydration and microstructural properties as a function of chemical composition and particle size distribution of cement, w/c and reaction temperature using the vector approach. In the three-dimensional microstructure of the developed HYMOSTRUC model, cement grains are displayed as arbitrarily distributed spheres, whereas hydrates are exhibited as growing spheres in the outward direction of the cement particles (Ye, Van Breugel and Fraaij, 2003). In HYMOSRUC, clinker tends to dissolve during the hydration process, forming a porous shell of hydrates around the unreacted particles. Small and remote clusters evolve initially around clinker particles by the progression of hydration; big clusters are then formed once the outer shell of other particles are surrounded by small grains, which leads to the development of hydrates in the outward direction (refer to **Figure 2.6**).

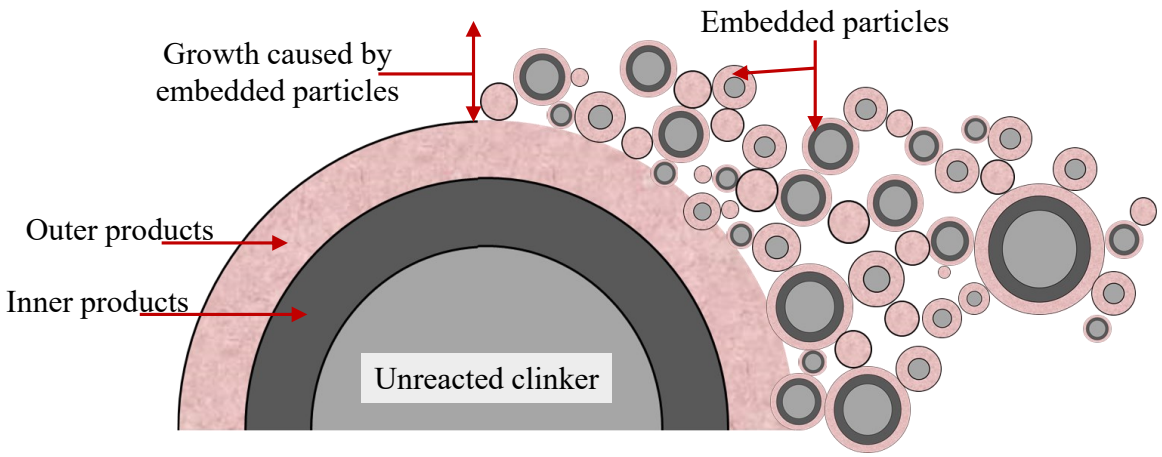

Figure 2.6: Formation of a hydrated matrix microstructure in HYMOSTRUC (modified from Ye, Van Breugel and Fraaij, 2003)

The properties such as development of hydration and microstructure, thermodynamic

equilibrium, volume changes in hydrated cement and the effect of geometrical changes of the microstructure on the creep behavior of hardening concrete can be obtained from the HYMOSTRUC.

2.3.3 DuCOM

DuCOM model was developed in the Concrete Laboratory of the University of Tokyo to predict the early age properties of concrete such as cement heat hydration, thermal conduction, moisture equlibrium and pore structure formation, and durability characteristics such as chloride ion transport, carbonation, corrosion of steel rebar and calcium ion leaching (Maekawa, Ishida and Kishi, 2009). The microstructure of the hydrates in the DuCOM model is predicted by using the heat generation during the hydration process, hence the mechanical properties are analytically evaluated. The predictions of this model are based on unhydrated core, inner products, C–S–H and free pore spaces as shown in **Figure 2.7**.

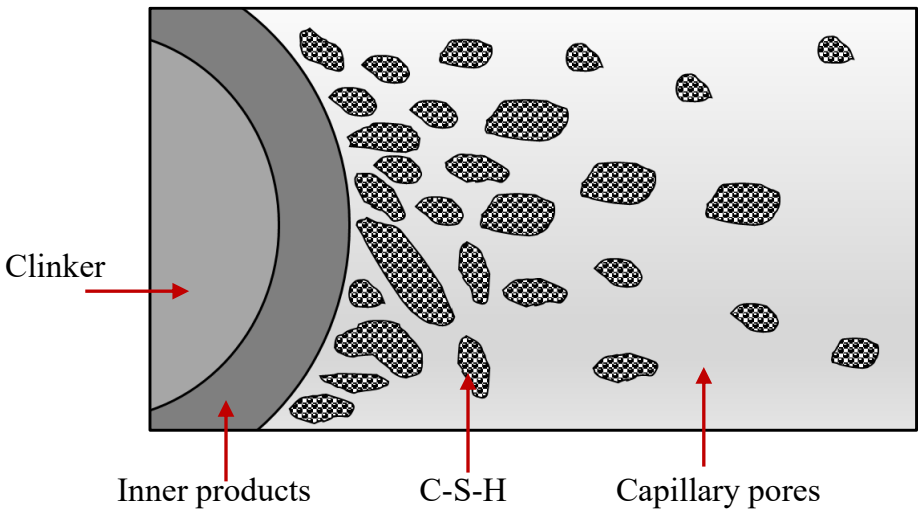

Figure 2.7: Microstructure of hydrated matrix in DuCOM model (modified from Maekawa, Ishida and Kishi, 2009)

2.3.4 Other existing models

Hlobil, Smilauer and Chanvillard (2016) proposed an analytical multi-scale model to air-entrained cement by approximating the finite element simulation, in which the volume fractions of hydrates are occupied from the abovementioned CEMHYD3D model and CemBase. A similar multi-scale model was developed by using the vector approach to predict the Young's modulus and Poisson's ratio of oil well cement (API class G) with varying temperatures (Bahafid et al., 2018). In the meantime, Mazaheripour et al. (2018) developed a model to predict the elastic behavior of hydrated cement paste using the lattice approach. The aforesaid HYMOSTRUC is used to simulate the microstructure of the cement paste in this model by considering the C-S-H and portlandite as the hydration products. The elastic modulus was finally predicted at the macroscale by establishing the properties to the lattice elements and by incorporating homogenization technique for upscaling.

Stefan et al., (2010) developed a model to compute the elastic properties of cement paste considering porosity, unreacted clinker and hydration products in the hydrated matrix. The volume fraction of each phase was calculated using empirical relationship (considering degree of hydration and w/c), and the mechanical properties of each phase was measured via nanoindentation techniques at the microscopic scale and via resonance frequencies techniques at macroscopic scale. The results obtained therein from finite element method and homogenization approach were compared and discussed. Similarly, by considering inner product, outer product and clinker as hydration products, Zheng et al. (2010) developed a simple model to compute the elastic modulus of cement paste using homogenization method.

A model to predict elastic properties such as elastic modulus and Poisson's ratio of mortar

was proposed by Wu et al., (2012) using the four hierarchical levels of multi-scale model consist of C-S-H solids, HD and LD C-S-H, hydrated cement matrix and finally mortar. The required elastic properties in nano and micro level solid phases were obtained using the molecular dynamics, and the volume fraction of each phase was derived from analytical relationships. In this model, the final property at macroscale was calculated using the homogenization technique. Furthermore, a multiphase micromechanical model for hybrid fiber reinforced concrete was suggested by Chen et al. (2016) to compute the elastic properties by considering concrete as three phase material (aggregate, ITZ and bulk paste). The volume fraction of ITZ was calculated using the relationship proposed by Lu and Torquato, (1992), and based on the previous studies, the elastic properties of each phase were assumed. At last, using the homogenization method, the elastic modulus and Poisson's ratio of hybrid fiber reinforced concrete was computed by assuming the ITZ as a single shell with constant uniform properties throughout the hydration process.

Moreover, a micro-mechanical modeling approach was proposed by Duplan et al., (2014). Based on the assumed and experimental values for elastic properties of different types aggregates (clay, sand and rubber), ITZ and cement paste, the elastic modulus of mortar was predicted using two different ways of homogenization method such as Mori–Tanaka method and self-consistent approach and compared with experimental results. A two-dimensional plane strain microstructural finite element model by considering the local stress concentration around the inclusions was developed by Das, Maroli and Neithalath, (2016) to predict the elastic behavior of the matrix. By considering the elastic properties of each phase in mortar such as hardened cement paste, quartz, ITZ for quartz, light weight aggregate and ITZ for light weight aggregate and generated representative element area consisted of

abovementioned phases, were numerically analyzed using finite elements by invoking periodic boundary conditions. Finally, the predicted results were compared with experimental results as well as the results of different homogenization methods.

2.4 Durability of cementitious material

Assessing the durability performance of both new and existing concrete structures remains one of the most significant challenges, particularly while considering the effective longevity of the structure. In turn, this is dictated by the capability of the concrete structures for a large extent to resist numerous deterioration processes such as transportation of ions, gas (mainly carbon dioxide) and moisture, alkali-aggregate reactions and frost damage (Hatanaka et al., 2003; Gasch, Eriksson and Ansell, 2019). Worth to note that among the varying processes, chloride ingression and carbonation are most serious degradation process in reinforced concrete structures, specifically for those exposed to such environments as air-bone chlorides in marine regions and deicing salts in cold regions (Chindaprasirt, Rukzon and Sirivivatnanon, 2008; Q. F. Liu et al., 2014; Xie, Dangla and Li, 2021). Under these environments, the abovementioned processes occur concurrently, thus leading to increase the risk of reinforcement corrosion. Additionally, the transport of ions involves chemical reactions between hydration products and pore solution, causing dissolution and precipitation in the hydrated matrix.

The microstructural changes due to the chloride ion ingression is conceptually shown in **Figure 2.8**. During the exposure condition (NaCl solution is considered herein for example), chloride ion enters the concrete structure through adsorption on the surface of the hydration products and diffusion through the pore network. The pH of the hydrated matrix is high

(approximately above 13), yet the pH of the exposure solution is typically neutral (pH 7). Therefore, pH of the exposed surface reduces due to the leaching out of OH- ion from the matrix. To maintain the chemical equilibrium in the exposed surface and solution, other ions such as Ca^{+2}, K^{+} also leach out from the matrix as shown in Figure 2.8. However, because of low concentration of Ca^{+2} ion in the pore solution and low pH in the exposed surface, portlandite and C-S-H dissolve to maintain the concentration Ca^{+2}. As the result, the porosity of the hydrated matrix increases with exposure time. In addition, the chloride ion penetration increases due the increased porosity, hence raises the risk of reinforcement corrosion. Chloride solid phases such as Friedel's salt also forms near to the exposed surface, while some part of the chloride ions are adsorbed by the surface area of the C-S-H (Song et al., 2021). The bound chloride by precipitation of Friedel's salt or adsorbed by C-S-H has no effect on the corrosion of steel bars. However, the free chloride in the pore solution causes the reinforcement corrosion in the concrete structure.

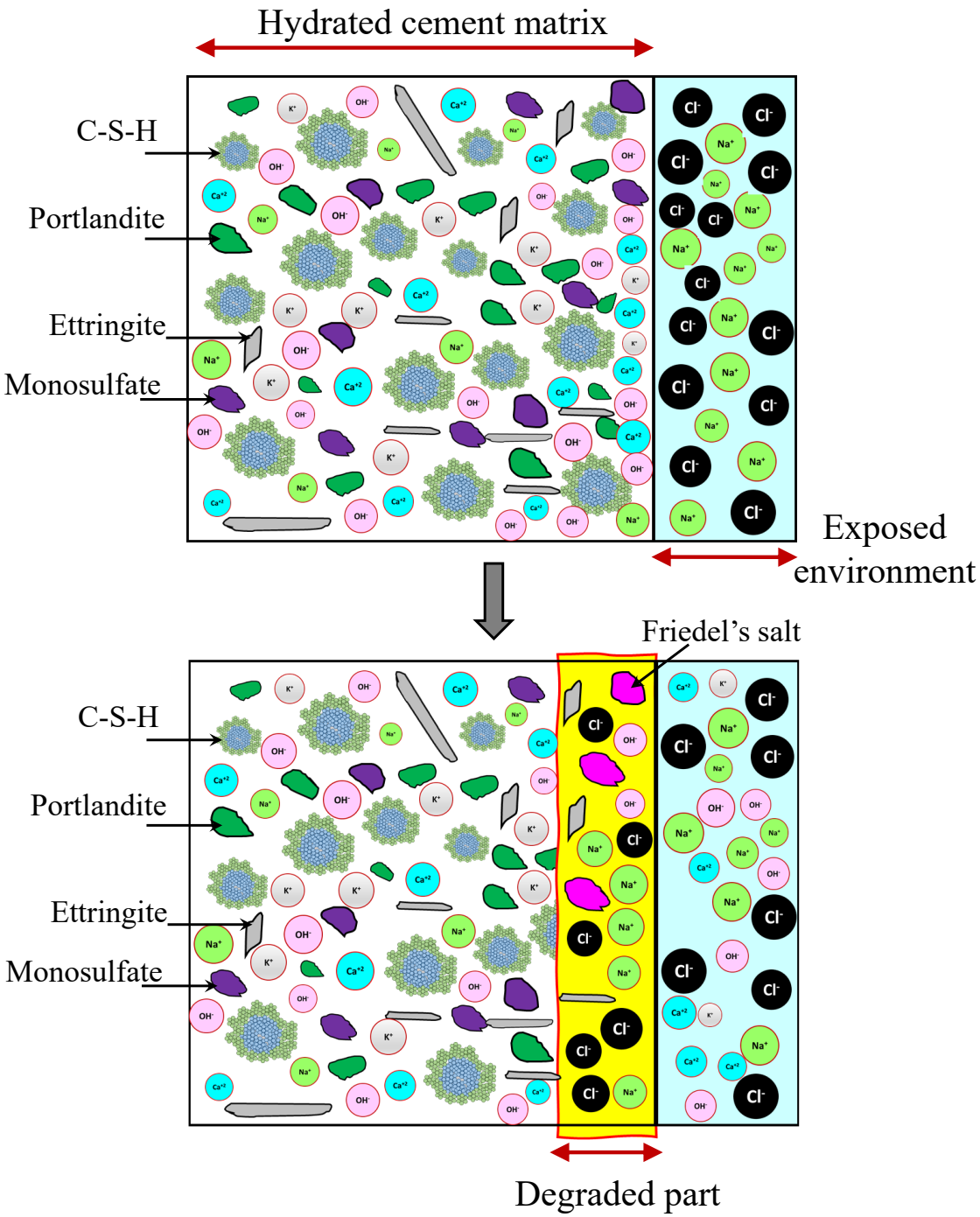

Figure 2.8: Schematic diagram for chloride ion transport in hydrated matrix

Carbonation of cement-based material is another complex process, altering the microstructural properties and performance of material underneath atmospheric conditions.

Decreasing the pH in carbonation is the utmost significant effect in the hydrated matrix, as the corrosion of reinforcement is accelerated by low pH due to the dissolution of thin oxide passive layer protecting the steel bars at lower alkaline conditions (Phung et al., 2016). Alternatively, carbonation shows in positive effects in cement basted material. During the carbonation process, the deposition of carbonation products (mainly calcite and silica gel) occurs in pores, benefits to matrix densification, and contributing to the development of mechanical properties and to the decrease of the transportation of hazardous ions (Phung et al., 2016; Song et al., 2021).

The structures near to marine environment undergo complicated chemical and physical reactions due to the combined ingression of chloride and carbonation. As previously indicated, the bound chloride phases such as Friedel's salt and adsorbed chloride by C-S-H have no effect on the reinforcement corrosion. However, most of the hydration products such as portlandite and C-S-H dissolve in the alkaline condition, which reduces the bound chloride phases in the hydrated matrix. Because, the portlandite and monosulfate which are essential to form the Friedel's salt, are dissolved by the carbonation, and due to the dissolution of C-S-H, only low amount of chloride would be adsorbed by C-S-H surface (Song et al., 2021). During the transportation of carbon dioxide gas, carbonates in the pore solution react with monosulfate to form carboaluminate phases such as hemi carboaluminate and mono carboaluminate. Incorporating the chloride ions into these carboaluminates phases are more difficult than monosulfate (Song et al., 2021). Thus, the chloride binding capacity in the hydrated matrix is decreased, leading to have more free chloride ions in the solution which triggers rapid corrosion of the reinforcement. It is manifest that the coupled reactive-transport models are necessary to understand the effect of transportation of ions and gas on

microstructure and mechanical properties of hydrated matrix for long-term analysis.

2.5 Existing model for transportation process

A coupled reactive transport model using COMSOL and GEMS packages coupled by Java interface was developed by Azad et al., in 2016 to simulate the ionic transport of porous matrix under the saturated condition. COMSOL was used for ions transportations using the Nernst–Planck equation, and GEMS was used for geochemical calculations supported by thermodynamic database of CEMDATA for cementitious material. The developed model was validated with OpenGeoSys-GEMS model and HYTEC model. Another COMSOL-PHREEQC model was developed via a multi-dimensional and multi species transport model for cement based materials (Guo et al., 2018). The open-source geochemical package called PHREEQC was used herein to calculate the thermodynamic calculations including the phase-equilibrium and surface complexation reactions, and Nernst-Planck Equation in COMSOL was used to predict the ions transportations under the saturated condition of the hydrated matrix based on the defined exposure conditions. The required input parameters such as ion concentrations in the pore solutions, amount of hydration products and porosity of the hydrated matrix were taken from the previous studies. The model was verified with experimental results of chloride ion penetration reported in the previous studies.

Furthermore, to simulate the multi-ionic transport through hydrated matrix, a combined model consisted of phase-equilibrium model, a surface complexation model, and a multi-component diffusion model was developed using PHREEQC (Elakneswaran et al., 2010). The adsorptions of chloride, potassium, and sodium on the surface of C-S-H were considered in this model. The predicted chloride profile was verified with raw experimental results of the

hardened cement paste exposed to sea water and the experiment results reported in previous studies.

Phung et al., (2016) has proposed a one-dimensional reactive transport model combined advection and diffusion to simulate the carbonation under controlled CO2 pressure. The carbonation degree, carbon dioxide uptake, amount of portlandite, porosity and transport properties over time as well as space could be able to predict based on the considered hydration products such as C-S-H and portlandite and calcite as carbonate phases. Very recently, a reactive transport model to concurrent chloride diffusion and carbonation of the concrete was developed by Xie, Dangla and Li, (2021). Here, similar to the assumptions made by Phung et al., (2016), portlandite and C-S-H were considered as hydration products, and calcite was taken as product from the carbonate phases. Moreover, in order to avoid the complications, they assumed that the binding of chloride ion occurs only on the surface of C-S-H. Another numerical model for combined transport of chloride ion and carbon dioxide gas was analytically developed by Shen et al., (2019), wherein the effects of temperature, relative humidity and concentration of carbon dioxide in the air were studied.

2.6 Limitations in the existing models

Based on the presented comprehensive literature review, it is clearly perceived that in most of the previously proposed models, the progression of microstructure could be predicted with certain assumptions and simplifications. In fact, the realistic capturing of cement microstructure is an intricate process, and by definition, the models represent an approximation of the reality. But apparently, more assumptions and simplifications possibly limit the application range and further developments of the models. There are also models,

with certain assumptions and simplifications, reasonably predicting the responses of cement materials. For example, better predictions have been reported to the models which only employed the C-S-H and portlandite as hydration products (Constantinides and Ulm, 2004; Koichi Maekawa, Ishida and Kishi, 2009; Zheng et al., 2010; Wu et al., 2012; Mazaheripour et al., 2018). In some models, detailed microstructure has been predicted by considering the cement paste as three phase material consisted of only the unhydrated clinker, hydration products and porosity (Stefan et al., 2010). Few proposed models have ignored the volume of C-S-H, but alternatively, considered only capillary porosity or gel space ratio to predict the mechanical properties such as compressive strength (Bentz, 1999; Termkhajornkit et al., 2014). For simplifying the computations, several studies have assumed the C-S-H matrix as a single matrix with constant gel porosity ignoring the two types of C-S-H formation (Bentz, 1999; Haecker et al., 2005; Koichi Maekawa, Ishida and Kishi, 2009; Lavergne et al., 2018). Moreover, the complex chemical reaction in the cement paste matrix is not considered in the previous works (van Breugel, 1995a; Koichi Maekawa, Ishida and Kishi, 2009).

Furthermore, while predicting the mechanical properties of mortar and concrete through microstructure, modelling the ITZ realistically into the concrete composite was continuously a challenging process. For instance, during the prediction of Young's modulus of concrete, Li et al. (Li et al., 1999) failed to capture the overlapping between ITZs, which inevitably affected the accuracy of the prediction. It is admitted that the unavailability of experimental data on ITZ is the major hurdle that limits the developments of reliable and insightful simulations of concrete, which consequently leads the researchers to deal with lot of assumptions on properties of ITZ (Duplan et al., 2014; Aouissi et al., 2016; Chen et al., 2016; Das, Maroli and Neithalath, 2016). Particularly, in most of the existing models, the ITZ layer

was assumed to be uniform with constant mechanical properties (Ramesh, Sotelino and Chen, 1996; Hashin and Monteiro, 2002; Aouissi et al., 2016). But, in real case, the clinker content in ITZ reveals a gradient increase with the distance from aggregate surface (Nadeau, 2002). Moreover, by ignoring time-dependent effects, the mechanical properties of ITZ were assumed to be a specific ratio/ function of cement paste properties (Duplan et al., 2014; Das, Maroli and Neithalath, 2016).

For modelling the transport properties, incorporation of hydration process, chemical reaction, transportation process and appropriate coupling among them are essential. However, due the complexity of the coupling process, most of the previously developed models did not consider the hydration reaction simultaneously with transportation process (Phung et al., 2016; Guo et al., 2018; Shen et al., 2019; Xie, Dangla and Li, 2021). Also, in most of them, hydrated matrix was assumed to be fully saturated and gas phase was assumed to be nil in the pore solution (Phung et al., 2016; Guo et al., 2018). Moreover, the models did not consider the detail chemical reaction occurring inside the hardened cement matrix, instead C-S-H and portlandite were assumed as hydration products and calcite was as carbonate phase (Phung et al., 2016; Shen et al., 2019; Xie, Dangla and Li, 2021). Yet in reality, there are several other hydration products including C-S-H, portlandite, ettringite, monosulfate, silicious hydrogarnet, Friedel's salt (from as chloride phase), calcite, carboaluminate phases (mono carboaluminat and hemicarboaluminate), silica gel and alumina gel forming during the reaction of carbon dioxide with hydration products. Their progression influences the pore structure of the matrix and the ion concentration in pore solution.

The outcomes of above studies evidence that the assumptions and simplifications do not necessarily affect the model outcomes as long as the consequences of the approach are

covered appropriately. However, to simulate the properties of cement-based material more realistically, the model should integrate all the constituents of hydration as well as transportation comprehensively. Also, to make the model valid for wide range of applications (i.e., generalization), the possible assumptions must be eliminated. Considering the previous limitations in mind, the present doctoral study has been undertaken to develop a new model to more realistically predict both mechanical and transport properties of cementitious materials.

CHAPTER 3

A TWO-STAGE MODEL FOR THE PREDICTION OF MECHANICAL PROPERTIES OF CEMENT PASTE

3.1 Introduction

The microstructure is one of the most important factors that governs the evolution of mechanical and transport properties of the Ordinary Portland Cement (OPC). When the OPC reacts with water, various hydration products are formed, filling the pore structure and leading to the formation of stiff product. Among the constituents, calcium silicate hydrate (C-S-H) and capillary porosity are two important factors which contributes to the strengthening (S˘milauer and Bittnar, 2006; Jennings et al., 2007; Al-Ostaz et al., 2010; Wang and Subramaniam, 2011; Termkhajornkit et al., 2014; Bahafid et al., 2018; Liu et al., 2019). The C-S-H matrix has a high specific surface area, and that typically forms to around 50 – 60 % of the hydrated cement paste; as the prime bonding agent, it tends to bind the steel reinforcements, aggregates, sand and other hydration products with each other in hydrated cement/ concrete (Papatzani, Paine and Calabria-Holley, 2015). Using scanning electron microscopy and nitrogen absorption methods, several researchers have demonstrated that the formation of C-S-H in the cement matrix occurs namely in two stages with different intrinsic characteristics (Lawrence and Young, 1973; Tennis and Jennings, 2000). At the early stage of the hydration process, the development of C-S-H occurs on the surface of cement particles, and with the time, the cement particles are partially/ fully covered by C-S-H layer. Subsequently, the formation of new C-S-H is induced within the space confined by the

existing C-S-H, as the diffusion process continues to be occurred through the previously formed C-S-H layer. The C-S-H formed under the confinement has higher density (hereafter referred to be HD C-S-H) compared to the C-S-H formed at the early stage as the outer product (hereafter referred to be LD C-S-H). Each of them forms not only with different densities, but also forms with different volume fractions (Tennis and Jennings, 2000; Bernard, Ulm and Lemarchand, 2003). As known, the porosity of the cement matrix decreases with increasing hydration time due to the formation of hydration products. During the hydration, however, the capillary porosity network establishes with different length scales depending on the water to cement ratio (w/c) (Wang and Subramaniam, 2011). The cement matrix becomes more susceptible when the capillary pores are evolved to be connected compared to that progress individually.

The understanding and predicting the microstructure of cement paste are no doubt the most complicated processes. However, with the aid of newly developed computer-based packages/ models, the prediction of microstructure of hydrated cement could be reasonably achievable in the recent decades. CEMHYD3D model (Bentz, 1999), HYMOSTRUC model (van Breugel, 1995b) and DuCOM model (Koichi Maekawa, Ishida and Kishi, 2009) are the well-known models for the prediction of microstructure and intrinsic properties of cementitious materials. The CEMHYD3D model is based on discretization approach, in which the microstructure of the cement matrix has been represented as a grid of discrete cubic elements. The prediction of this model is bounded to the microstructure and compressive strength, and the gel space ratio has been used for the prediction of compressive strength. In the HYMOSTRUC model, vector approach is used for the prediction of microstructure, simulating the cement hydration as growth of spherical particles with overlapping. In this

model, the C-S-H and portlandite (CH) (prime components by weight) have been considered for the determination of microstructure. On the other hand, the microstructure of the hydrates in the DuCOM model is predicted by using the heat generation during the hydration process, hence the mechanical properties are analytically evaluated. The predictions of this model are based on unhydrated core, inner products, C-S-H and free pore spaces. In the recent past, several simplified empirical and analytical models have also been proposed for the predictions of volume of unreacted clinker, hydration products and capillary porosity, hence linked to the mechanical properties of cement paste (Constantinides and Ulm, 2004; Haecker et al., 2005; Stefan et al., 2010; Zheng et al., 2010; Wu et al., 2012; Hlobil, Šmilauer and Chanvillard, 2016; Bahafid et al., 2018; Lavergne et al., 2018; Mazaheripour et al., 2018). Among them, Hlobil, Smilauer and Chanvillard (2016) have proposed an analytical multi-scale model to air-entrained cement by approximating the finite element simulation, in which the volume fractions of hydrates had been occupied from the abovementioned CEMHYD3D model and CemBase. A similar multi-scale model has also been developed by using the vector approach to predict the Young's modulus and Poisson's ratio of oil well cement (API class G) with varying temperatures (Bahafid et al., 2018); as the reaction mechanisms of oil well cement differ from that of OPC, this model could not fit well for the simulations on OPC.

In most of the previously proposed models, the progression of microstructure could be predicted with certain assumptions and simplifications. In fact, the realistic capturing of cement microstructure is an intricate process, and by definition, the models represent an approximation of the reality. But apparently, more assumptions and simplifications possibly limit the application range and further developments of the models. There are also models, with certain assumptions and simplifications, reasonably predicting the responses of cement

materials. For example, better predictions have been reported to the models which only employed the C-S-H and portlandite as hydration products (Constantinides and Ulm, 2004; Koichi Maekawa, Ishida and Kishi, 2009; Zheng et al., 2010; Wu et al., 2012; Mazaheripour et al., 2018). In some models, detailed microstructure has been predicted by considering the cement paste as three phase material consisted of only the unhydrated clinker, hydration products and porosity (Stefan et al., 2010). Few proposed models have ignored the volume of C-S-H, but alternatively, considered only capillary porosity or gel space ratio to predict the mechanical properties such as compressive strength (Bentz, 1999; Termkhajornkit et al., 2014). For simplifying the computations, several studies have assumed the C-S-H matrix as a single matrix with constant gel porosity ignoring the two types of C-S-H formation (Bentz, 1999; Haecker et al., 2005; Koichi Maekawa, Ishida and Kishi, 2009; Lavergne et al., 2018). The outcomes of above studies evidence that the assumptions and simplifications do not necessarily affect the model outcomes as long as the consequences of the approach are covered appropriately. However, to simulate the cement responses more realistically, the model should integrate all the constituents of hydration comprehensively. Also, to make the model valid (generalization) for wide range of applications, the possible assumptions must be eliminated. Therefore, addressing the limitations found in the currently available models, a two-stage model is proposed here to predict the volume fraction and mechanical properties of OPC more appropriately.

The model proposed in this research work consists of two stages, Stage-1: prediction of volume fraction of hydrates and Stage-2: multi-scale model. Thermodynamic model coupled with cement hydration model is used to predict the detailed microstructure of the hydrated cement. For the prediction of volume fraction of the hydrates, two types of C-S-H are

considered into account in a more realistic manner. The multi-scale model is proposed to predict the mechanical properties such as compressive strength, Young's modulus and Poisson's ratio using the hydration results. As C-S-H and capillary porosity are the most dominant components for the development of mechanical properties, C-S-H space ratio is incorporated in the place of gel space ratio. Finally, all the model predictions at each stage are validated using the experimental results available in the literature.

Significance and originality

The study presented herein fills several research gaps found in the previous models as outlined in the previous section. The formation of two types of C-S-H with the distinct properties is originally considered in the model. Unlike most of the previously proposed models (in which the simplified gel space ratio concept has been used, eliminated the vital role of C-S-H), the computation of mechanical properties herein is based on the detailed microstructure of hydrated cement paste. Besides, among the hydration products, the priority is given to the volume fraction of two types of C-S-H and capillary porosity, which could realistically simulate the responses of the cement paste. Moreover, the detailed computation for the prediction of chemical shrinkage is carried out using the reaction rate of clinker mineral from the cement hydration model, and subsequently, the capillary porosity is predicted more accurately by considering the two types of C-S-H, chemical shrinkage and other possible hydration products. In the application point of view, the Stage-1 model can be used to predict the volume fraction of hydration products, hence it can be effectively related to the mechanical and transport properties of cementitious material. The proposed Stage-2 model can potentially be used for the selection of construction material, designs and structural analysis with the time dependent material properties, while reducing the waste of time, cost,

material and manpower compared to that in the conventional approaches.

3.2 Model description

Figure 3.1 presents the entire outline of the two-stage model proposed in this research work (called **HyMeC**). As illustrated, the fundamental characteristics such as clinker compositions, physical properties, boundary conditions and mixture recipe are the required input parameters of this model. The hydrated OPC matrix typically consists of C-S-H, portlandite, ettringite, monosulfate, hydrotalcite, Fe-siliceous hydrogarnet, capillary pores and etc. The volumetric prediction of the hydrates is envisioned in Stage-1 of this model. The basis of Stage-1 includes the relative humidity model, thermodynamic model, cement hydration model and model for the volumetric prediction, and those models are described in the subsequent sections. In Stage-2, the mechanical properties of cement paste have been systematically predicted from the volume fractions of the hydrates computed in Stage-1. The overall modelling approach is comprehensively described below.

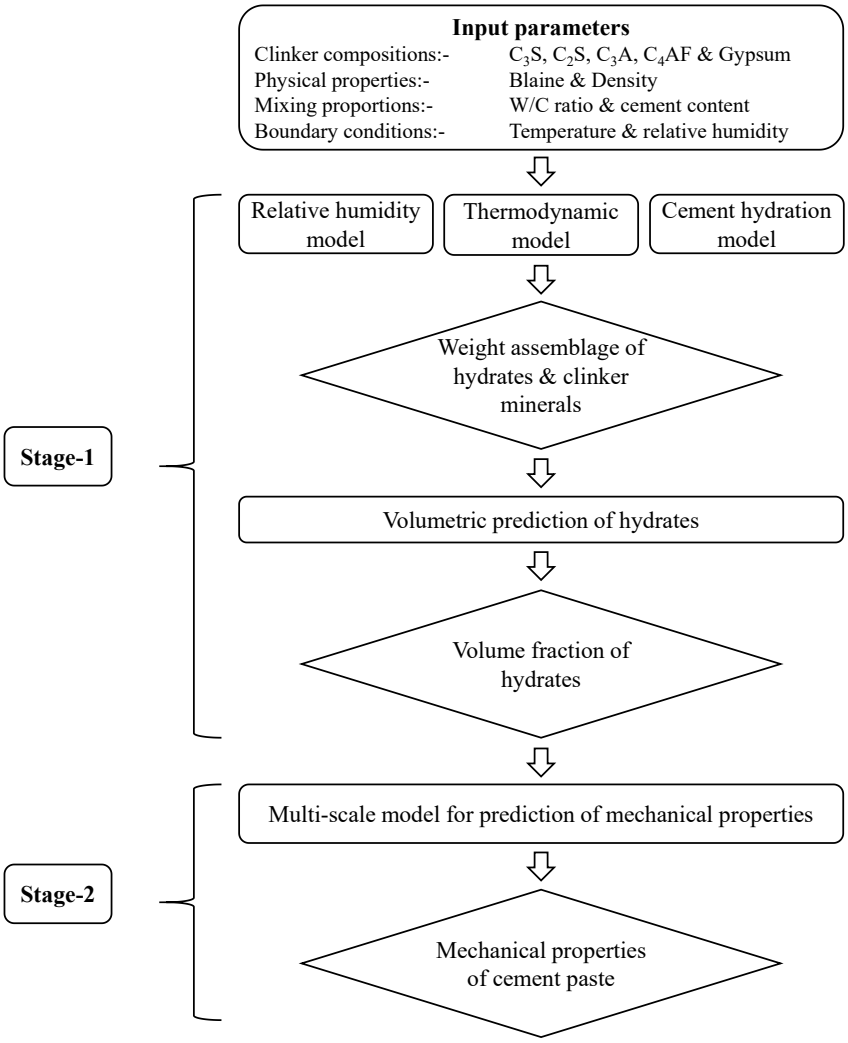

Figure 3.1: Schematic diagram for the proposed model

3.2.1 Relative humidity (RH) model

RH significantly influences the formation of hydration products and mechanical properties, as the rate of hydration reaction decreases with decreasing RH of the cement paste (Jiang, Sun and Wang, 2006; Wyrzykowski and Lura, 2016). Moisture diffusion and self-desiccation are the main reasons for the decreasing of internal RH of hydrated cement paste especially in low w/c paste. Due to the decrease in internal RH (in the pore spaces) of the hydrated cement paste, the reaction of hydration would occur at slower rates and, development of material

properties may be hampered, particularly in cement with low w/c compared to that with fully saturated condition (Chen et al., 2013). Therefore, the proposed two-stage model required to employ the appropriate evolution of RH with hydration process for accurate prediction of hydrates and mechanical properties. As a preliminary step, simple empirical formulas were developed (by regression method, wherein the outcome variable was RH, and the predictor variables were hydration period and w/c ratio) for sealed conditions using experimental results reported in the previous studies, to predict the internal RH of hydrated cement paste with different w/c as presented in Eq. (3.1) and (3.2).

For w/c > 0.4,

$$RH\ (\%) = 100\ \ t^{\left(0.07\ \left(\frac{w}{c}\right)-0.0435\right)} \tag{3.1}$$

For w/c ≤ 0.4,

$$RH\ (\%) = 100\ t^{\left(0.375\left(\frac{w}{c}\right)^2-0.0375\left(\frac{w}{c}\right)-0.0625\right)} \tag{3.2}$$

where, w/c is water cement ratio, and t is hydration period. As the RH rapidly decreases in low w/c paste (w/c ≤ 0.4) under the sealed condition compared to that at high w/c paste (w/c > 0.4), two formulas were derived herein to predict the realistic behavior of internal RH with different w/c ratio.

3.2.2 Thermodynamic model

Several studies have revealed that the thermodynamic model linked with complete set of precise thermodynamic databases, could reliably predict phase assemblages of hydrated cement and chemical compositions (Feng, Miao and Bullard, 2014; Lothenbach et al., 2019).

Herein, the thermodynamic calculations were performed using Geochemical software PHREEQC (an open-source package). This software has also been used previously by several researchers to predict the hydration products of cementitious material (Elakneswaran et al., 2016, 2019; Zhang et al., 2017). The thermodynamically stable solid phases and pore solution composition in the hydrated cement matrix (with hydration time) are predicted from the reaction of clinker mineral using the phase equilibrium module in PHREEQC. The equilibrium calculations in phase-equilibrium module in PHREEQC are based on the solving the law of mass action (LMA) equations (Lothenbach and Zajac, 2019). The Cemdata18 (Lothenbach et al., 2019) along with PHREEQC default thermodynamic database (Parkhurst and Appelo, 1999) were used in this work.

3.2.3 Cement hydration model

The popular cement hydration model developed by Parrot and Killoh (L.J. Parrot and Killoh, 1984) was adopted in this study. As previously demonstrated by several researchers (Lothenbach, Matschei, et al., 2008; Feng, Miao and Bullard, 2014; Lavergne et al., 2018) this model could accurately predict the realistic dissolution rate of individual clinker minerals as a function of hydration time. The prediction of this model is based on set of empirical formulas described in Eq. (3.3) – Eq. (3.9). Initially, nucleation and growth rate (Eq. 3.3), diffusion rate (Eq. 3.4) and hydrates shell formation rate (Eq. 3.5) are calculated as a function of previous hydration rate of the specific clinker minerals. Afterwards, the controlling rate of hydration is selected based on the minimum of nucleation and growth rate (Eq. 3.3), diffusion rate (Eq. 3.4) and hydrates shell formation rate (Eq. 3.5). Finally, hydration degree (α_t^m) for the time t and mineral m is computed from Eq. (3.6) for the time interval Δt by considering the specific surface area, water cement ratio, temperature and relative humidity of the cement

paste.

Nucleation and growth rate ($R_{t,1}^m$)

$$R_{t,1}^m = \frac{K_1}{N_1}(1-\alpha_t^m)(-\ln(1-\alpha_t^m))^{(1-N_1)} \quad (3.3)$$

Diffusion rate ($R_{t,2}^m$)

$$R_{t,2}^m = \frac{K_2(1-\alpha_t^m)^{(\frac{2}{3})}}{1-(1-\alpha_t^m)^{(\frac{1}{3})}} \quad (3.4)$$

Hydrates shell formation ($R_{t,3}^m$)

$$R_{t,3}^m = K_3(1-\alpha_t^m)^{N_3} \quad (3.5)$$

Hydration degree of a clinker mineral (α_t^m)

$$\alpha_t^m = \alpha_{t-1}^m + \Delta t \cdot \min(R_{t,1}^m, R_{t,2}^m, R_{t,3}^m) \cdot \beta_{w/c} \cdot \lambda_{RH} \cdot \frac{A}{A_0} \cdot \exp\left(\frac{E_a^m}{R}\left(\frac{1}{T_0}-\frac{1}{T}\right)\right) \quad (3.6)$$

where,

$$\beta_{w/c} = (1+3.333\cdot\left(H^m\cdot\frac{w}{c}-\alpha_{t-1}\right))^4 \qquad for\ \alpha_{t-1} > H^m\cdot\frac{w}{c} \quad (3.7)$$

$$\beta_{w/c} = 1 \qquad for\ \alpha_{t-1} \le H^m\cdot\frac{w}{c} \quad (3.8)$$

$$\lambda_{RH} = \left(\frac{RH-0.55}{0.45}\right)^4 \quad (3.9)$$

where, w/c is the water cement ratio, α_{t-1} is the total degree of hydration at the previous time step, RH is relative humidity, A is the Blaine surface area of the cement (m^2/kg), A_0 is the reference surface area of cement (385 m^2/kg), E_a^m is the apparent activation energy of

clinker mineral, T0 is the reference temperature (293.15 K), T is the temperature, and K_1, N_1, K_2, K_3, N_3, H are equation constants related to the type of clinker mineral. The values of constants used for the calculations (Eq. 3.3 – 3.9) are tabulated in **Table 3.1** (Lothenbach, Le Saout, et al., 2008; Lothenbach, Matschei, et al., 2008).

Table 3.1: The values of constants for the calculations of hydration degree of clinker minerals

	C_3S	**C_2S**	**C_3A**	**C_4AF**
K_1	1.5	0.5	1	0.37
N_1	0.7	1	0.85	0.7
K_2	0.05	0.006	0.04	0.015
K_3	1.1	0.2	1	0.4
N_3	3.3	5	3.2	3.7
H	1.8	1.35	1.6	1.45
Ea (J/mol)	41,570	20,785	54,040	34,087

Herein, to predict the solid assemblage of hydration products and dissolution of clinker minerals by weight percentage with hydration period, the coupled thermodynamic and cement hydration model (Elakneswaran et al., 2016) was used. As the next step, the model was expanded to predict the volume fraction of hydrates which are the input parameters for the multi-scale model i.e., Stage-2 (**Figure 3.1**).

3.2.4 Prediction of volume fraction of the hydrates

As discussed earlier, the formation of two types of C-S-H (LD C-S-H and HD C-S-H) were considered in this model to predict the volume fraction of hydrates more accurately. The total

weight of C-S-H matrix predicted from the thermodynamic model was further distinguished as LD C-S-H and HD C-S-H using the relationship (Eq. 10) proposed by Tennis and Jennings (Tennis and Jennings, 2000). In their experimental work, surface area of C-S-H was measured by nitrogen adsorption, hence the Eq. 3.10 was developed through multiple linear regression. Here, the proposed relationship directly pronounces the mass ratio of LD C-S-H, as the surface area that had been measured by nitrogen adsorption was only contributed by the LD C-S-H.

$$M_r = 3.017.\frac{w}{c}.\alpha - 1.347.\alpha + 0.538 \quad (3.10)$$

where Mr is ratio of the mass of LD C-S-H to the total mass of C-S-H, w/c is water cement ratio and α is degree of hydration. The average densities of both C-S-H were obtained from the literature (Jennings et al., 2007), 2000 kg/m^3 and 1700 kg/m^3 for HD and LD C-S-H respectively. Basically, the total volume of gel porosity in the cement is reliant to the volume of C-S-H matrix. As the thermodynamic model could not predict the gel porosity, the reliable porosity values for LD C-S-H and HD C-S-H were obtained from the literatures, which are 36% and 26 % respectively (Jennings et al., 2007).

Due to molar volume difference of the hydration products and clinker minerals, there is a reduction in the sum of reaction products compared to reactants during the hydration process, and this difference can be defined as chemical shrinkage. This shrinkage typically causes self-desiccation and autogenous shrinkage, leading to cracking and failure in low water cement paste (Zhutovsky and Kovler, 2009; Chen et al., 2013; Hu et al., 2018). In the previous research works, the chemical shrinkage was either neglected or assumed to be constant percentage of reacted cement for simplifying the computations (Termkhajornkit et al., 2014),

(Bentz, 2006). However, those assumptions made for chemical shrinkage would considerably affect the volume prediction of capillary porosity. Therefore, in this proposed model, the detail calculation for the prediction of chemical shrinkage were carried out. The chemical shrinkage coefficients of each type of clinker minerals are shown in **Table 3.2** (Bentz, Lura and Roberts, 2005).

Table 3.2: Chemical shrinkage coefficients

Cement phase	**Coefficient/ (g water/ g solid cement phase)**
C_3S	0.0704
C_2S	0.0724
C_3A (Convert all C_3A to ettringite)	0.171
C_3A (Convert all C_3A to Monosulfoaluminate)	0.115
C_4AF (Convert all C_4AF to ettringite)	0.117
C_4AF (Convert all C_4AF to Monosulfoaluminate)	0.086

The volume of all the other hydration products was computed by using their molar volumes. Finally, the capillary porosity of the cement matrix was estimated as balance of the system, obtained from the difference between initial volume and final volume of hydration products, chemical shrinkage and unreacted clinker minerals as described in Eq. (3.11).

$$\Phi_{Cap} = V_i - (V_{UC} + V_{HP} + V_{CS}) \quad (3.11)$$

where, Φ_{Cap} is volume of capillary porosity, V_{CS} is chemical shrinkage, V_i is initial volume of cement paste, V_{UC} is volume of unreacted clinker and V_{HP} is volume of hydration products.

3.2.5 Multi-scale model for predicting mechanical properties

In the proposed two-stage model, Stage-2 incorporates the multi-scale model (**Figure 3.1**), systematically correlating the nano structural properties of C-S-H to micro performance of cement paste in three hierarchical levels as conceptually illustrated in **Figure 3.2**. In Level 1, the C-S-H matrix consists of LD C-S-H and HD C-S-H was considered at the characteristic scale of 1 - 100 nm. Capillary porosity was included with C-S-H matrix in Level 2 at the scale of 100 nm - 10 µm, referred as C-S-H foam **(Figure 3.2**). Finally, unreacted clinker minerals and other hydration products were added to the model at Level 3. The characteristic scale of the cement paste (Level 3) ranges 10 - 100 µm. In order to predict the mechanical properties of the cement paste (compressive strength, Young's modulus and Poisson's ratio) from the nano C-S-H matrix, the volume fraction of hydration products, clinker minerals and capillary porosity obtained from the Stage-1 analysis, were used as the input parameters.

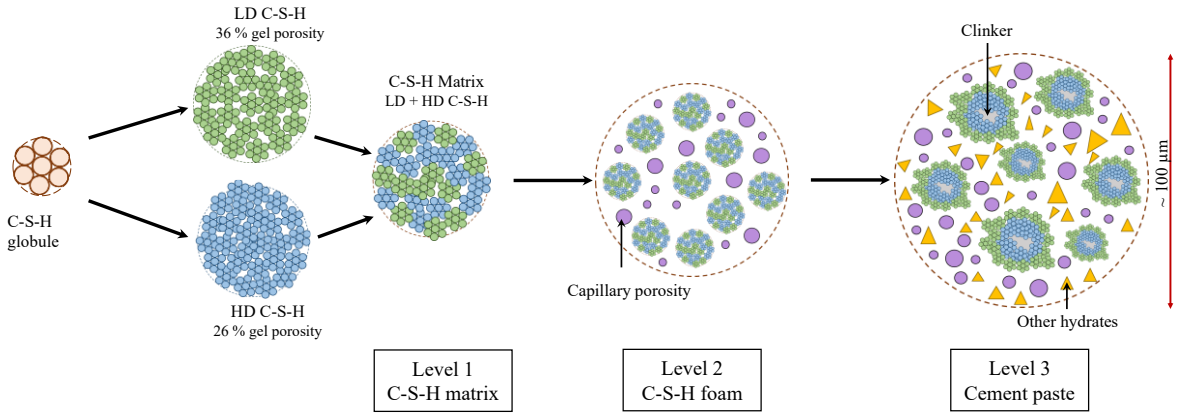

Figure 3.2: Three levels of the multi-scale model: from C-S-H matrix to cement paste

Compressive strength

As per the hierarchical flow, the compressive strength of cement paste was predicted from the

compressive strength of C-S-H matrix, from Level 1 to Level 3 (**Figure 3.2**). The volume fraction of HD C-S-H existing in total C-S-H (Φ_{CSH-HD}) was calculated by using Eq. (3.12). The volume fraction of HD C-S-H ($V_{HD\ CSH}$) and total volume fraction of C-S-H (V_{CSH}) were obtained at the volumetric prediction of hydration products.

$$\Phi_{CSH-HD} = \frac{V_{HD\ CSH}}{V_{CSH}} \tag{3.12}$$

Depending on the volume fraction of HD C-S-H exists in total C-S-H, the actual packing density of C-S-H matrix (η_{CSH}) was interpolated using Eq. (13).

$$\eta_{CSH} = \eta_{CSH-LD} + (\eta_{CSH-HD} - \eta_{CSH-LD})\,\Phi_{CSH-HD} \tag{3.13}$$

where, η_{CSH-LD} and η_{CSH-HD} are the packing densities of LD C-S-H and HD C-S-H respectively, and their values were found to be respectively 0.63 and 0.76 (Constantinides and Ulm, 2007). This packing density of C-S-H matrix can be directly related to the tensile strength of C-S-H matrix ($f_{t,CSH}$) as presented in Eq. (3.14) (Nemecek et al., 2018).

$$f_{t,CSH} = f_{t,glob}\ exp\left(\frac{1.293\left(\eta_{CSH}^{13.011} - 1\right)}{\eta_{CSH}}\right) \tag{3.14}$$

where, $f_{t,glob}$ is the apparent tensile strength of C-S-H globule, and which was found to be 320 MPa (Hlobil, Šmilauer and Chanvillard, 2016). Finally, to predict the compressive strength of C-S-H matrix ($f_{c,CSH}$), the Griffith model (Griffith, 1924) was employed. Generally, the constitutive behaviour of quasi-brittle materials (such as cement paste, mortar and concrete) can be described by the following theories: plasticity, failure mechanics and damage mechanics (Bažant and Planas, 1998; Jirásek and Rolshoven, 2009; Kim and Abu Al-Rub, 2011). As similar theories (fracture material model, isotropic damage law and Rankine

criterion) were used to derive Griffith theory, it is more likely to be applicable to cementitious materials. Assuming that the scale down of cement (i.e. C-S-H matrix and foam) would also disclose the brittle characteristics similar to hardened cement paste, the Griffith strength ratio correspond to the brittle response (σ_c/σ_t of 8, where σc is the compressive strength and σt is tensile strength) was used to relate the tensile strength of C-S-H matrix ($f_{t,CSH}$) and compressive strength of C-S-H matrix ($f_{c,CSH}$). Similar assumptions could also be found in previous works (Hlobil, Šmilauer and Chanvillard, 2016; Šmilauer, Hlobil and Hlaváček, 2017).

In the second level, the compressive strength of C-S-H foam which includes C-S-H matrix and capillary porosity was computed by using the C-S-H space ratio. It should be noted that in the previous studies (Bentz, 1999; Lam, Wong and Poon, 2000; Termkhajornkit et al., 2014), the C-S-H space ratio has not been considered, but instead, the gel space ratio was used to simplify the computations. However, as well known, the C-S-H takes the leading role as the active binding phase in the cement matrix (Hu et al., 2014); therefore, the C-S-H space ratio (γ_{CSH}) proposed by Hlobil, Šmilauer and Chanvillard (Hlobil, Šmilauer and Chanvillard, 2016) was appropriately considered in this level (Eq. 3.15).

$$\gamma_{CSH} = \frac{V_{CSH}}{V_{CSH}+\Phi_{Cap}} \tag{3.15}$$

where, V_{CSH} is the total volume fraction of C-S-H and Φ_{Cap} is the volume fraction of capillary porosity, and these could be obtained from the Stage-1 analysis. As presented in Eq. (3.16), the compressive strength of C-S-H foam ($f_{c,CSH\ foam}$) can be correlated with the C-S-H space ratio (γ_{CSH}) (Hlobil, Šmilauer and Chanvillard, 2016). Here, the $f_{c,CSH}$ is the compressive strength of C-S-H matrix which has been obtained in the previous level (Hlobil,

Šmilauer and Chanvillard, 2016).

$$f_{c,CSH\ foam} = f_{c,CSH}\ exp\ (-\frac{A(1-\gamma_{CSH}^{B})}{\gamma_{CSH}}) \quad (3.16)$$

A and B defined by Eq. (3.17) and Eq. (3.18) respectively, are the parameters as the function of β which is the factor used to define the spatial distribution of C-S-H (gradient) within the cement paste. As known, the amorphous C-S-H gel occupies the largest volume fraction in the microstructure of hardened cement paste, and its spatial distribution is therefore largely responsible for the mechanical properties. Typically, the distribution factor ranges between 0.4 and 1.0, depends on several factors such as heterogeneous nucleation, precipitation of C-S-H and cement fineness (Hlobil, Šmilauer and Chanvillard, 2016).

$$A = 1.101\ exp\ (-\frac{0.296(\beta-1)}{\beta}) \quad (3.17)$$

$$B = -11.058\beta^{1.987} + 16.191\beta \quad (3.18)$$

In the final level (Level 3), the multi-scale model was extended to predict the compressive strength of cement paste (considered representative volume element (RVE) size is 100 μm) which consist of C-S-H matrix, capillary porosity, unreacted clinker minerals and other hydration products. The Eq. (3.19) describes the prediction of the compressive strength of cement paste ($f_{c,cp}$) from the compressive strength of C-S-H foam ($f_{c,CSH\ foam}$), (Hlobil, Šmilauer and Chanvillard, 2016).

$$f_{c,cp} = f_{c,CSH\ foam}(0.758 + (1 - 0.758)\ exp(-29.3\Phi_{inclusion})) \quad (3.19)$$

where, $\Phi_{inclusion}$ is the volume fraction of solids other than the C-S-H matrix, and which was calculated from volume fraction of hydrates obtained in Stage-1. Finally, the compressive

strength results predicted from the proposed model were compared with the experimental results available in the literatures.

Young's modulus

The Young's modulus of the cement paste was also predicted using the multi-scale model (**Figure 3.2**). In Level 1, the Young's modulus of C-S-H matrix (E_{CSH}) was computed with the confluence of two types of C-S-H matrix as a function of volume fraction of HD C-S-H existing in total C-S-H (Φ_{CSH-HD}) (Eq. 3.20). The Young's modulus of LD C-S-H (E_{LD_CSH}) and HD C-S-H (E_{HD_CSH}) were found to be 21.2 GPa and 27 GPa respectively (Constantinides and Ulm, 2004).

$$E_{CSH} = E_{LD\_CSH} + (E_{HD\_CSH} - E_{LD\_CSH})\Phi_{CSH-HD} \quad (3.20)$$

The Young's modulus of C-S-H foam (E_{CSH_foam}) was then calculated from the results obtained in Level 1 using the relationship expressed in Eq. (3.21) (Hlobil, Šmilauer and Chanvillard, 2016).

$$E_{CSH\_foam} = E_{CSH}\, exp(C\, \frac{\gamma_{CSH}^{D} - 1}{\gamma_{CSH}}) \quad (3.21)$$

Here, γ_{CSH} is the C-S-H space ratio, and the parameters C and D can be explained in terms of β (Eq. (22) and Eq. (23) respectively).

$$C = 0.82\, exp\,(-4.949\, \frac{\beta^{0.02} - 1}{\beta^{2.8}}) \quad (3.22)$$

$$D = 1.818\, exp\,(4.310\, \frac{\beta^{0.02} - 1}{\beta^{2.8}}) \quad (3.23)$$

Finally, the predicted modulus of C-S-H foam (Level 2) was used to predict the Young's

modulus of the cement paste (E_{cp}) from Eq. (3.24) (Hlobil, Šmilauer and Chanvillard, 2016).

$$E_{cp} = E_{CSH\_foam}\,(1 + \Phi_{inclusion}\left(0.0102E_{incl} + 0.278E_{CSH_{foam}}^{0.2}\right)) \qquad (3.24)$$

where, E_{incl} is the is the Young's modulus of solids in cement matrix excluding C-S-H. The E_{incl} was calculated as summation of volume fraction multiplies by its Young's modulus ($\sum_i E_i \cdot V_i$) presented in **Table 3.3**.

Table 3.3: The Young's modulus and Poisson's ratio of all the constituents of hydrated cement matrix

Inclusions	Young's modulus (GPa)	Poisson's ratio	Reference
C_3S	135	0.3	(Velez et al., 2001)
C_2S	130	0.3	(Velez et al., 2001)
C_3A	145	0.3	(Velez et al., 2001)
C_4AF	125	0.3	(Velez et al., 2001)
Portlandite	42.3	0.324	(Haecker et al., 2005)
Ettringite	26	0.4	(Zajac et al., 2018)
Monosulfate	30.2	0.3	(Zajac et al., 2018)
Fe-Siliceous hydrogarnet	167	0.3	(Zajac et al., 2018)
Hydrotalcite	30.2	0.3	(Zajac et al., 2018)
Gypsum	45.7	0.33	(Haecker et al., 2005)

Poisson's ratio

In Level 1, the bulk modulus ($K_{LD/HD\ CSH}$) and shear modulus ($G_{LD/HD\ CSH}$) of the LD C-S-H and HD C-S-H were individually computed from Eq. (3.25) and Eq. (3.26) respectively using moduli of the C-S-H crystals (Al-Ostaz et al., 2010). The bulk and shear moduli of C-S-H

crystals are found to be 43 GPa and 26 GPa respectively (Manzano et al., 2007).

$$K_{LD/HD\ CSH} = \frac{4\ G_S\ (1-\Phi)}{3\Phi+4(\frac{G_S}{K_S})} \tag{3.25}$$

$$G_{LD/HD\ CSH} = \frac{G_S\ (1-\Phi)\ (8G_S+9K_S)}{6\Phi(2G_S+K_S)+8G_S+9K_S} \tag{3.26}$$

where, K_S is the bulk modulus and G_S is the shear modulus of the C-S-H crystals, and Φ is the gel porosity. Based on the Eq. (3.27) and Eq. (3.28), the bulk (K_{CSH}) and shear (G_{CSH}) moduli of C-S-H matrix were interpolated using the volume fraction HD C-S-H existing in the total C-S-H (Φ_{CSH-HD}).

$$K_{CSH} = K_{LD\_CSH} + (K_{HD\_CSH} - K_{LD\_CSH})\Phi_{CSH-HD} \tag{3.27}$$

$$G_{CSH} = G_{LD\_CSH} + (G_{HD\_CSH} - G_{LD\_CSH})\Phi_{CSH-HD} \tag{3.28}$$

where, K_{LD_CSH} and K_{HD_CSH} are the bulk moduli of LD and HD C-S-H respectively obtained from Eq. (3.25), and G_{LD_CSH} and G_{HD_CSH} are shear moduli of LD and HD C-S-H from Eq. (3.26).

In Level 2, to predict the Bulk modulus (K_{CSH_foam}) and shear modulus (G_{CSH_foam}) of the C-S-H foam, the Eq. (3.25) and Eq. (3.26) were modified by replacing the bulk (K_{CSH}) and shear (G_{CSH}) moduli of C-S-H matrix and capillary porosity (Φcap) in the place of bulk and shear moduli of C-S-H crystals and gel porosity as expressed in Eq. (3.29) and Eq. (3.30). The bulk and shear moduli of C-S-H matrix were obtained from Eq. (3.27) and Eq. (3.28).

$$K_{CSH\_foam} = \frac{4\ G_{CSH}\ (1-\Phi cap)}{3\Phi cap+4(\frac{G_{CSH}}{K_{CSH}})} \tag{3.29}$$

$$G_{CSH\_foam} = \frac{G_{CSH}\,(1-\Phi cap)\,(8G_{CSH}+9K_{CSH})}{6\Phi cap(2G_{CSH}+K_{CSH})+8G_{CSH}+9K_{CSH}} \quad (3.30)$$

In Level 3, the unreacted clinker minerals and other hydration products were additionally added to the matrix of Level 2. In the Part I of Level 3, the unreacted clinker minerals were inserted to predict the bulk modulus of homogenized martial which includes C-S-H matrix, capillary porosity and unreacted clinker minerals as graphically illustrated in **Figure 3.3**.

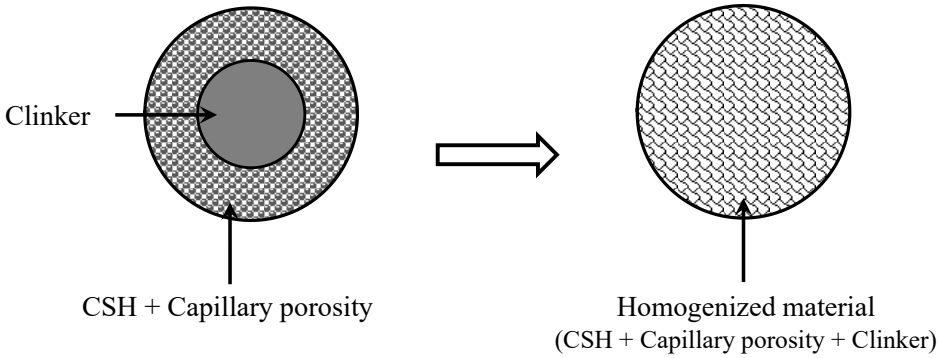

Figure 3.3: Conceptual illustration of homogenizing the material (Part I of Level 3)

The Eq. (3.31) expresses the prediction of bulk modulus of homogenized material (K_e) in terms of bulk and shear modulus of C-S-H foam, bulk modulus of unreacted clinker ($K_{clinker}$) and volume fraction of clinker in the homogenized material (f_c) (Zheng et al., 2010). The bulk modulus of unreacted clinker ($K_{clinker}$) was obtained as summation of volume fraction of clinker multiply by its bulk modulus ($\sum_i K_i \cdot V_i$), and the individual Ki values were calculated using the values of Young's modulus and Poisson's ratio of clinker minerals which are listed in **Table 3.3**.

$$K_e = K_{CSH\,foam} + \frac{(K_{clinker}-K_{CSH\,foam})f_c}{1+\frac{(1-f_c)(K_{Clinker}-K_{CSH\,foam})}{K_{CSH\,foam}+\frac{4}{3}G_{CSH\,foam}}} \quad (3.31)$$

As the next part (Part II) of the prediction of bulk modulus of cement paste, the other hydration products were also added into the previous material (Figure 3.3) as shown in **Figure 3.4.**

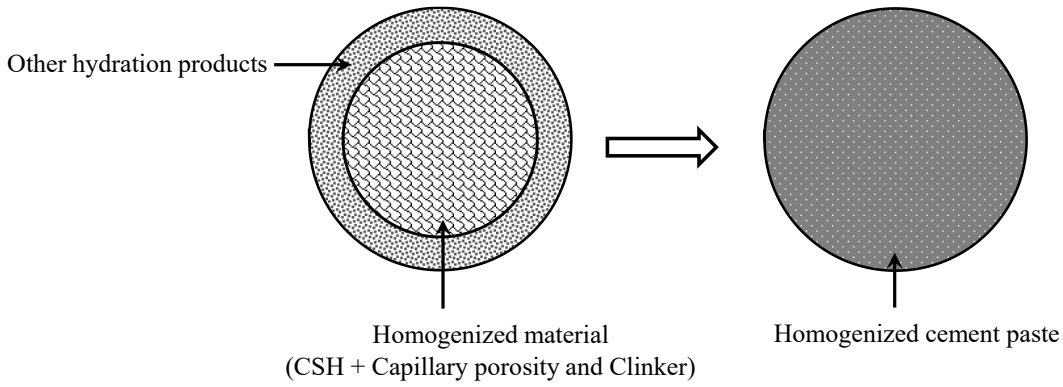

Figure 3.4: Conceptual illustration of homogenized cement paste

To predict the bulk modulus of the cement paste (K_{cp}), the Eq. (3.31) was amended by replacing the bulk (K_m) and shear (G_m) moduli of other hydration products, bulk modulus of homogenized material (K_e) and volume fraction of homogenized material in the cement paste (f_{hm}) in the place of bulk ($K_{CSH\ foam}$) and shear ($G_{CSH\ foam}$) moduli of C-S-H foam, bulk modulus of unreacted clinker ($K_{clinker}$) and volume fraction of clinker in the homogenized material (f_c) as expressed in Eq. (3.32). The bulk (K_m) and shear (G_m) moduli of other hydration products were calculated as summation of volume fraction multiplies by its bulk/ shear modulus ($\sum_i K_i \ or \ G_i \cdot V_i$). The corresponding information of Ki and Gi were computed using Young's modulus and Poisson's ratio data presented in Table 3.3.

$$K_{cp} = K_m + \frac{(K_e - K_m) f_{hm}}{1 + \frac{(1 - f_{hm})(K_e - K_m)}{K_m + \frac{4}{3} G_m}} \tag{3.32}$$

Theoretically, two sets of moduli are required for the computation of Poisson's ratio of a

material; therefore, bulk modulus (Eq. 32) of the cement paste together with Young's modulus (obtained from Eq. (24)) were used herein to predict the Poisson's ratio (ν) from the fundamental relationship presented in Eq. (33). Finally, the predicted results were validated with experimental results available in the previous studies.

$$\nu = \frac{3K_{cp} - E_{cp}}{6K_{cp}} \tag{3.33}$$

3.3 Results and discussion

3.3.1 Verification of RH model

The variations of internal RH of sealed cement paste of w/c 0.2-0.5 predicted from the proposed Eq. (3.1) and (3.2) are illustrated in **Figure 3.5** and compared with experimental results of Jiang et al. (Jiang, Sun and Wang, 2006). It can be seen that the predicted results are quite close to the experimental results. As expected, the maximum reduction of RH was observed in w/c of 0.2, followed by w/c of 0.3. It can also be found that the drop of RH increases with decreasing w/c ratio due to the deficiency of water for the hydration reaction, leading to consume loosely bound water for hydration in low w/c paste. The predicted internal RH of w/c 0.5 dropped to 95 % after 300 days, while for the w/c ratio of 0.2 at the same hydration period was about 73 %. At the same time, the experimental results after 300 days were 93.5% and 78.8% for w/c of 0.5 and 0.2 respectively. The similar tendency also was reported by previous researchers (Chen et al., 2013; Wyrzykowski and Lura, 2016).

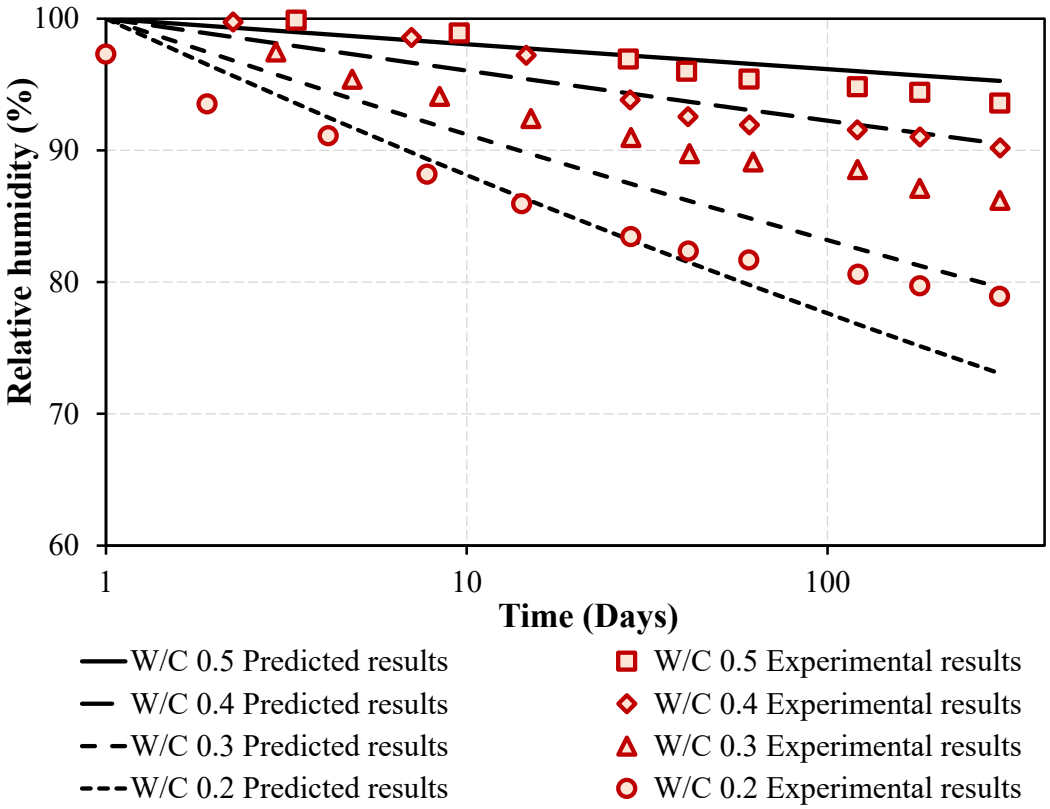

Figure 3.5: Validation of RH with hydration period for w/c ratio of 0.2-0.5.

3.3.2 Prediction of volume fraction of hydrates

Figure 3.6 presents the variation of entire phase assemblage in volume with hydration period predicted in Stage-1 at the given physical and chemical properties (C_3S 62.2 %, C_2S 18.3 %, C_3A 5.6 % and C_4AF 9.8 % Blaine specific surface area 311 m2/kg and density 3.16 g/cm^3) for w/c ratio of 0.4 and the temperature at 20 °C as the reference. It can be seen that the proportion of clinker content and capillary porosity were high in the cement paste initially. With the increasing hydration period, the volume of clinker minerals decrease as hydration reaction takes place, followed by the increase in the volume of hydration products. The hydration products such as C-S-H, portlandite, ettringite, monosulfate, hydrotalcite and Fe-

siliceous hydrogarnet are comprehensively predicted from the Stage-1 model as a function of hydration period. Among the hydration products, the C-S-H (solid C-S-H and gel) and portlandite are found to be existing in high quantity, and considerable amount of ettringite and siliceous hydrogarnet are also confirmed. This prediction is in a very good agreement with the fractions reported in many previous works (Tennis and Jennings, 2000; Elakneswaran et al., 2016; Zajac et al., 2018), demonstrating the accurate predictability of the model (Stage-1) proposed herein.

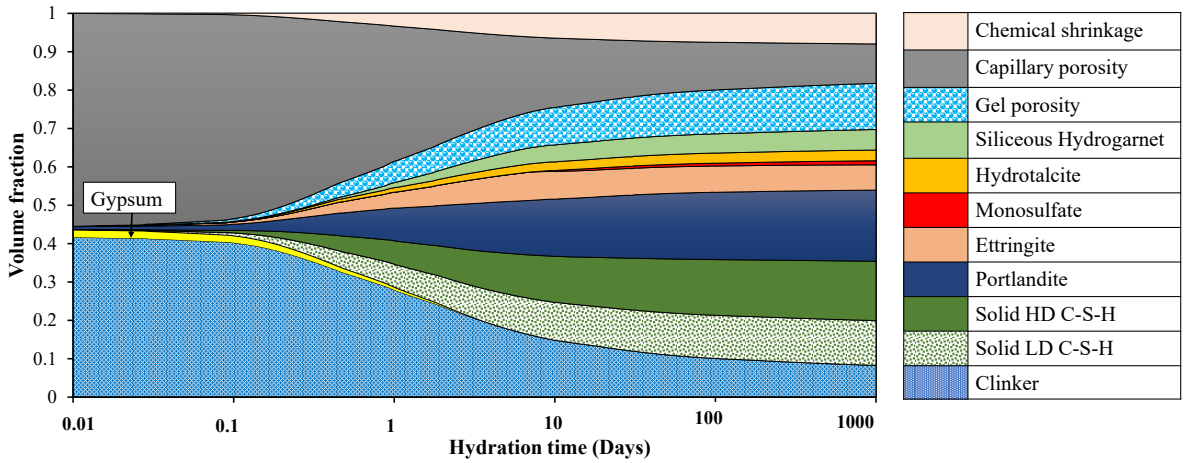

Figure 3.6: Mineral assemblage of hydrated OPC with hydration period for w/c of 0.4.

Verification of chemical shrinkage

Figure 3.7 presents the predictability of the chemical shrinkage obtained from the proposed model (Stage-1). It can be seen that the predicted results show fairly a good agreement with the experimental results obtained from the previous study (Igarashi and Maruyama, 2011) for w/c ratio 0.4 and 0.55. As predicted, the amount of chemical shrinkage increases with hydration period with a decreasing rate, and this tendency is similar to that observed by several other researchers (Deschner et al., 2012; Le Saoût et al., 2013). By the end of 320

days, the experimental and predicted chemical shrinkages (w/c of 0.4) are 0.0724 and 0.0777 respectively, and for the w/c of 0.55, the shrinkages are respectively 0.0646 and 0.0729, suggesting the accurate predictability of the model. It can also be seen, during the entire hydration process, higher chemical shrinkage is obtained for lower w/c ratio. As explained in the previous section, this is due to the molar volume effects i.e., higher the content of cement volume causes higher the hydration reactions, leading to high volume reduction in cement paste.

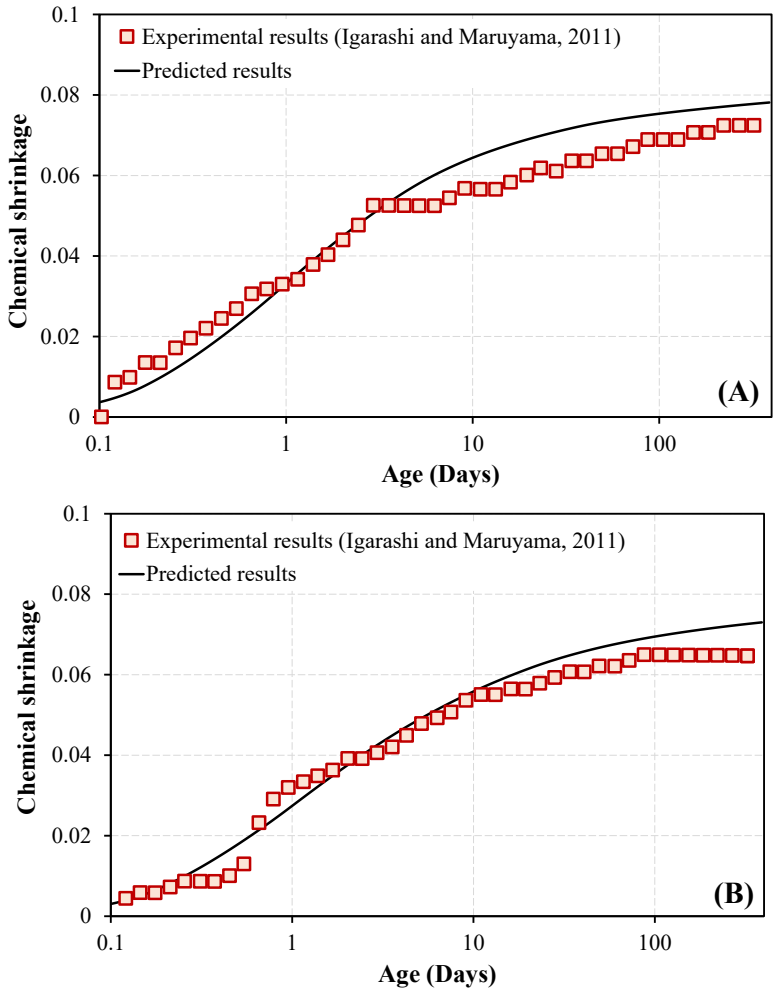

Figure 3.7: Validation of chemical shrinkage with hydration period for W/C ratio of (A) 0.4 and (B) 0.55.

Verification of capillary porosity

The capillary porosity verses the hydration period is presented in **Figure 3.8**, comparing the results obtained from the proposed model with the experimental results reported by Igarashi and Maruyama (Igarashi and Maruyama, 2011) for the w/c of 0.4 and 0.55. The space employed by the water in the cement matrix is known to be the capillary pores (Sant, Bentz and Weiss, 2011), and the predicted results excellently capture the typical non-linear decrease with the increase in the hydration period. The initial porosity is apparently high, and when hydration is in progress, the formation of hydration products continues to fill the existing voids system, leading to a denser microstructure with decreasing porosity. In other words, the decrease in porosity is equal to the increase in the solid fraction within the cement paste. Several other researchers have also reported the similar tendency for both short and long periods (Sant, Bentz and Weiss, 2011; Wang and Subramaniam, 2011; Singh et al., 2015). The predicted capillary porosity of fresh mix is approximately 53 % and 62 % for w/c ratio 0.4 and 0.55 respectively, and the experimental results shows 56 % and 64 %. Only 5 % and 3 % variations are observed between predicted and experimental results at the initial stage. After the 320 days of hydration, experimental results for the w/c of 0.4 and 0.55 are 19.1 % and 28.4 % respectively, which are almost same as the predicted results (19.2 % and 28.5 %).

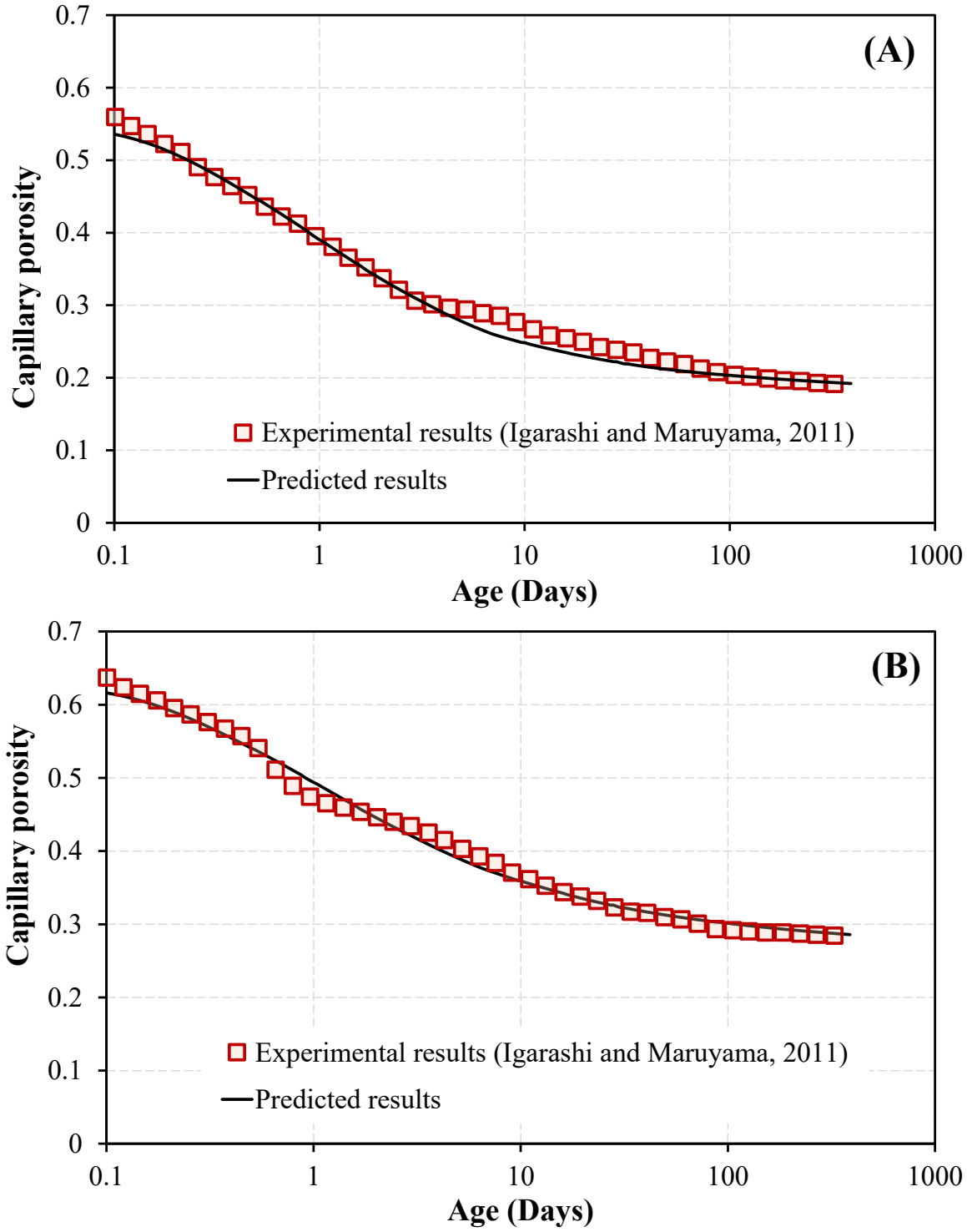

Figure 3.8: Variation of capillary porosity with hydration period for w/c of (A) 0.4 and (B) 0.55.

3.3.3 Prediction and verification of compressive strength

The **Figure 3.9** and **Figure 3.10** illustrate the predictability of the proposed model for the compressive strength with two independent sets of experimental results with hydration period obtained from previous studies. The predicted results for w/c ratios of 0.3, 0.4, 0.5 and 0.6 are compared with experiment results (the experiments were in accordance with that reported by Yoda et al. (Yoda et al., 2018) (**Figure 3.9**), and **Figure 3.10** shows the comparison between predicted and experimental results for w/c 0.4 and 0.55 taken from the study of Maruyama and Igarashi (Maruyama and Igarashi, 2014). The compressive strength of the hardened cement paste is size dependant; therefore, the considered RVE size of the cement paste in model needs to reasonably match with size of the experiment specimens. As per the previous reports, the RVE size of 100 μm or above could reliably capture the strength responses of the cement specimens of 100~200 mm in height or length (Rupasinghe et al., 2017; Königsberger et al., 2018). In this study, the considered RVE of hardened cement paste corresponds to 100 μm, and the size of the experiment specimens used herein to validate is 100 mm in height and 50 mm in diameter, suggesting compatibility for reliable predictions. As the loading faces of the specimens were polished well prior to the compression tests in both experimental works (Maruyama and Igarashi, 2014; Yoda *et al.*, 2018), the experimental boundary conditions can be considered to be in consistent with the model.

The proposed model shows excellent prediction for different w/c ratio ranging from 0.3-0.6 with varying hydration time. It is also observed that the cement paste with low w/c ratio gains higher compressive strength compared to that of high w/c ratio, which is in a very good agreement with the results reported by several researchers (Takahashi et al., 1997; Maruyama and Igarashi, 2014; Yoda et al., 2018). This could be predominantly attributed to high

production of C-S-H (prime binding agent) occurred in cement paste with low w/c ratio (consisting high cement volume) during hydration. Moreover, the porosity decreases with decreasing w/c ratio, leading the paste to a denser microstructure. As presented in Eq. (3.15), the C-S-H space ratio therefore increase with decreasing w/c ratio, which eventually results the higher compressive strength in low w/c paste as observed in **Figure 3.9** and **Figure 3.10**. It can also be seen that the model slightly underpredicts the early strength of the cement paste compared to the experimental results reported by Maruyama and Igarashi (Maruyama and Igarashi, 2014) (**Figure 3.10**). However, in **Figure 3.9**, the proposed model accurately predicts the early strength for w/c ratios of 0.4-0.6. After 07 days of hydration period, the compressive strength model shows a very good agreement with both independent sets of experimental data (**Figure 3.9** and **Figure 3.10**).

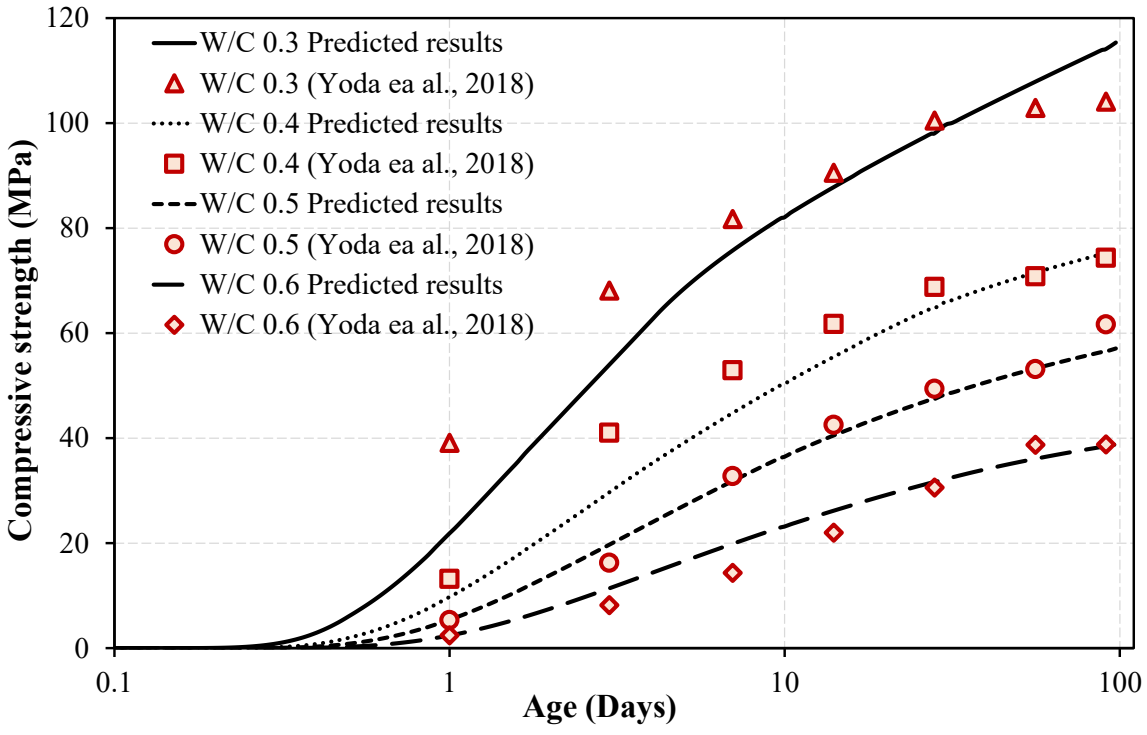

Figure 3.9: Development of the compressive strength for w/c 0.3 – 0.6.

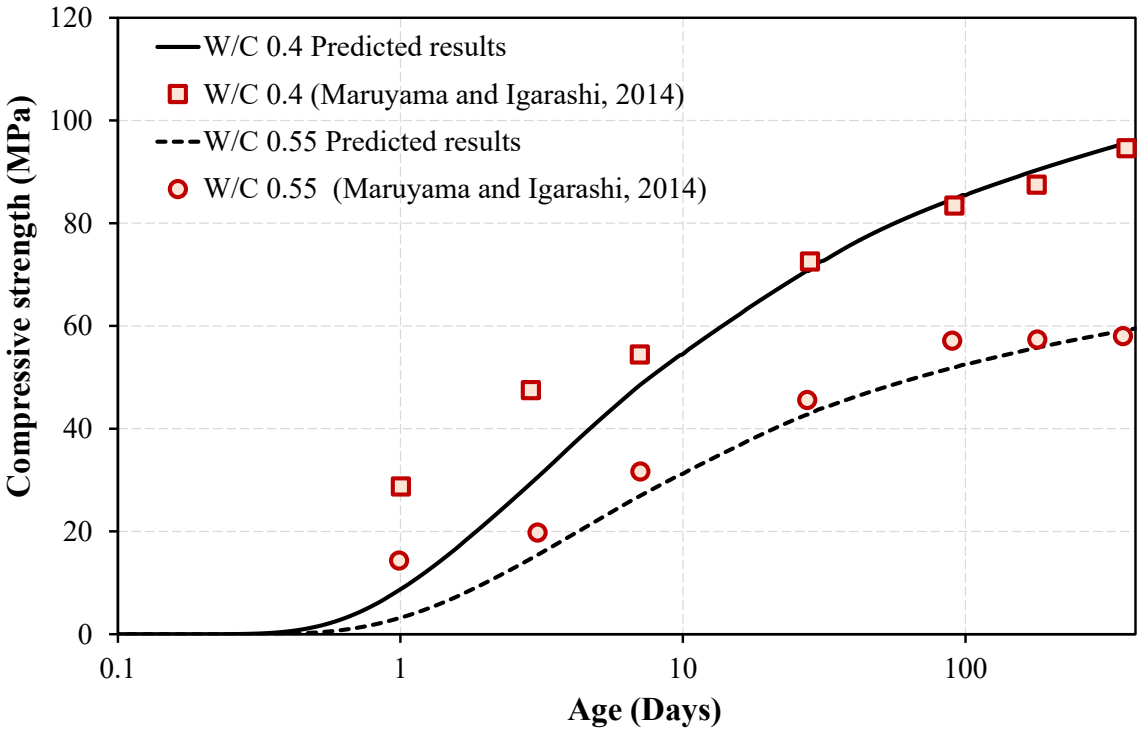

Figure 3.10: Development of the compressive strength for w/c 0.4 and 0.55.

The 0.7 of β value described in Eq. (3.17) and (3.18) showed the best fit to w/c of 0.3; similarly, the value of 0.8 to w/c 0.4 and the value of 1.0 to w/c of 0.5, 0.55 and 0.6. It is worth to note that the prediction suggests an increasing tendency of β with the increase in w/c ratio up to 0.5, and then it remains relatively to be a constant. This could possibly be due to the reason that high w/c paste (w/c > 0.4) contains enough water for the hydration reaction, which leads the C-S-H precipitation evenly distributed compared to that in low w/c paste. The previous study has suggested that the β values fall within the range of 0.4 - 1.0 (Hlobil, Šmilauer and Chanvillard, 2016), and that fairly agrees with the values attained in this study. However, the tendency of β has not been fully assessed yet covering all the w/c ratios in practice, hence a comprehensive study on β is recommended for future work.

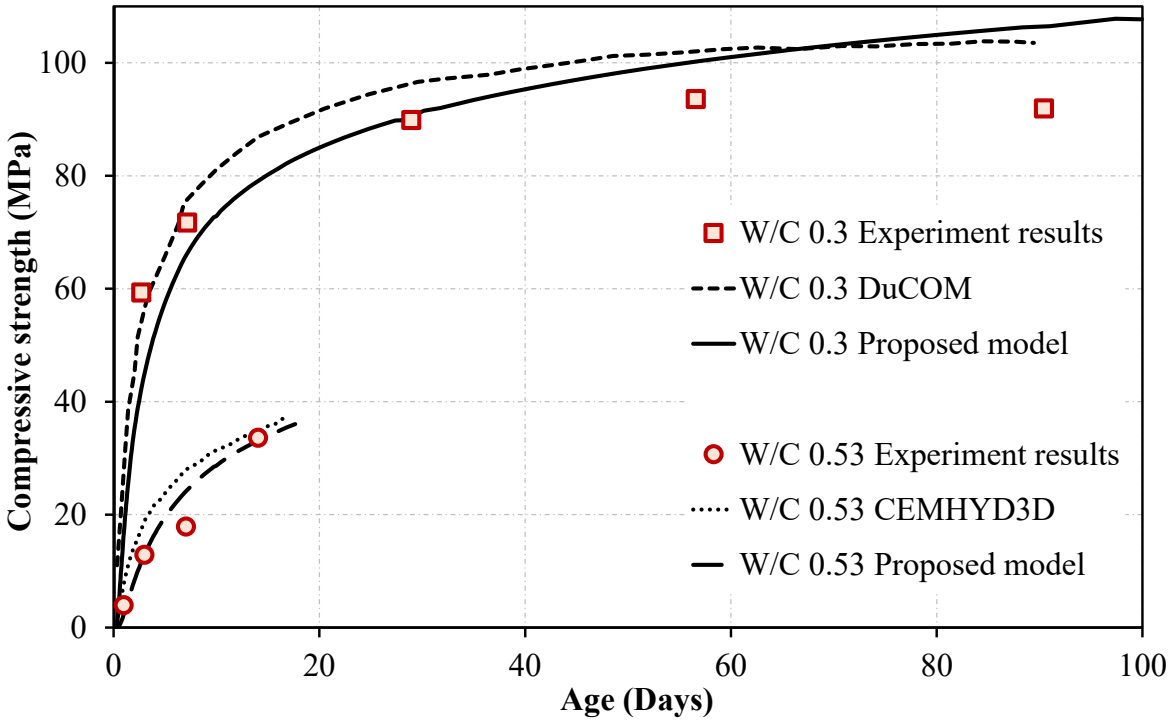

Figure 3.11: Comparison of compressive strengths predicted in the proposed model and existing models

As indicated earlier, CEMHYD3D and DuCOM models are some of the most frequently used models to predict the microstructure and mechanical properties of cementitious materials. Therefore, the predictability of the proposed model is compared with the predictions involving CEMHYD3D and DuCOM models, using the data available in the literature (Koichi Maekawa, Ishida and Kishi, 2009; Z. Liu et al., 2014) (**Figure 3.11**). In fact, the above models were developed based on different concepts. Hydration mechanism of DuCOM model was developed based on heat generation during the hydration process, hence the mechanical properties are analytically evaluated (Koichi Maekawa, Ishida and Kishi, 2009). In CEMHYD3D, on the other hand, the digital image of 3D microstructure was used to model the microstructure (Bentz, 1999); it should be mentioned that the prediction results adopted

herein for comparison had been encompassed the gel space ratio concept for evaluating the compressive strength [(Z. Liu et al., 2014). The comparison, as seen in **Figure 3.11**, shows a very good agreement between existing models (CEMHYD3D and DuCOM) and the proposed scheme which involves coupled thermodynamic and cement hydration models for computing the microstructure.

The effect of proposed RH model on predicting the compressive strength of cement paste (using the input parameters reported in Yoda et al (Yoda et al., 2018)) for w/c 0.3-0.6 is demonstrated in **Figure 3.12**. The predicted compressive strength for sealed condition (the variation of RH was predicted using Eq. (3.1) and Eq. (3.2)) and fully saturated condition (RH equals to 1) are compared. The high deviation is observed between saturated and sealed condition for w/c 0.3 (approximately 26 % higher in saturated condition after 100 days), followed by 0.4 (nearly 6 % difference after 100 days). Previously, Chen et al. (Chen et al., 2013) also have reported a similar tendency for heat of hydration at saturated and sealed conditions for the cement paste of w/c 0.3 (about 19 % difference after 7 days) and 0.4 (difference of 3 % for the same age). Furthermore, it can be clearly seen that the variation between the results predicted from saturated and sealed conditions decreases with increasing w/c ratio, and the effect of RH can be neglected for w/c higher than 0.4. This observation confirmed that access to the external water permits higher degree of hydration in the low w/c paste (w/c 0.3 and 0.4). On the other hand, the effect of external water is negligible for the high w/c paste (w/c 0.5 and 0.6), as they contain enough water for the hydration reactions. As demonstrated, the overall realistic behaviours are clearly reflected by the proposed model.

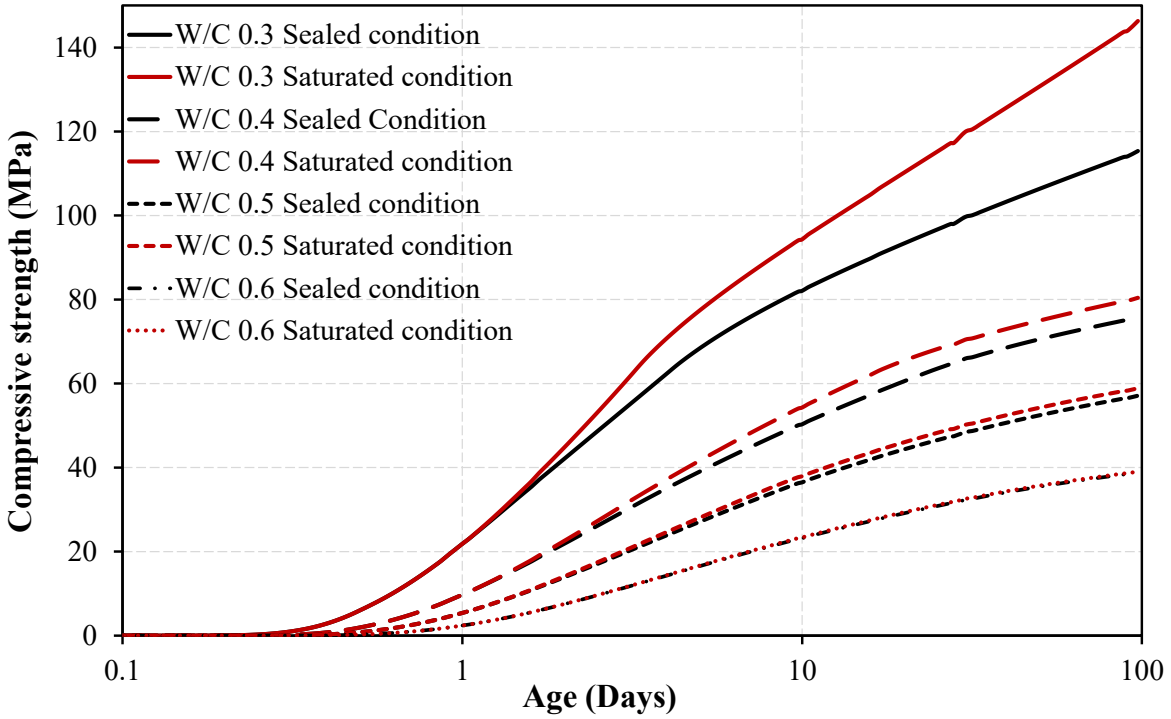

Figure 3.12: Comparison of predicted compressive strength under sealed and saturated condition.

3.3.4 Prediction and verification of Young's modulus

The predicted and experimental results of the Young's modulus of cement paste for w/c ratios of 0.4 and 0.55 are shown in **Figure 3.13**. According to **Figure 3.13**, the proposed model exhibits good agreement with experimental results obtained from the previous study (Maruyama and Igarashi, 2014). The Young's modulus values used herein for validations were determined from two different experimentations: ultrasonic tests and compression loading tests. The experimental size of the hardened cement paste used for ultrasonic test was 40 × 40 × 160 mm, and the specimens of φ50 × 100 mm was used for loading tests. As discussed in the previous section, for a reliable validation of the model, size compatibility between model RVE size and experimental size of hardened cement paste needs to be

carefully considered. For instance, Smilauer and Bittnar (2006) evaluated the effect of RVE size in predicting the Young's modulus, demonstrated that 50 μm might be the reasonable minimum size, above which the model reliably captures the evolution of Young's modulus during whole hydration period, regardless of the experimental size. Followed by, few studies have revealed that incorporating higher RVE sizes (pretty much above 50 μm) in model insignificantly impacts on size compatibility, hence preserving the predictability of Young's modulus. Therefore, the experimental data sets adopted herein for validation appears to be compatible with the RVE size of the model.

It can be observed that the development of Young's modulus reveals the similar tendency as explained for the development of compressive strength (**Figure 3.9** and **Figure 3.10**). Regardless of w/c ratios, the values tend to increase exponentially at first, and afterwards increase with a decreasing rate towards a stable state. Also, higher values of Young's modulus are predicted for the low w/c paste i.e., w/c ratio of 0.4 compared to that of 0.55. In addition to reported by Maruyama and Igarashi (Maruyama and Igarashi, 2014), similar trends in Young's modulus were also observed by previous researchers (Stefan et al., 2010; Wang and Subramaniam, 2011; Mazaheripour et al., 2018). Similar β values which have been demonstrated as used for the prediction of compressive strength in previous section, were used herein (Eq. 3.22 and 3.23), and they could predict the Young's modulus also more accurately.

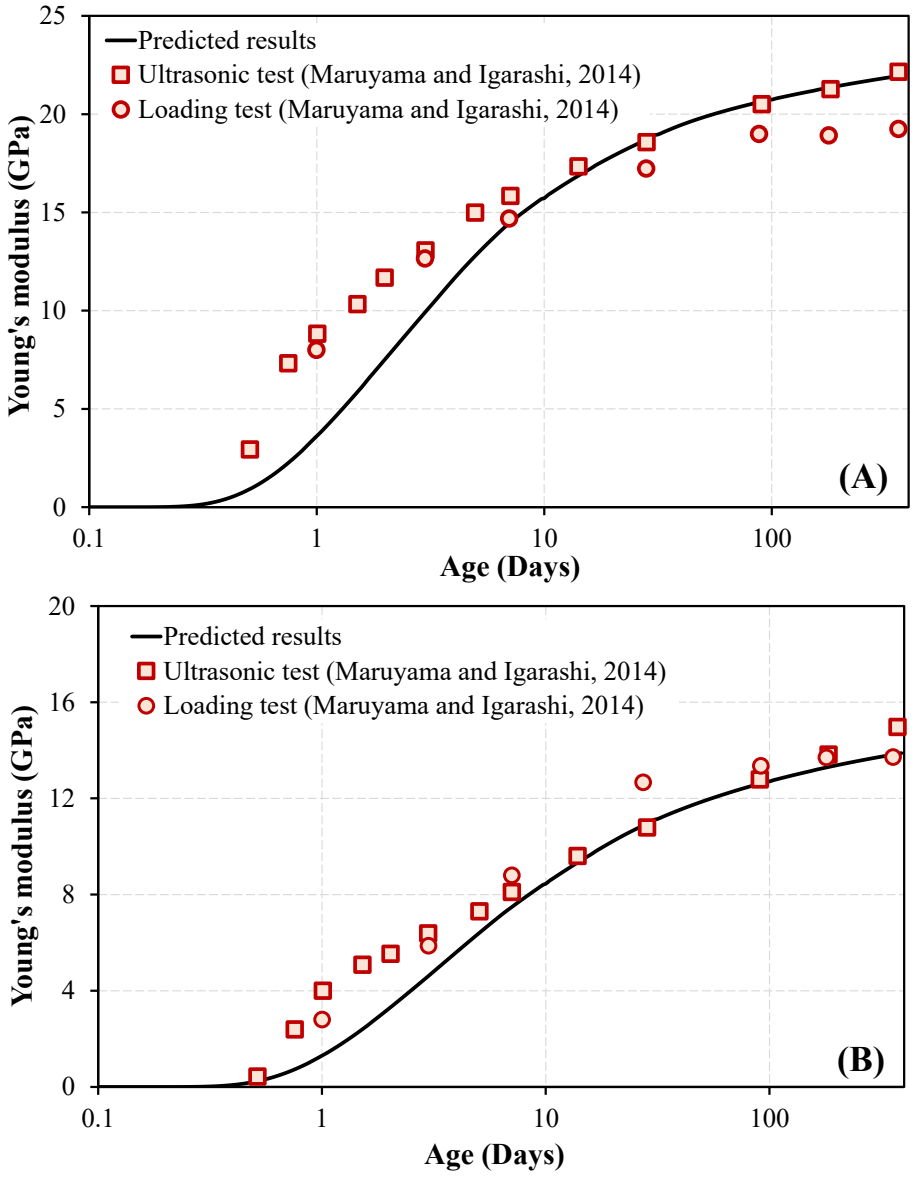

Figure 3.13: Comparison of Young's modulus of cement paste for w/c (A) 0.4 and (B) 0.55

3.3.5 Prediction and verification of Poisson's ratio

Figure 3.14 presents the evolution of the Poisson's ratio of cement paste obtained from the proposed two-stage model for the w/c ratios of 0.4 and 0.55, comparing the experimental results of Maruyama and Igarashi (Maruyama and Igarashi, 2014). The predicted results show slightly an over estimation of Poisson's ratio during the early age of hydration process. The

model proposed herein for the Poisson's ratio relies on two important assumptions such as (i) the cement matrix is sphere, and (ii) the total volume of capillary porosity has been considered to be with C-S-H matrix (with neither other hydration products nor unreacted clinker). And, these assumptions could possibly be the reason for the overprediction of Poisson's ratio at the early stage. However, after around 10 days of hydration period, the results obtained from the model agree well with the experimental results. For example, after 180 days, the experimental and predicted results of Poisson's ratio for w/c of 0.4 are 0.27 and 0.25 respectively, and 0.26 and 0.30 are obtained for w/c of 0.55. As cement particles exist in suspension form in the water during the early stage, the Poisson's ratio of fresh mix is equal to Poisson's ratio of water (0.5) (Stefan et al., 2010b; Maruyama and Igarashi, 2014), and that has been excellently captured in the proposed model. When the hydration is in progress, the Poisson's ratio of paste decreases due to the formation of denser microstructure by replacing the solids in the place of water. It can also be seen that the Poisson's ratio increases with increase in w/c ratio, as reported by Stefan et al. (Stefan et al., 2010), and the observed propensity is quite similar to that observed for capillary porosity (**Figure 3.8**).

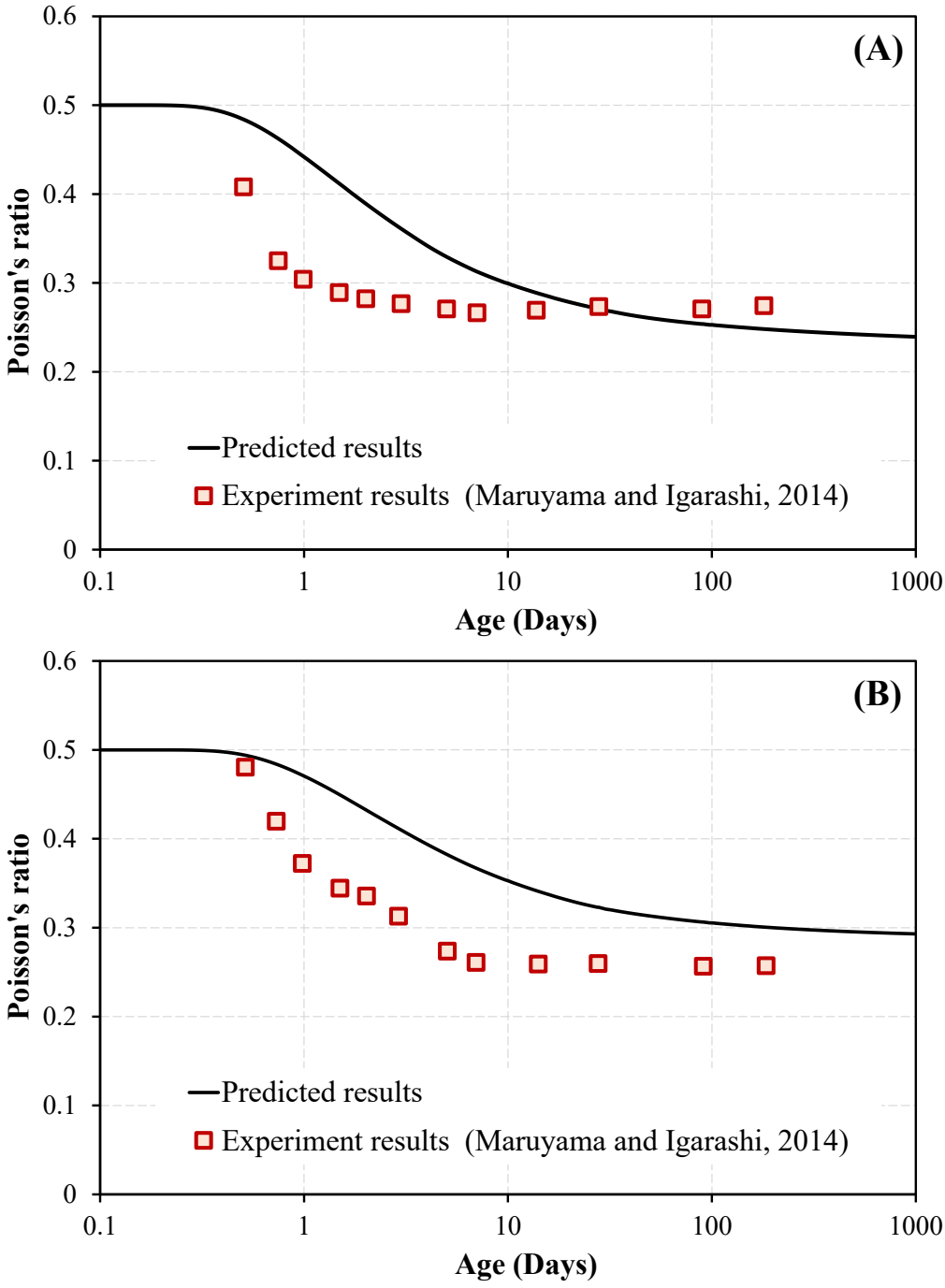

Figure 3.14: Evolution of Poisson's ratio of cement paste for w/c (A) 0.4 and (B) 0.55.

3.4 Conclusions

In this research work, a two-stage model has been proposed to predict the mechanical

properties of OPC paste such as compressive strength, Young's modulus and Poisson's ratio from the development of microstructure during the hydration process. In Stage-1, the volume fraction of hydrates has been predicted by integrating (i) relative humidity model (ii) thermodynamic model, (iii) cement hydration model and (iv) model for volumetric prediction. The multi-scale model (3 levels from C-S-H matrix to cement paste) has been developed in Stage-2 for predicting the above mechanical properties using the volume hydrates obtained from Stage-1. From the analysis of the successfully developed model, the following conclusions are drawn.

The behaviors of the relative humidity during the hydration process have been realistically reflected through the proposed relationships as a function of w/c ratio and hydration period, and the predicted results exhibit a fairly good agreement with experimental results for w/c of 0.2-0.5. The microstructure and porosity of the hydrated cement paste, in terms of volume fraction, have been predicted using the integrated Stage-1 model, which comprehensively expresses the variation of phase assemblage with hydration process for long periods. The predicted chemical shrinkage and capillary porosity shows a very good agreement with reported experimental results of w/c 0.4 and 0.55 in Stage-1 analysis. The proposed multi-scale model (Stage-2) demonstrates accurate predictability of the mechanical properties of cement paste. The predicted compressive strength excellently captures the realistic values for the w/c ratios ranging from 0.3 – 0.6, and similarly, the Young's modulus is predicted. The computation of Poisson's ratio also shows relatively good agreement with the available experimental data of two w/c (0.4 and 0.55). However, the model slightly overpredicts the Poisson's ratio at early stage (before 10 days); thus, further validations are required with more independent experimental results to generalize the Poisson's ratio model.

CHAPTER 4

PROPOSING A THREE-PHASE MODEL FOR PREDICTING THE MECHANICAL PROPERTIES OF MORTAR AND CONCRETE

4.1 Introduction

Mortar and concrete are the most widely used building materials in the global construction industry. Owing to the diverse components such as cement hydrates, aggregates, and cement-aggregate interfacial zones, they highly reveal a complicated microstructure. Number of previous studies disclosed that their behaviours on the application of loads are determined by intrinsic properties, which, at the micro-scale, are influenced by the water/cement ratio (w/c), clinker compositions and degree of hydration of cement, while aggregate properties play a significant role at the macroscale (Nadeau, 2003; Königsberger et al., 2018). The properties of bulk paste existing in the matrix of mortar and concrete are time dependent. As the crystalline and semi-crystalline hydrates continue to evolve with hydration period, the materials become more complicated to understand (Elakneswaran et al., 2016; Noguchi et al., 2021). Therefore, optical determination of the mechanical properties of mortar and concrete from their microstructure is of a great interest in industrial applications these days.

The occurrence of cement-aggregate interface (also referred to as interfacial transition zone, ITZ) is related to the wall-effect originated by the aggregate surface that disturbs the normal packing of cement particles (Hashin and Monteiro, 2002; Nadeau, 2002; Gao et al., 2018).

During casting, the spatial arrangement of anhydrous grains becomes looser in the vicinity of aggregate particles. In addition, micro-bleeding of fresh mix leads to the accumulation of water near the surface of aggregate particles during the vibration of mixture and before setting. As the result, clinker content exhibits an increasing distribution with the distance from the aggregate surface, and a higher local w/c is attained in the ITZ of fresh mortar and concrete (Hashin and Monteiro, 2002). In fact, the ITZ is not a definite zone, but a region of transition, and a thickness ranging between 10–40 μm is documented for typical mortars and concrete (Hashin and Monteiro, 2002; Nadeau, 2002; Bernard and Kamali-Bernard, 2015; Zhu et al., 2017). Because of its high porosity compared to bulk paste matrix, ITZ is typically considered to reveal adverse effects on the performance of mortars and concretes, particularly on transport and mechanical properties to a great extent (Hashin and Monteiro, 2002; Nadeau, 2002; Bernard and Kamali-Bernard, 2015; Zhu et al., 2017).

The thickness of the ITZ is found to be influenced by various casting factors such as curing age, w/c ratio, aggregates properties (type, roughness, shape and size), aggregate content and supplementary cementitious materials (Nadeau, 2002; Elsharief, Cohen and Olek, 2003; Gao et al., 2014; Zhu, Provis and Chen, 2018; Huang et al., 2019). Recently, Huang et al. (2019) investigated the ITZ properties of both normal aggregates and light weight aggregates. Their outcomes indicated that the ITZ between light weight aggregate and cement paste is stronger and bonded without visible cracks compared to normal weight aggregates. High surface roughness of the lightweight aggregate can be the reason, which allows to have an effective mechanical interlocking, bringing advantages related to the strength of the aggregate-cement system. It should also be noted that w/c ratio at the interface would be low due to high water absorption of the lightweight aggregates, which leads to increased interfacial bonding

strength in ITZ. Due to the tightened environmental policy on limiting aggregate exploitation and ever-increasing price, finding substitutes for natural aggregate has drawn a great deal of attention (Toghroli, Sajedi and Ibrahim, 2018; Ferraro et al., 2020; Jiang, Ling and Shi, 2020). Involving artificial aggregates can be one potential alternative; following are some of such widely used materials: coal fly ash, paper ash, cement kiln dust, municipal solid waste incineration fly ash and bottom ash (Gesoğlu, Özturan and Güneyisi, 2006; Gunning, Hills and Carey, 2009; Colangelo, Messina and Cioffi, 2015). Jiang et al. (Jiang, Ling and Shi, 2020) studied the performance of artificial aggregates on strength, ITZ and drying shrinkage, concluded that the artificial aggregates using waste concrete powder exhibits an enhancement on ITZ thickness, i.e., lower ITZ thickness (30 μm) was obtained for artificial aggregates compared to that of natural aggregate (60 μm) while improving mechanical properties of ITZ. This was attributed to the further reaction in aggregates located at the outer layer made by waste concrete powder with cement matrix, thus resulting in low porosity.

The concrete is characterized as a multi-phase material with several different representative scales. At macroscopic scale, concrete is regarded as a homogeneous material, while at mesoscopic scale, it is pondered to be consisting of coarse aggregates and mortar matrix (Bernard and Kamali-Bernard, 2015). Further subdivisions of the mortar matrix produce fine aggregates and hardened cement paste with pores embedded inside. It is well known that it is unsuitable to model the concrete at a single scale, as its intrinsic features range from nanometer-sized pores to millimeter-sized aggregates. Therefore, a multi-scale model can be more appropriate to link different length features of concrete, hence to evaluate macro-mechanical properties from micro-composition and micro-mechanical properties (Chen et al., 2016; Haile et al., 2019). During the analysis, the properties computed at one scale,

micrometers for instance, are inputted to the subsequent scale of the model, such as millimeters. For evaluating the effective properties of multi-inclusion composites (such as mortar and concrete), homogenization stepping scheme was repeatedly shown to be an effective pathway (Gal and Kryvoruk, 2011; Chen et al., 2016; Brown, Allison and Sanchez, 2018; Haile et al., 2019; Li and Li, 2019). In this homogenization method, the properties are assessed by averaging the stress and strain fields of material representative volume element (RVE) featuring a ‘‘mesoscopic” length scale which is much larger than the characteristic length scale of particles (inhomogeneities), but smaller than the characteristic length scale of a macroscopic specimen (Chen et al., 2016).

As yet, many research were undertaken to determine the Young’s modulus and Poisson’s ratio of concrete by both analytical and numerical methods. Earlier days, researchers attempted to model the concrete simply as a two-phase material consisting coarse aggregates and mortar matrix (Nilsen and Monteiro, 1993; Simeonov and Ahmad, 1995). Although the two-phase model could provide approximate estimations, insightful results were not achieved. The variation between real values and estimated values (in two-phase models) was later found to be due to the ignorance of ITZ in concrete (Nilsen and Monteiro, 1993). Thenceforth, the three-phase concept was incorporated by researchers in their models proposed to concrete by considering the ITZ as a single layer around aggregates (Nilsen and Monteiro, 1993; Simeonov and Ahmad, 1995). It should be noted, however, modelling the ITZ realistically into the concrete composite was continuously a challenging process. For instance, during the prediction of Young’s modulus of concrete, Li et al. (1999) failed to capture the overlapping between ITZs, which inevitably affected the accuracy of the prediction. In fact, the unavailability of experimental data on ITZ is the major hurdle that limits the developments

of reliable and insightful simulations of concrete, which consequently leads the researchers to deal with lot of assumptions on properties of ITZ (Duplan et al., 2014; Aouissi et al., 2016; Chen et al., 2016; Das, Maroli and Neithalath, 2016). Particularly, in most of the existing models, the ITZ layer was assumed to be uniform with constant mechanical properties (Ramesh, Sotelino and Chen, 1996; Hashin and Monteiro, 2002; Aouissi et al., 2016). But, in real case, the clinker content in ITZ reveals a gradient increase with the distance from aggregate surface (Nadeau, 2002). Moreover, by ignoring time-dependent effects, the mechanical properties of ITZ were assumed to be a specific ratio/ function of cement paste properties (Duplan et al., 2014; Das, Maroli and Neithalath, 2016). Therefore, it is still needed to develop reliable models by considering both gradient and time-dependent effects in ITZ for precise computations of Young's modulus and Poisson's ratio of concrete.

The model proposed in this research work systematically integrates (i) cement hydration model, (ii) thermodynamic model, (iii) multi-scale model and (iv) homogenization scheme to predict the mechanical properties of mortar and concrete in a realistic manner. By representing mortar/ concrete as a three-phase composite material and based on previously proposed model for w/c distribution in ITZ by Nedeau (2002), the mechanical properties of ITZ and bulk paste/ mortar is computed with hydration period separately. Unlike most of the previously proposed models (wherein constant properties of ITZ and bulk paste were used), the computation of mechanical properties of ITZ and bulk paste is based on the detailed microstructure of hydrated cement paste including two types of C-S-H, capillary porosity, chemical shrinkage and other hydration products. Since the microstructure of cement matrix varies depending on curing time, chemical composition of clinker, w/c and curing temperature, the realistic computations of ITZ and bulk paste are emphasized in this proposed framework.

Finally, the homogenization method is applied to predict the mechanical properties of the materials. The validity of the proposed model is verified with independent sets of experimental data, and the effect of ITZ on the Young's modulus and Poisson's ratio is investigated through sensitivity analysis for mortar and concrete.

4.2 Modelling strategy

The steps followed in the proposed model for mortar and concrete are clearly depicted in **Figure 4.1**. The fundamental parameters such as clinker compositions, properties of clinker and aggregates, mixture recipe and boundary conditions are the necessary input parameters for computations. As conceptually illustrated in **Figure 4.2**, both the mortar and concrete are considered as three-phase materials: (i) mortar: fine aggregates, ITZ and bulk paste, and (ii) concrete: coarse aggregates, ITZ and mortar. It should be noted, as the ITZ consists of low amount of clinker and high amount of water, it can be reasonably considered as a cement paste with higher w/c (compared to the initial w/c of fresh concrete mix/ mortar mix). The required mechanical properties of ITZ and bulk paste are separately computed from the cement paste model developed in our previous work (Krishnya, Yoda and Elakneswaran, 2021). Finally, homogenization method was used to predict the mechanical properties of mortar and concrete. The elaboration of modelling approach can be found in subsequent sections.

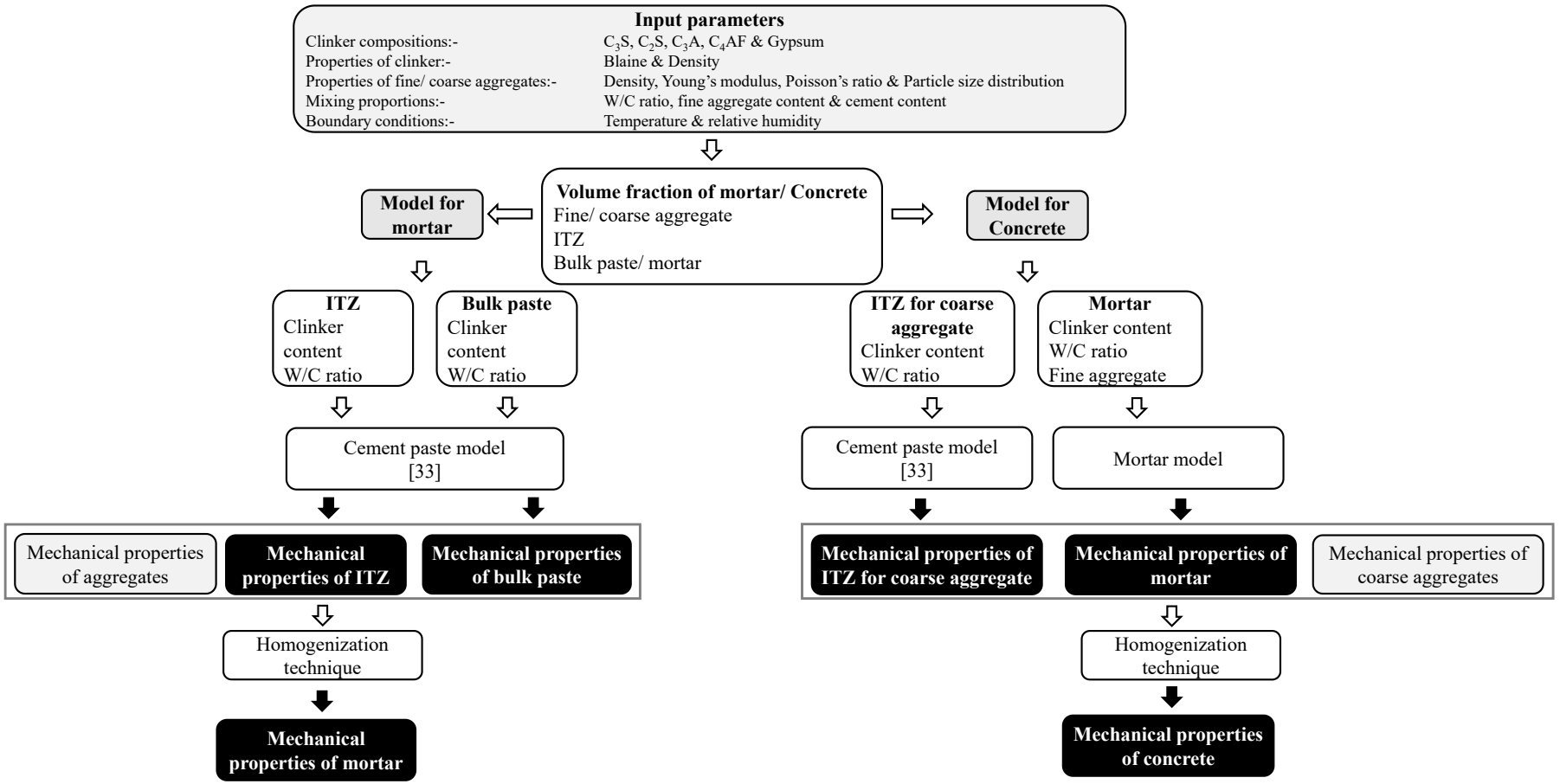

Figure 4.1: Flow diagram of the model proposed for mortar and concrete

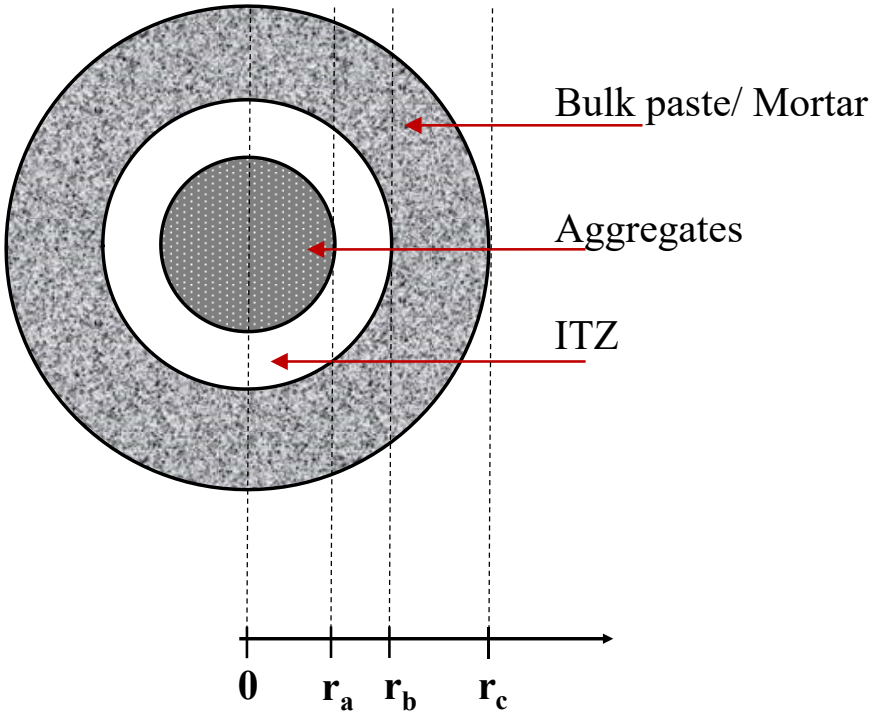

Figure 4.2: Schematic diagram indicating three-phase of modelled mortar/ concrete

4.2.1 Properties of ITZ

The development of ITZ imposes adverse effect on the mechanical properties; therefore, the properties of ITZ such as volume fraction and mechanical properties are required to be predicted in a realistic manner. As discussed earlier, the aggregate properties are one of the parameters that determine the thickness of the ITZ (Zheng, Wong and Buenfeld, 2009; Zheng, Zhou and Jin, 2012), and the mechanical properties of ITZ vary with the hydration period. Therefore, for a specific degree of hydration (i.e., for a specific curing period), the ITZ can be considered as a single shell with uniform mechanical properties. Moreover, based on the previous studies, the thickness is presumed to be 15 μm for fine aggregate in mortar and 40

μm for coarse aggregate in concrete (Ma and Li, 2014; Maghsoodi, 2018; Li, Li and Wang, 2019).

The volume fraction of aggregate in typical concrete is more than 60%, thereby the spacing between adjacent aggregates can only be a few times the typical ITZ thickness (Garboczi and Bentz, 1997; Rupasinghe et al., 2017). Similar to that implemented in previous studies, the volume fraction of ITZ is computed herein by considering the overlapping of ITZ shells using the 'void exclusion probability' (Lu and Torquato, 1992). Principally, the void exclusion probability is the volume fraction of the space not occupied by all the spheres and ITZ shells, i.e., fraction of the bulk paste. Hence, the ITZ volume fraction f_{ITZ} for an ITZ thickness of h can be expressed as,

$$f_{ITZ} = (1 - f_{agg})(1 - \exp(-\pi\rho(\alpha_1 h + \alpha_2 h^2 + \alpha_3 h^3))) \quad (4.1)$$

where,

$$\alpha_1 = \frac{4\langle R^2\rangle}{1-f_{agg}} \quad (4.2)$$

$$\alpha_2 = \frac{4\langle R\rangle}{1-f_{agg}} + \frac{12\epsilon_2\langle R^2\rangle}{(1-f_{agg})^2} \quad (4.3)$$

$$\alpha_3 = \frac{4}{3(1-f_{agg})} + \frac{8\epsilon_2\langle R\rangle}{(1-f_{agg})^2} + \frac{16A\epsilon_2^2\langle R^2\rangle}{3(1-f_{agg})^3} \quad (4.4)$$

$$\epsilon_2 = \frac{2\pi\langle R^2\rangle}{3} \quad (4.5)$$

with A being equal to 2, 3, and 0 for the Carnahan-Starling, scaled- particle, and Percus-Yevick approximation, respectively (Lu and Torquato, 1992). However, by comparing with numerical exact model data, Garboczi and Bentz (Garboczi and Bentz, 1998) suggested that

A = 0 is always the best choice for the simulation, thus, A is taken as zero in this work. ρ is the total number of aggregates per unit volume, and α_1, α_2 and α_3 are functions of mean aggregate radius $\langle R \rangle$ and mean square aggregate radius $\langle R^2 \rangle$ according to the aggregate size distribution. According to previous studies (Garboczi and Bentz, 1998; Dridi, 2013), with the assumption of uniform distribution by volume of aggregates, the remaining parameters are calculated from aggregate size distribution as,

$$\rho = \sum \frac{9 f_{agg} f_i}{4\pi (r_{i+1}^3 - r_i^3)} ln \frac{r_{i+1}}{r_i} \tag{4.6}$$

$$\langle R^n \rangle = \sum \frac{9 f_{agg} f_i}{4\pi \rho (r_{i+1}^3 - r_i^3)} \int_{r_i}^{r_{i+1}} r^{n-1} \, dr \tag{4.7}$$

f_{agg} is the volume fraction of aggregate. f_i is the fraction of the total volume of aggregate that has a radius between r_i and r_{i+1}, $r_i < r_{i+1}$. A typical sieve analysis is expressed in terms of the mass fraction passing or retained by a certain sieve size, which can easily be converted to the form given here. If aggregates of different size have all the same density, then mass fractions are the same as volume fractions. Once the ITZ volume fraction is known, the volume fraction of bulk paste (f_{bulk}) is obtained by simple subtraction.

To represent the concrete or mortar of practical use, the proportion of each phase constituent in the composite sphere should satisfy the following conditions (refer to Figure 4.2) (Zheng, Zhou and Jin, 2012).

$$f_{agg} = \frac{r_a^3}{r_c^3} \tag{4.8}$$

$$f_{agg} + f_{itz} = \frac{r_b^3}{r_c^3} \tag{4.9}$$

The local volume fraction of anhydrous cement in bulk paste ($\alpha_{c,bulk}$) and ITZ ($\alpha_{c,ITZ}$) are computed from Nadeau (Nadeau, 2002). Moreover, the effective w/c of bulk paste and ITZ is calculated based on Eq 4.10.

$$w/c_{bulk\ or\ ITZ} = \frac{1-\alpha_{c,bulk}\ or\ \alpha_{c,ITZ}}{\rho_c \alpha_{c,bulk}\ or\ \alpha_{c,ITZ}} \quad (4.10)$$

4.2.2 Multi-scale model

In computational material science, concrete is characterized as a multi-phase material with different representative scales (Bernard and Kamali-Bernard, 2015). At mesoscopic scale, it is focused to be consisting of coarse aggregates and mortar matrix; the mortar matrix can be subdivided as fine aggregates and hardened cement paste; the hardened cement paste consists of several hydration products, unreacted clinker and capillary porosity. Therefore, a multi-scale model can be more appropriate for realistically predicting the behaviour of concrete and evaluating the impact of compositions on the mechanical properties. **Figure 4.3** presents the organization of the multi-scale model proposed in this study, describing the levels and constitutions for modelling the concrete.

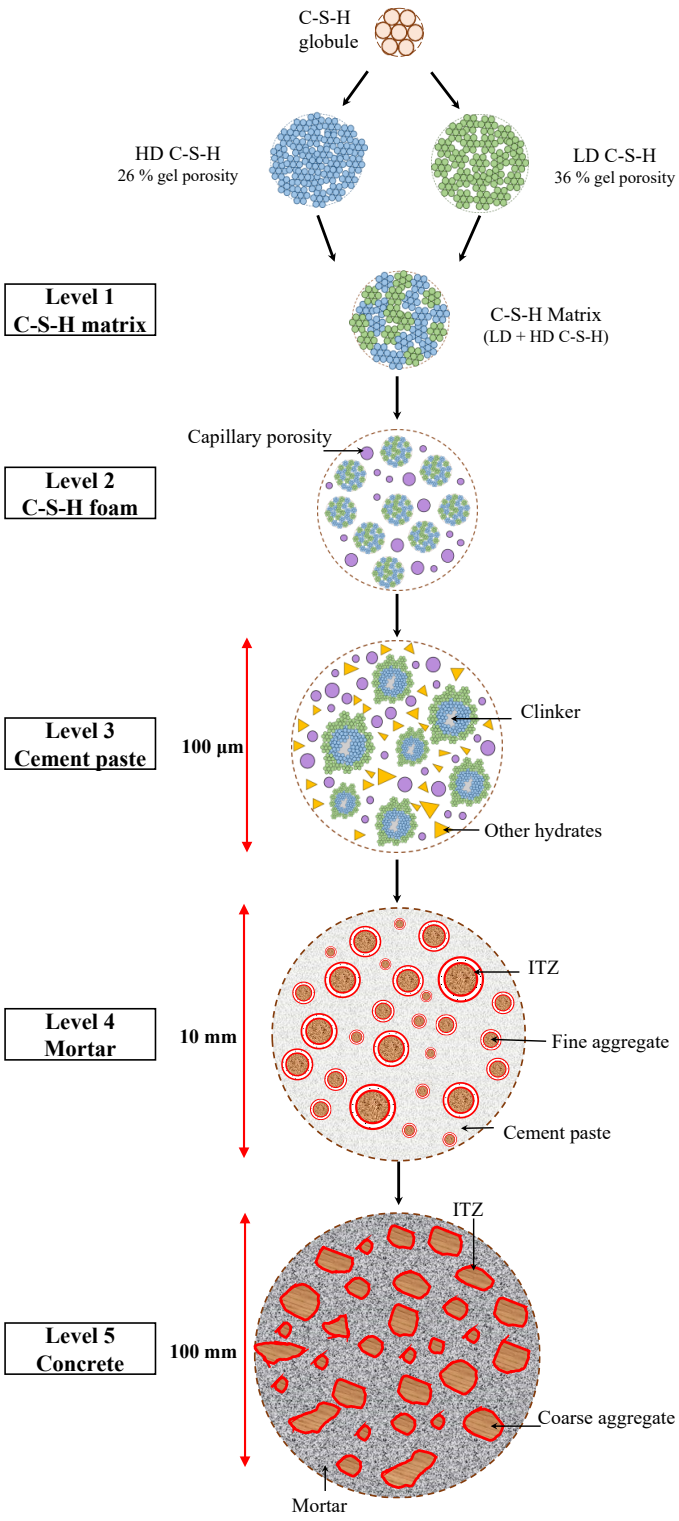

Figure 4.3: Representation of hierarchical model (multi-scale) proposed for concrete

Model description for cement paste

The development of cement paste model (Level 1-3 of the multi-scale model) is described briefly in this section. It should be noted that further detail of cement paste model can be found in our previous work (Krishnya, Yoda and Elakneswaran, 2021). Here, as the first step, the popular hydration model proposed by Parrot and Killoh (1984) was implemented to predict the hydration products based on the considered input parameters such as clinker composition, boundary condition and mixing conditions. Thermodynamic calculations were performed using the open source geochemical (IPHREEQC) based on the estimated dissolution rate of clinker minerals to predict the hydration products. Using the predicted volume fraction of hydration products such as two types of C-S-H (Low density C-S-H and High-density C-S-H), portlandite, ettringite, monosulfate, hydrotalcite, Fe-siliceous hydrogarnet and calculated chemical shrinkage based on the reaction rate of each clinker minerals, the capillary porosity with hydration period was predicted. The multi-scale model initiating from C-S-H matrix (Level 1) and ending up with cement paste (Level 3) was then used to predict the mechanical properties of cement paste. **Figure 4.4** depicts the overall procedure adopted in the cement paste model.

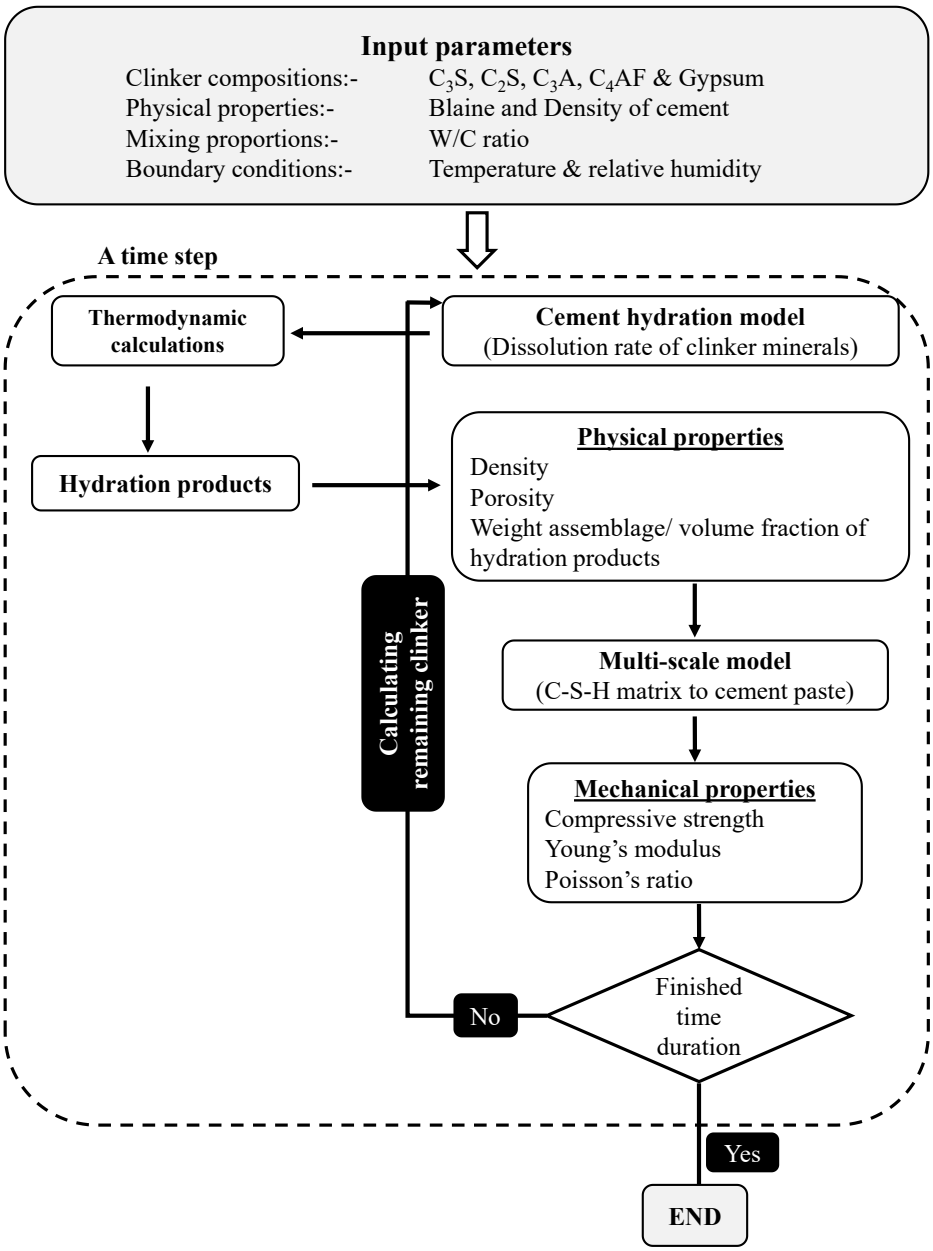

Figure 4.4: Flow diagram illustrating the procedure used to develop the cement paste model

Model description for mortar

In the model proposed for mortar, the aggregate is assumed to be inert with the cement in order to eliminate the complexity of the model. The properties of ITZ and bulk paste vary with w/c ratio, degree of reaction, aggregate content, and clinker properties. As illustrated in

Figure 4.1, to predict the mechanical properties of ITZ and bulk paste, following parameters are required: (i) clinker content, (ii) w/c ratio and (iii) volume fraction of ITZ and bulk paste. Clinker content in ITZ and bulk paste is obtained from Nadeau (Nadeau, 2002), while the w/c ratio and volume fraction are computed using Eq. 4.10 and Eq. 4.1, respectively. The above-mentioned computations are then inputted to cement paste model (which is the integration of cement hydration model, thermodynamic model, and multi-scale model) to predict the mechanical properties. The predicted mechanical properties (of ITZ and bulk paste), volume fraction of all three phases and considered mechanical properties of fine aggregate are finally used to predict the mechanical properties of mortar such as Young's modulus and Poisson's ratio using the homogenization method (as illustrated in **Figure 4.5**).

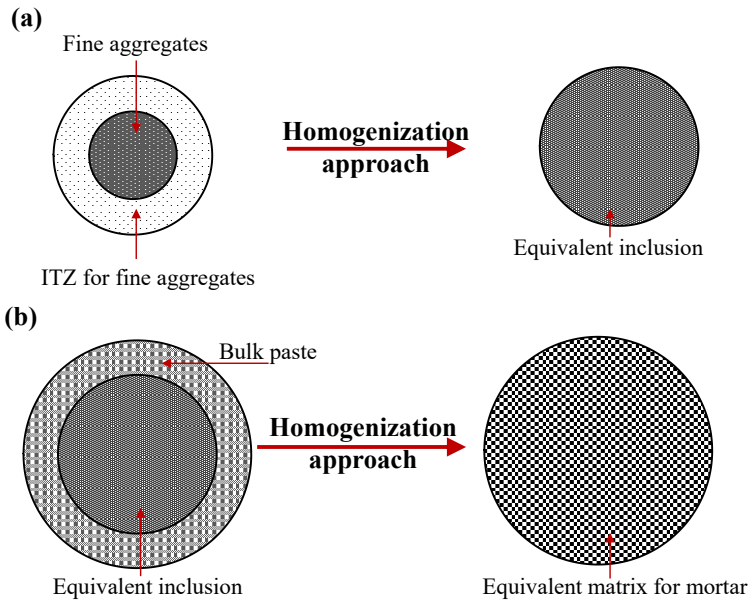

Figure 4.5: Two step homogenization procedure of mortar: (a) the first step homogenization of fine aggregates and ITZ and (b) the second step homogenization of equivalent inclusion and bulk paste

The two-step homogenization method employed herein was developed by Christensen and

Lo (1979). The method is based on three-phase sphere model for two-phase composite material, which was developed to compute the effective bulk and shear modulus by assuming that each individual aggregate has homogeneous particle size with equivalent elastic properties and radius. The origin of this model was from the study by Eshelby (Christensen and Lo, 1979). Following the evaluations, Christensen (1979) concluded that the homogenization model can be more reliable than other generally used models such as differential scheme and Mori-Tanaka model (1973), because the stress-strain field interactions between different inclusions were considered in this model (Li, Zhao and Pang, 1999). This homogenization model was also implemented in several previous studies to predict the effective properties of mortar and concrete (Li, Zhao and Pang, 1999; Chen et al., 2016). As per the first step, the effective properties of two-phase composite made up of fine aggregates and ITZ (shown in Figure 4.5(a)) are computed based on Eq. 4.11- Eq. 4.19 (Christensen and Lo, 1979).

$$K_{equ} = K_{ITZ} + \frac{\emptyset_{agg}(K_{agg}-K_{ITZ})(3K_{ITZ}+4G_{ITZ})}{3K_{ITZ}+4G_{ITZ}+3(1-\emptyset_{agg})(K_{agg}-K_{ITZ})} \tag{4.11}$$

$$B\left(\frac{G_{equ}}{G_{ITZ}}\right)^2 + C\left(\frac{G_{equ}}{G_{ITZ}}\right) + D = 0 \tag{4.12}$$

$$B = 8\left(\frac{G_{agg}}{G_{ITZ}} - 1\right)(4 - 5\nu_{ITZ})\eta_1\emptyset_{agg}^{\frac{10}{3}} - 2\left(63\left(\frac{G_{agg}}{G_{ITZ}} - 1\right)\eta_2 + 2\eta_1\eta_3\right)\emptyset_{agg}^{\frac{7}{3}} +$$

$$252\left(\frac{G_{agg}}{G_{ITZ}} - 1\right)\eta_2\emptyset_{agg}^{\frac{5}{3}} - 50\left(\frac{G_{agg}}{G_{ITZ}} - 1\right)(7 - 12\nu_{ITZ} + 8\nu_{ITZ}^2)\eta_2\emptyset_{agg} + 4(7 -$$

$$10\nu_{ITZ})\eta_2\eta_3 \tag{4.13}$$

$$C = -4\left(\frac{G_{agg}}{G_{ITZ}} - 1\right)(1 - 5\nu_{ITZ})\eta_1\emptyset_{agg}^{\frac{10}{3}} + 4\left(63\left(\frac{G_{agg}}{G_{ITZ}} - 1\right)\eta_2 + 2\eta_1\eta_3\right)\emptyset_{agg}^{\frac{7}{3}} -$$

$$504\left(\frac{G_{agg}}{G_{ITZ}} - 1\right)\eta_2\emptyset_{agg}^{\frac{5}{3}} + 150\left(\frac{G_{agg}}{G_{ITZ}} - 1\right)(3 - \nu_{ITZ})\nu_{ITZ}\eta_2\emptyset_{agg} + 3(15\nu_{ITZ} - 7)\eta_2\eta_3 \quad (4.14)$$

$$D = 4\left(\frac{G_{agg}}{G_{ITZ}} - 1\right)(5\nu_{ITZ} - 7)\eta_1\emptyset_{agg}^{\frac{10}{3}} - 2\left(63\left(\frac{G_{agg}}{G_{ITZ}} - 1\right)\eta_2 + 2\eta_1\eta_3\right)\emptyset_{agg}^{\frac{7}{3}} +$$

$$252\left(\frac{G_{agg}}{G_{ITZ}} - 1\right)\eta_2\emptyset_{agg}^{\frac{5}{3}} + 25\left(\frac{G_{agg}}{G_{ITZ}} - 1\right)(\nu_{ITZ}^2 - 7)\eta_2\emptyset_{agg} - 3(5\nu_{ITZ} + 7)\eta_2\eta_3 \quad (4.15)$$

$$\eta_1 = \left(\frac{G_{agg}}{G_{ITZ}} - 1\right)(49 - 50\nu_{agg}\nu_{ITZ}) + 35\left(\frac{G_{agg}}{G_{ITZ}}\right)(\nu_{agg} - 2\nu_{ITZ}) + 35(2\nu_{agg} - \nu_{ITZ}) \quad (4.16)$$

$$\eta_2 = 5\nu_{agg}\left(\frac{G_{agg}}{G_{ITZ}} - 8\right) + 7\left(\frac{G_{agg}}{G_{ITZ}} + 4\right) \quad (4.17)$$

$$\eta_3 = \frac{G_{agg}}{G_{ITZ}}(8 - 10\nu_{ITZ}) + (7 - 5\nu_{ITZ}) \quad (4.18)$$

$$\emptyset_{agg} = \frac{f_{agg}}{f_{agg} + f_{ITZ}} \quad (4.19)$$

where K_{equ} and G_{equ} are the effective bulk modulus and shear modulus of the equivalent inclusions after the first step of homogenization. K_{agg}, G_{agg} and ν_{agg} are the bulk modulus, shear modulus and Poisson's ratio of fine aggregates. K_{ITZ}, G_{ITZ} and ν_{ITZ} are the bulk modulus, shear modulus and Poisson's ratio of ITZ, and which are obtained from the previous work (Krishnya, Yoda and Elakneswaran, 2021).

Since the mortar consisting of bulk paste and equivalent inclusion (as elucidated **in Figure**

4.5(b)), the effective mechanical properties of mortar can be similarly computed by homogenization approach. The Eq. 4.11 - Eq. 4.19 are amended by replacing the effective properties of equivalent inclusion ($\emptyset_f$, G_{equ}, K_{equ} and ν_{equ}) and bulk paste properties (G_{bulk}, K_{bulk} and ν_{bulk}) in the place of aggregate properties ($\emptyset_{agg}$, G_{agg}, K_{agg} and ν_{agg}) and ITZ properties (G_{ITZ}, K_{ITZ} and ν_{ITZ}) to predict effective bulk modulus and shear modulus of mortar (K_{mor}, G_{mor}). The formula for volume fraction of equivalent inclusion in mortar is provided in Eq. 4.20. The bulk paste properties (G_{bulk}, K_{bulk} and ν_{bulk}) are obtained from the previous work (Krishnya, Yoda and Elakneswaran, 2021).

$$\emptyset_f = \frac{f_{agg} + f_{ITZ}}{f_{agg} + f_{ITZ} + f_{bulk}} \tag{4.20}$$

$$E_{mor} = \frac{9K_{mor}G_{mor}}{3K_{mor}+G_{mor}} \tag{4.21}$$

$$\nu_{mor} = \frac{3K_{mor}-2G_{mor}}{2(3K_{mor}+G_{mor})} \tag{4.22}$$

Theoretically, two sets of moduli are required for the computation of Young's modulus and Poisson's ratio of a material; therefore, bulk modulus of mortar (K_{mor}) together with shear modulus of mortar (G_{mor}) were used herein to predict the Young's modulus (E_{mor}) and Poisson's ratio (ν_{mor}) from the fundamental relationship presented in Eq. 4.21 and Eq. 4.22. Finally, the predicted results were validated using experimental results.

Model description for concrete

In the proposed model (refer **Figure 4.1**), concrete is reliably assumed as three phase material consisting of coarse aggregate, ITZ and mortar. In order to eliminate the complexity of the simulation, coarse aggregate is considered as chemically inactive with cement paste similar

to that considered for fine aggregate. The volume fraction of ITZ for coarse aggregate ($f_{C.ITZ}$) is computed with aid of Eq. 4.1 using the particle size distribution of coarse aggregate and ITZ thickness. Similar procedure that has been described for mortar is used to estimate the clinker content and w/c in ITZ for coarse aggregate and mortar (existing in concrete). Based on the computed w/c and clinker content, the mechanical properties of ITZ paste is predicted using the cement paste model (Krishnya, Yoda and Elakneswaran, 2021). Besides, the mechanical properties of mortar are predicted using the computed w/c, clinker content and fine aggregate content as described in model description for mortar section. The predicted mechanical properties (of ITZ and mortar), volume fraction of all three phases and considered mechanical properties of coarse aggregate are finally used to predict the mechanical properties of concrete using the homogenization method (illustrated in **Figure 4.6**).

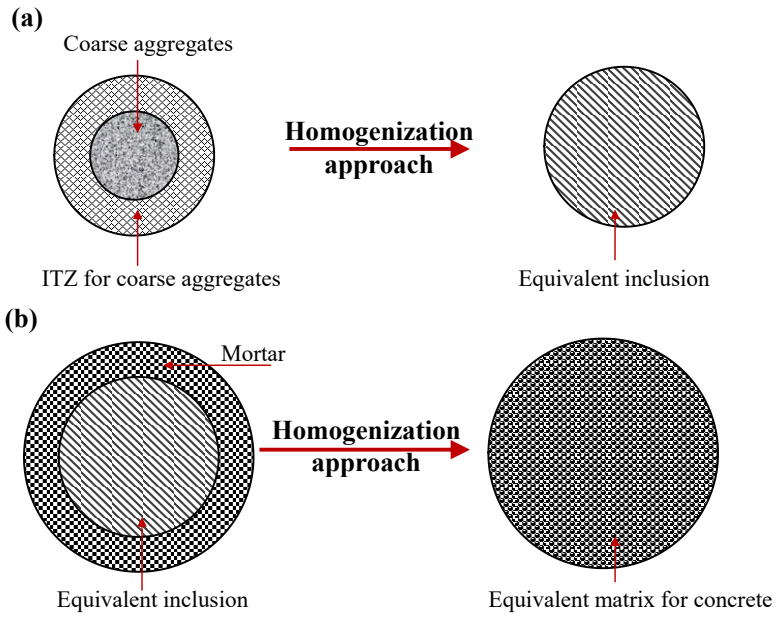

Figure 4.6: Two step homogenization procedure for concrete: (a) the first step homogenization of coarse aggregates and ITZ and (b) the second step homogenization of equivalent inclusion and mortar matrix

As elucidated in **Figure 4.6(a)**, the coarse aggregates and ITZ are considered in the first step. The Eq. 11 – Eq. 19 has been modified by replacing coarse aggregates properties ($\emptyset_{C.agg}$, $G_{C.agg}$, $K_{C.agg}$ and $\nu_{C.agg}$) and ITZ properties of coarse aggregates ($G_{C.ITZ}$, $K_{C.ITZ}$ and $\nu_{C.ITZ}$) in the place of fine aggregates properties ($\emptyset_{agg}$, G_{agg}, K_{agg} and ν_{agg}) and ITZ properties of fine aggregates (G_{ITZ}, K_{ITZ} and ν_{ITZ}) to predict the bulk ($K_{equ,\ con}$) and shear modulus ($G_{equ,\ con}$) of equivalent inclusion for concrete. The formula for volume fraction of coarse aggregate in equivalent inclusion is given in Eq. 4.23.

$$\emptyset_{C.agg} = \frac{f_{C.agg}}{f_{C.agg}+f_{C.ITZ}} \tag{4.23}$$

where, $f_{C.agg}$ is the volume fraction of coarse aggregate in concrete.

In the second step, the equivalent inclusion and mortar matrix are considered for the homogenization method as shown in **Figure 4.6(b)**. The effective mechanical properties of concrete can be similarly computed by homogenization approach. The Eq. 4.11 - Eq. 4.19 were altered by replacing the effective properties of equivalent inclusion ($\emptyset_{C.f}$, $G_{equ,con}$, $K_{equ,con}$ and $\nu_{equ,\ con}$) and mortar properties (G_{mor}, K_{mor} and ν_{mor}) in the place of coarse aggregate properties ($\emptyset_{C.agg}$, $G_{C.agg}$, $K_{C.agg}$ and $\nu_{C.agg}$) and ITZ properties of coarse aggregates ($G_{C.ITZ}$, $K_{C.ITZ}$ and $\nu_{C.ITZ}$) to predict effective bulk modulus and shear modulus of concrete (K_{Con}, G_{Con}). The volume fraction of equivalent inclusion in concrete is given in Eq. 4.24.

$$\emptyset_{C.f} = \frac{f_{C.agg} + f_{C.ITZ}}{f_{C.agg}+ f_{C.ITZ}+ f_{mor}} \tag{4.24}$$

where, f_{mor} is volume fraction of mortar in concrete. Once the volume fraction of ITZ for coarse aggregate is known, the volume fraction of mortar (f_{mor}) is obtained by simple

subtraction ($f_{mor} = 1 - f_{C.agg} - f_{C.ITZ}$).

The Young's modulus (E_{Con}) and the Poisson's ratio (ν_{Con}) of concrete are predicted from the fundamental relationship presented in Eq. 4.21 and Eq. 4.22 by replacing the concrete moduli in the place of mortar properties. Finally, the predictability of the model is validated using the experimental results available in the literature.

4.3 Results and discussion

4.3.1 Sensitivity analysis of ITZ

Figure 4.7 presents the Young's modulus of mortar and concrete predicted as a function of hydration period for different ITZ thickness. It should be mentioned that the prediction corresponds to the w/c of 0.6. The considered volume fraction of fine aggregate for mortar is 0.6, and cement: fine aggregate: coarse aggregate weight ratio for concrete is 1: 1.5: 3.2. The results clearly demonstrate that increasing the thickness of the ITZ results in a reduction in predicted Young's modulus. It is well known that the ITZ is the weakest zone in mortar and concrete (Zhu et al., 2018). The increase in ITZ thickness directly upsurges the volume fraction of ITZ, leading to the decrease in effective elastic modulus of the mortar and concrete. Similar behavior was observed by Simeonov and Ahmad (1995) and Li et al. (1999). However, when the ITZ thickness exceeds 15 μm for mortar and 40 μm for concrete, the predicted results do not show significant variation (refer **Figure 4.7**). It is apparent that the volume fraction of ITZ increases with the increasing thickness, yet the volume fraction of bulk paste decreases, ensuing a negative effect on effective Young's modulus. Meanwhile, the local w/c in ITZ and bulk paste increases with ITZ thickness based on the model proposed by Nadeau (2002), which leads to a positive effect on modulus. Since the above effects compromise each

other, further increase in ITZ thickness does not show significant reduction in final outcomes. Relatively a similar ITZ thickness (in a range between 10-50 μm) was also reported for sand and coarse aggregates in many previous works (Hashin and Monteiro, 2002; Nadeau, 2002; Bernard and Kamali-Bernard, 2015; Zhu et al., 2017). On the above basis, therefore, the ITZ thicknesses of 15 and 40 μm are reliably chosen for the computations in the proposed model.

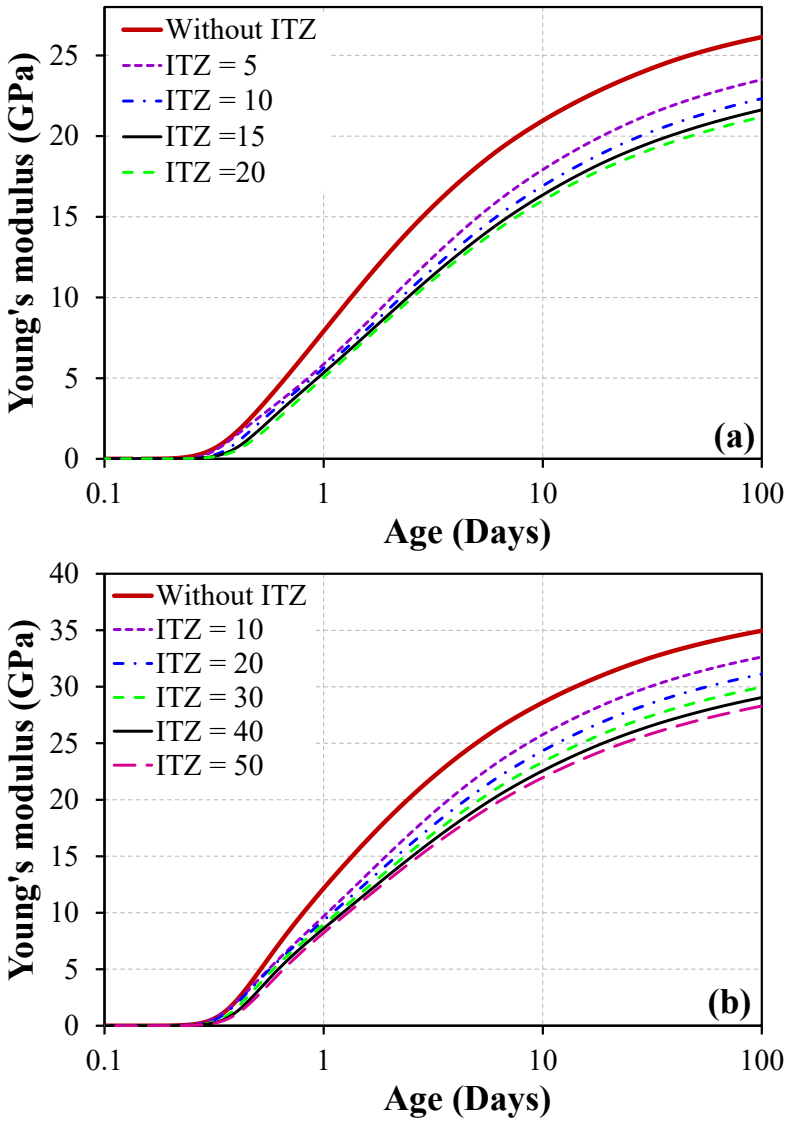

Figure 4.7: Variation of Young's modulus with hydration period for different ITZ thickness (a) for mortar and (b) for concrete

4.3.2 Young's modulus of mortar

To reveal the predictability of the proposed model, the predicted Young's moduli of mortar are compared with two independent sets of experimental results (refer **Figure 4.8** and **Figure 4.9**). In **Figure 4.8**, the raw experimental data were employed for the comparison. The experimental conditions and procedures corresponding to the set of data compared in **Figure 4.8** are detailed in Appendix A. The data used in **Figure 4.9** for validating the predicted results were obtained from previous report (TSUKAHARA, KATO and UOMOTO, 2000). The comparisons indicate that the predicted results exhibit a good agreement with both experimental sets for range of w/c and aggregate volume fractions. Slight variations are however witnessed in certain readings. For instance, 5 GPa variation could be seen between experimental and predicted results for the mortar with w/c of 0.4, aggregate volume fraction of 0.6 and curing period of 28 days (in **Figure 4.8**). It should be noted that in computations, the Young's modulus and Poisson's ratio of fine aggregate were considered to be 37.7 GPa and 0.2 respectively (Kawakami, 2005).

Regardless of w/c and aggregate volume fractions, the Young's modulus increases with hydration period. Besides, relatively higher values are predicted for the mortar with lower w/c, which is in consistent with that of hydrated cement paste. This could mainly be attributed to the increased formation of prime binding agent (i.e., C–S–H) at low w/c during the hydration. In due course, the decrease in the porosity could lead to the development of denser microstructure (Krishnya, Yoda and Elakneswaran, 2021), resulting an increase in Young's modulus of mortar matrix with hydration period. Moreover, for a specific w/c ratio, high moduli are computed for high content of fine aggregate (refer to **Figure 4.8** and **Figure 4.9**). This is because of the increased stiff inclusion in the paste and decreased effective water

content, which lead to the decrease in porosity in bulk paste (Scrivener, Lyon and Laugesen, 2004b; Gao et al., 2014). The tendencies predicted herein for Young's modulus of different cases are in consistent with those reported in previous studies (Tsukahara, Kato and Uomoto, 2000; Wriggers and Moftah, 2006; Teramoto, Igarashi and Maruyama, 2011; Duplan et al., 2014; Di Bella et al., 2015).

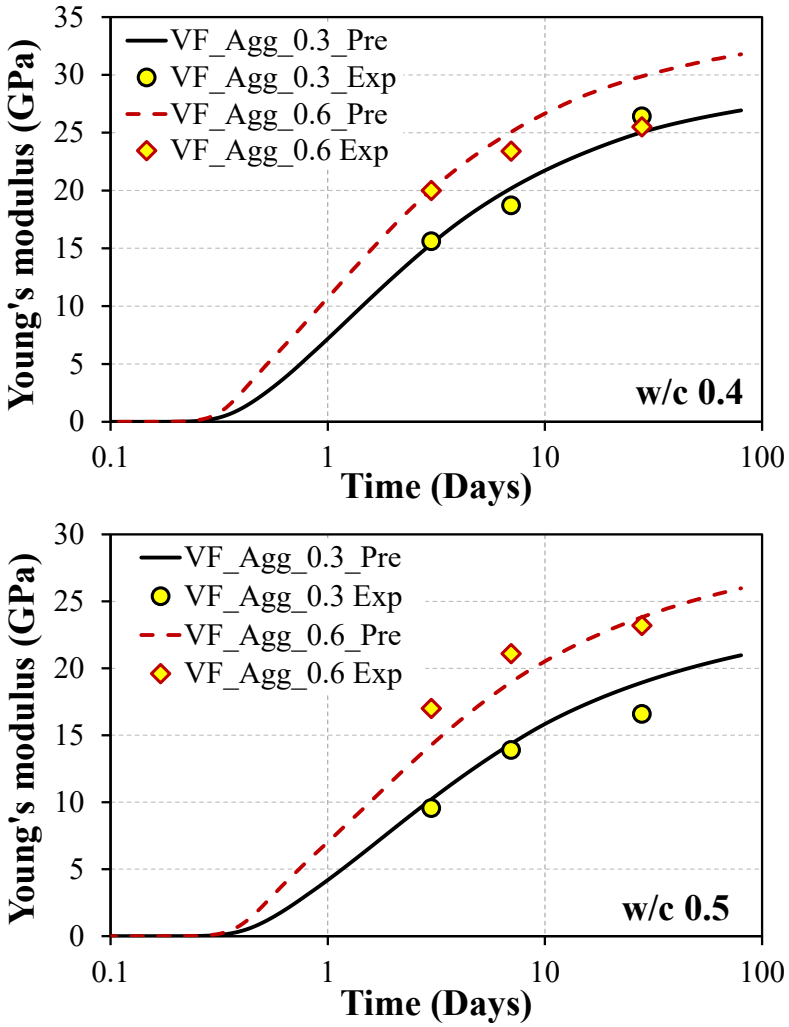

Figure 4.8: Validation of Young's modulus with hydration period for w/c ratio of 0.4 and 0.5 (VF_Agg stands for volume fraction of aggregate)

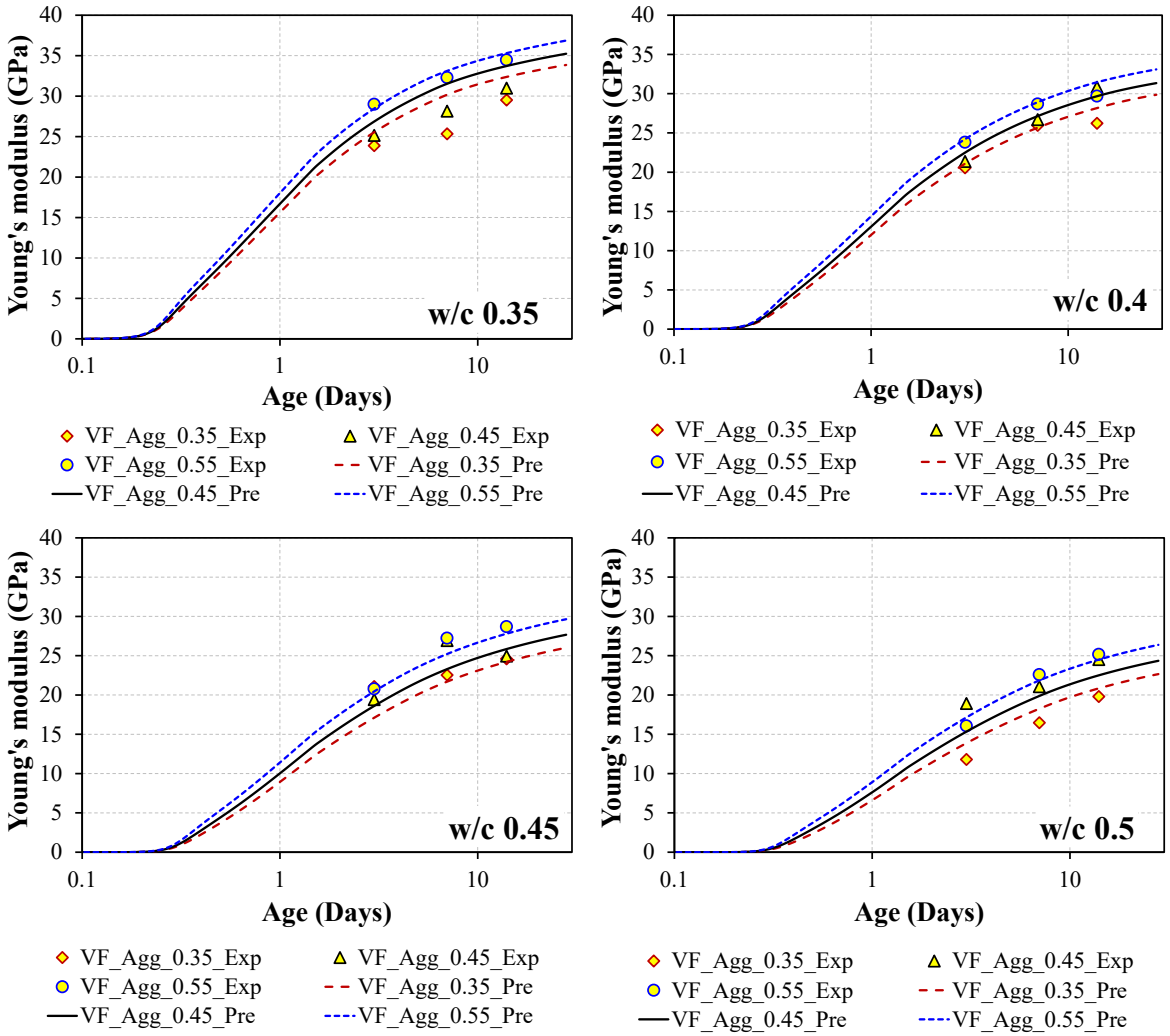

Figure 4.9: Development of Young's modulus of the mortar for w/c 0.35-0.5 and volume fraction of aggregate 0.35-0.55 (the experiment results were obtained from ref. (Tsukahara, Kato and Uomoto, 2000)) (VF_Agg stands for volume fraction of aggregate)

Figure 4.10 presents the compilation of predicted Young's modulus plotted against the experimental results of mortars corresponding to w/c ratios ranging from 0.3 to 0.55 and aggregate volume fraction from 0.2 to 0.6. The experimental data were obtained from both measurements and literature (Tsukahara, Kato and Uomoto, 2000; Teramoto, Igarashi and Maruyama, 2011). As illustrated in **Figure 4.10**, the predicted results of Young's modulus fall

within the error range of 5 GPa for all three sets of experiment results. Based on the sets of comparisons (**Figure 4.8**, **Figure 4.9** and **Figure 4.10**), it is perceived that the proposed model can be reliable for predicting the Young's modulus of mortar with different w/c ratios and aggregate volume fractions.

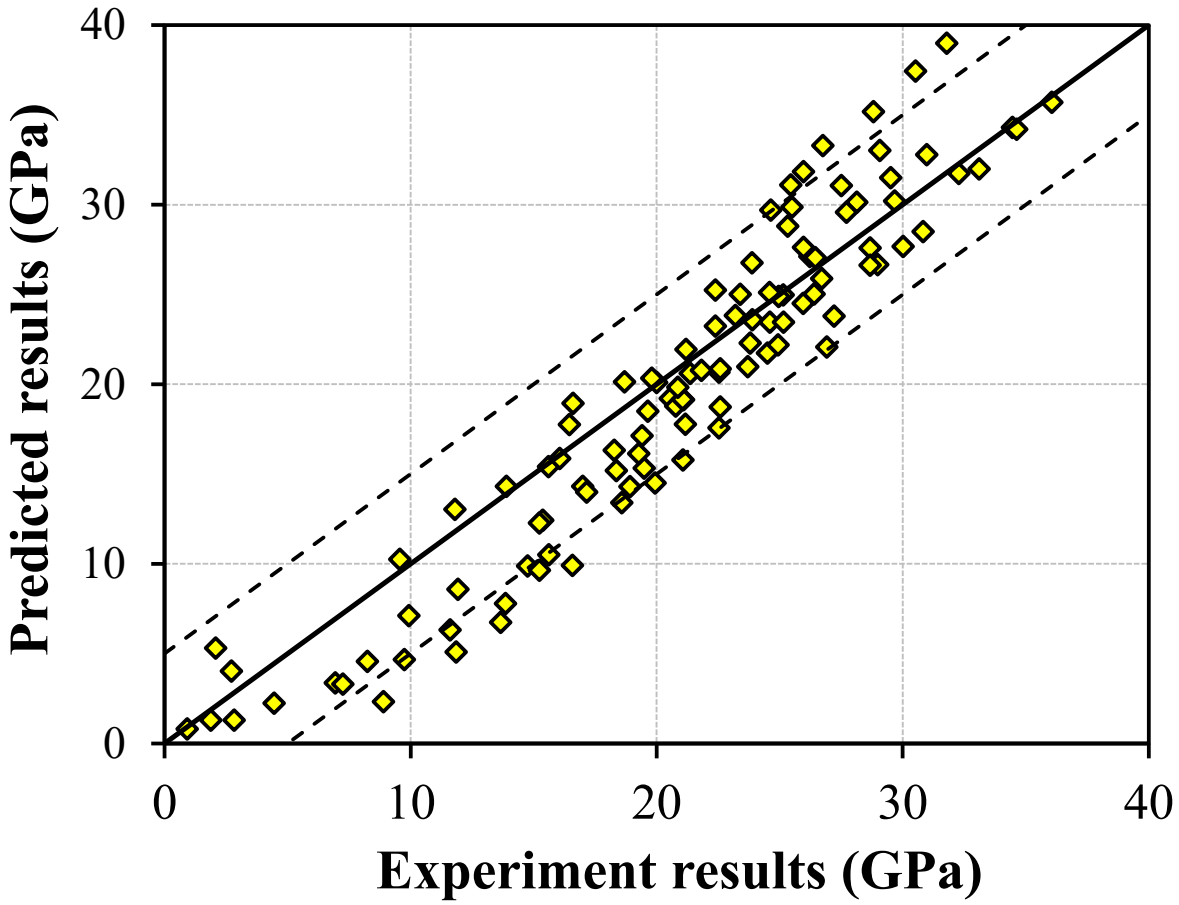

Figure 4.10: Comparison of predicted Young's modulus plotted against the experiment results

4.3.3 Poisson's ratio of mortar

Figure 4.11 presents the variation of Poisson's ratio of mortar with hydration period for w/c

of 0.3, 0.4 and 0.5 and fine aggregates volume fraction of 0.3 and 0.6 (The experimental conditions and procedures corresponding to the experiment data presented in **Figure 4.11** are detailed in Appendix A). It can be observed that the predicted results appear to slightly overestimate the Poisson's ratio for w/c ratio of 0.5, while those show a better agreement with experimental results for the w/c ratios of 0.3 and 0.4. The tendency observed for w/c ratio of 0.5 increases with increasing hydration period, which is in contrast with those observed for other w/c ratios. In fact, during the early stage, the mortar exists in suspension form within the water, thus the Poisson's ratio of fresh mix is equal to Poisson's ratio of water (0.5) (Bernard, Ulm and Lemarchand, 2003; Stefan et al., 2010a), and which is captured by the proposed model (**Figure 4.11**). When the hydration is in progress, the Poisson's ratio of mortar decreases due to the formation of denser microstructure by replacing the solids in the place of water. Thus, the increasing tendency observed for w/c of 0.5 might be due to experimental error. It can also be noticed that the Poisson's ratio increases with the increase in w/c ratio, which is similar to the tendency observed for cement paste (Maruyama and Igarashi, 2014; Krishnya, Yoda and Elakneswaran, 2021). For a specific water cement ratio, the Poisson's ratio decreases with the increase in volume fraction of fine aggregates (refer to **Figure 4.11**). It is clear that sand is considerably stiffer than the cement paste; therefore, the increasing stiffer inclusions in paste tends to restrain the lateral expansion of the softer matrix. In fact, both Young's modulus and Poisson's ratio of the aggregate influence the elastic properties such as Poisson's ratio and elastic modulus of mortar (Narayan Swamy, 1971).

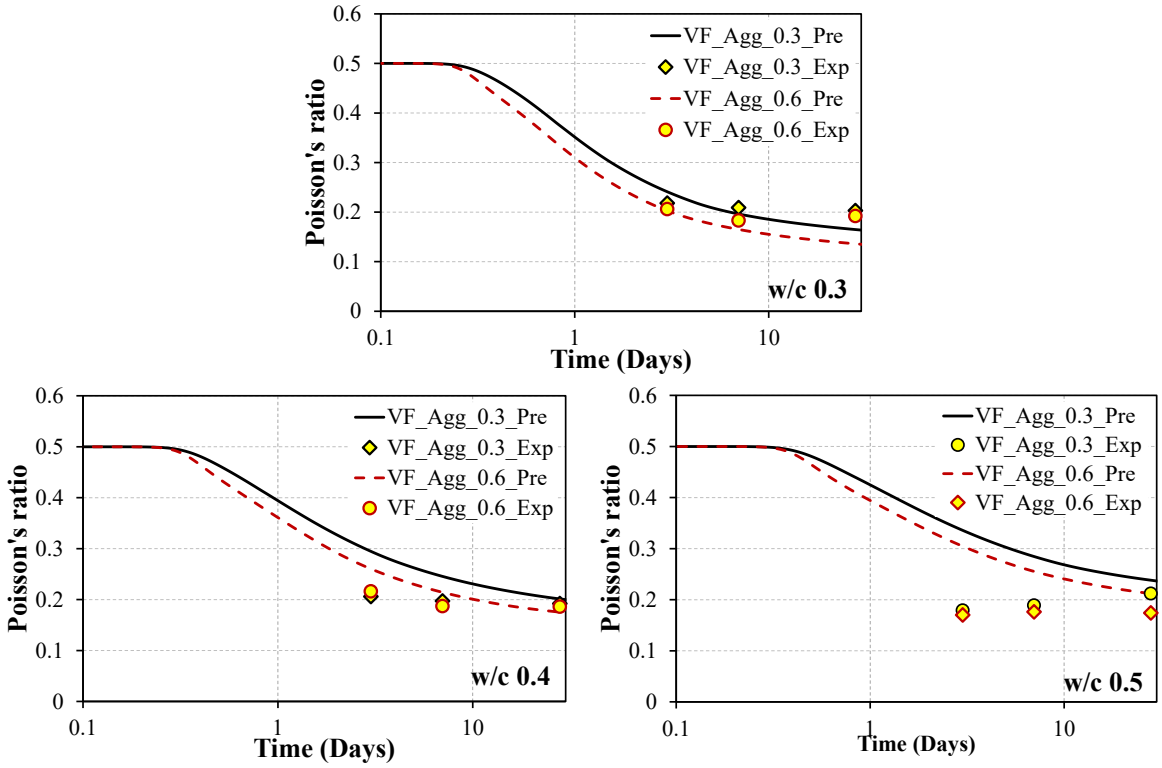

Figure 4.11: Validation of Poisson's ratio of the mortar for w/c 0.3-0.5 with volume fraction of aggregate 0.3 and 0.6 (VF_Agg stands for volume fraction of aggregate)

4.3.4 Young's modulus of concrete

Figure 4.13, Figure 4.14 and **Figure 4.14** illustrate the predictability of the model for the Young's modulus of concrete with different independent sets of experimental results obtained from raw experimental results and previous studies. **Figure 4.13** shows the comparison of Young's modulus for different w/c ratio and different types of cement (Type I and Type V). The experiment results used herein for the comparison belong to Han and Kim (Han and Kim, 2004). The second set of experimental data compared in **Figure 4.144** were obtained from Corinaldesi and Moriconi (Corinaldesi and Moriconi, 2009) for w/c, volume fraction of fine aggregate and volume fraction of coarse aggregates of 0.56, 0.12 and 0.5, respectively. During

the computation, the Young's modulus and Poisson's ratio of coarse aggregates were considered to be 50 GPa and 0.18, respectively (Kawakami, 2006), and for the fine aggregates, they were respectively 37.7 GPa and 0.20. Based on the considered aggregates properties, the proposed model shows a good capability to predict the Young's modulus of concrete for different w/c and wide range of aggregates content. There are however slight variations observed for some points (refer **Figure 4.133**), which could possibly be due to the assumptions made during prediction. Since the required parameters such as particle size distribution and properties of aggregates (Young's modulus and Poisson's ratio) were not available in the literature, they were assumed based on the instructions given in literature. Additionally, the aggregates were assumed to be inert and ITZ properties to be constant with distance from aggregate for a specific time. Nevertheless, the development of Young's modulus of concrete reveals almost a similar tendency of the development of Young's modulus of mortar.

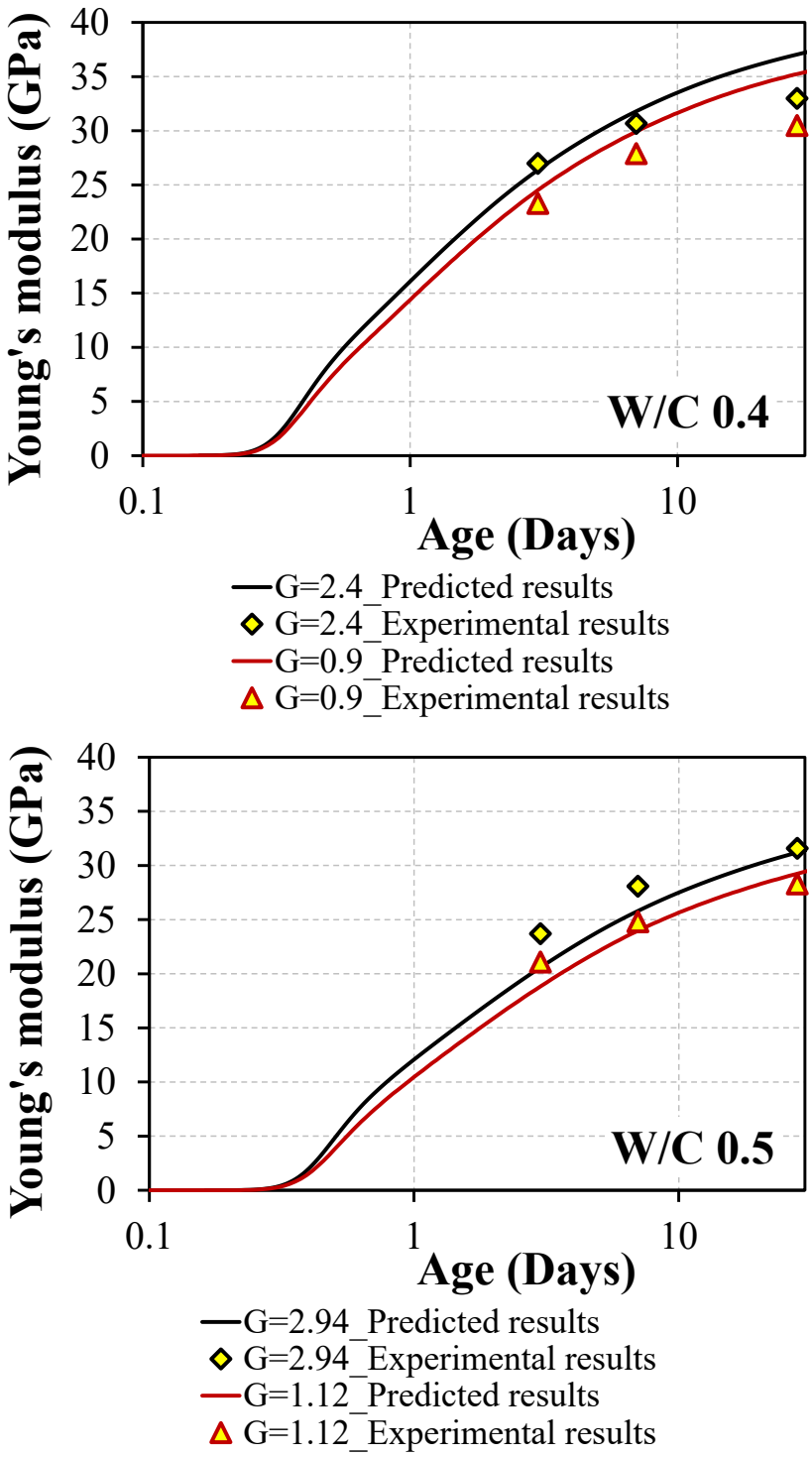

Figure 4.12: Validation of Young's modulus with hydration period for w/c ratio of 0.4 and 0.5 (G stands for weight ratio coarse aggregate/cement)

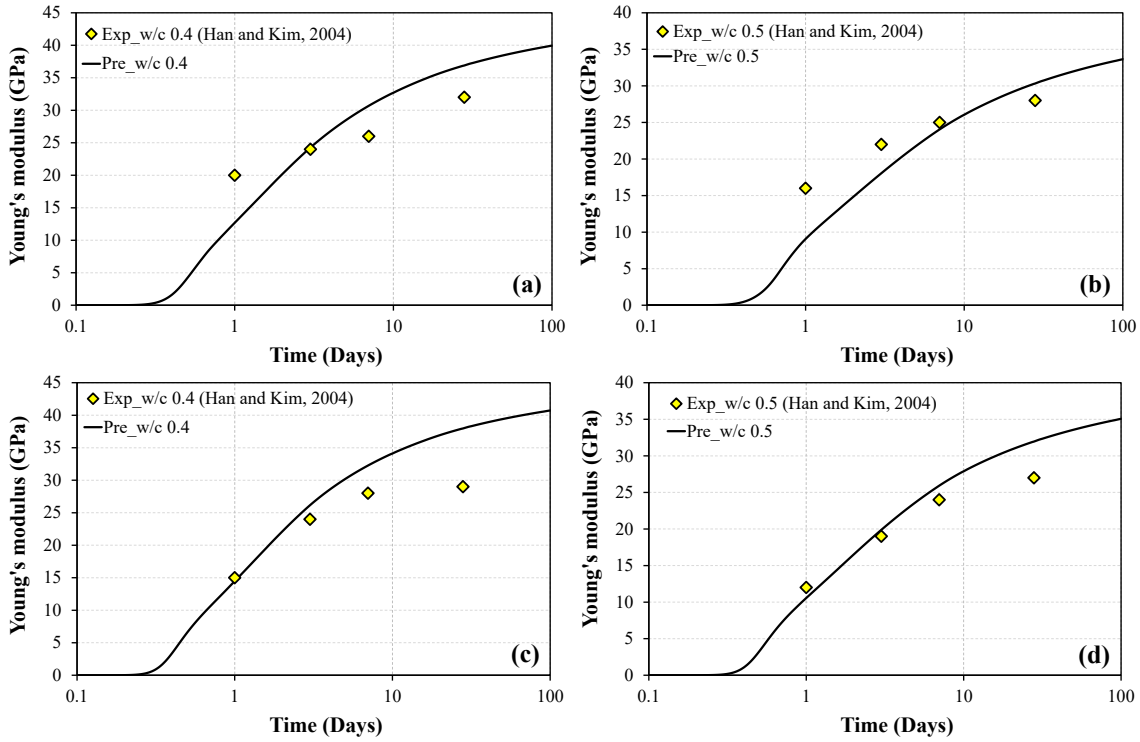

Figure 4.13: Validation of Young's modulus of concrete (experiment results were obtained from ref. (Han and Kim, 2004) of (a) and (b) for Type I cement and (c) and (d) for Type V cement.

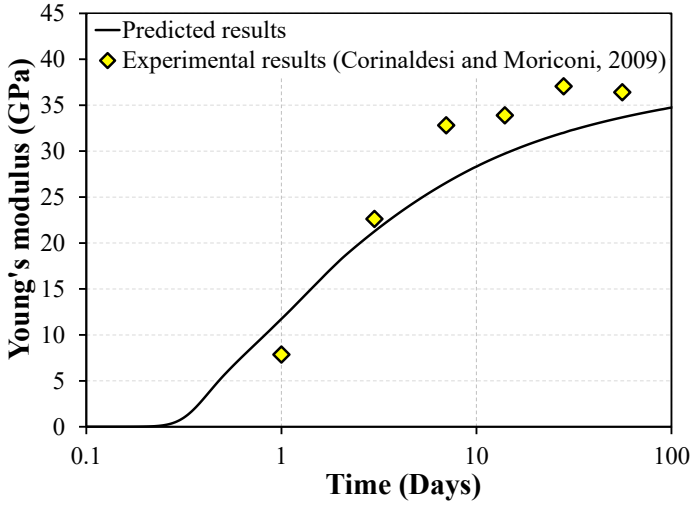

Figure 4.14: Validation of Young's modulus of concrete (experiment results were obtained from ref (Corinaldesi and Moriconi, 2009))

Figure 4.155 shows the overall validation for 30 number of measured Young's modulus of concrete with the w/c of 0.4 to 0.6. All the experiment results were taken from previous studies (Han and Kim, 2004; Corinaldesi and Moriconi, 2009; Klein, Lenz and Mazer, 2020). The predicted results of Young's modulus fall within the error range of 5 GPa for all three sets of experiment results as depicted in **Figure 4.155**. Based on the sets of validations (**Figure 4.13**, **Figure 4.14, Figure 4.154** and **Figure 4.155**), it is verified that the proposed model can be reliable for predicting the Young's modulus of concrete with different w/c ratios and aggregate volume fractions

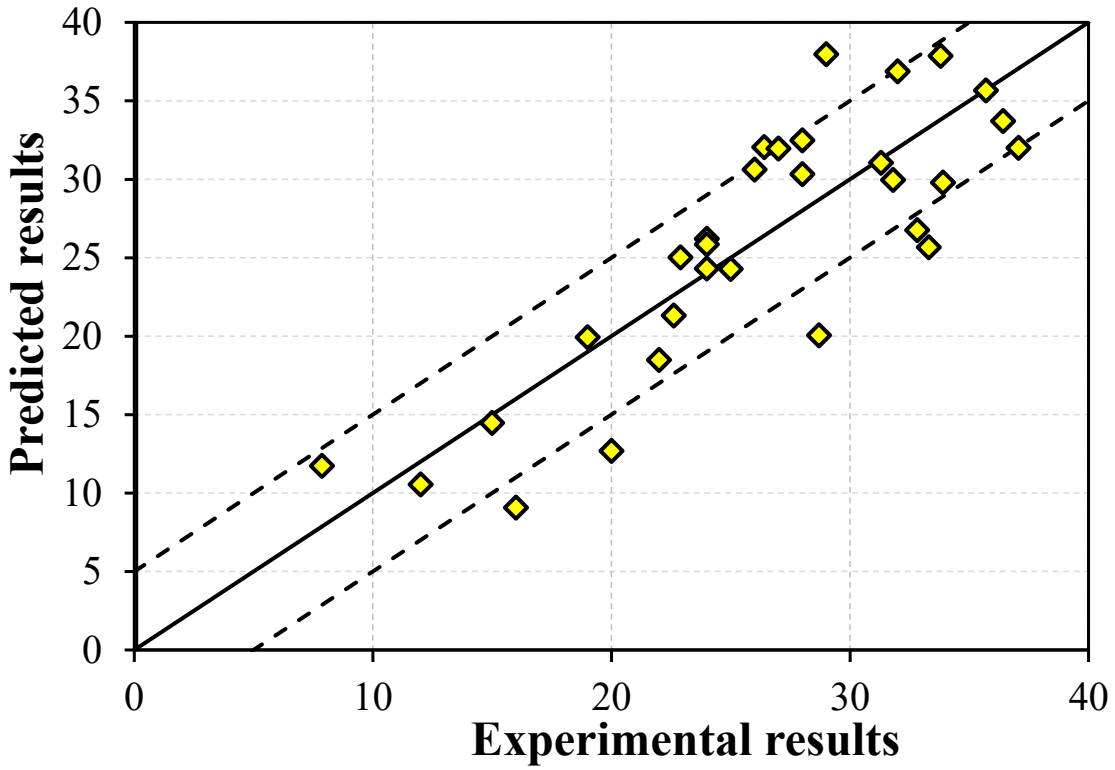

Figure 4.15: Comparison of predicted Young's modulus plotted against the experiment results

4.3.5 Poisson's ratio of concrete

The variation of Poisson's ratio with hydration period from raw experimental results and predicted results is illustrated in **Figure 4.176** and the validation of Poisson's ratio with hydration period of concrete for w/c of 0.5, sand to cement ratio of 1.5 and coarse aggregate to cement ratio of 3 is presented in **Figure 4.17**. The experiment results used for the comparison were taken from Allos and Martin (1981). The predicted results show relatively good agreement with experiment results (after 10 days in **Figure 4.17**); however, the model appears to overpredicts the Poisson's ratio at the early stage (see **Figure 4.17**). However, the predicted results as illustrated in **Figure 4.176** shows good agreement with raw experimental results. According to the prediction, the Poisson's ratio of concrete decreases with the increase in hydration period. This is understandable that the formation of denser microstructure during the hydration replaces the solids in the place of water. Particularly, the greatest decrease in Poisson's ratio occurs until 10 days, and after 10 days, the decrease becomes very mild. A similar behaviour was also observed by Narayan Swamy (1971).

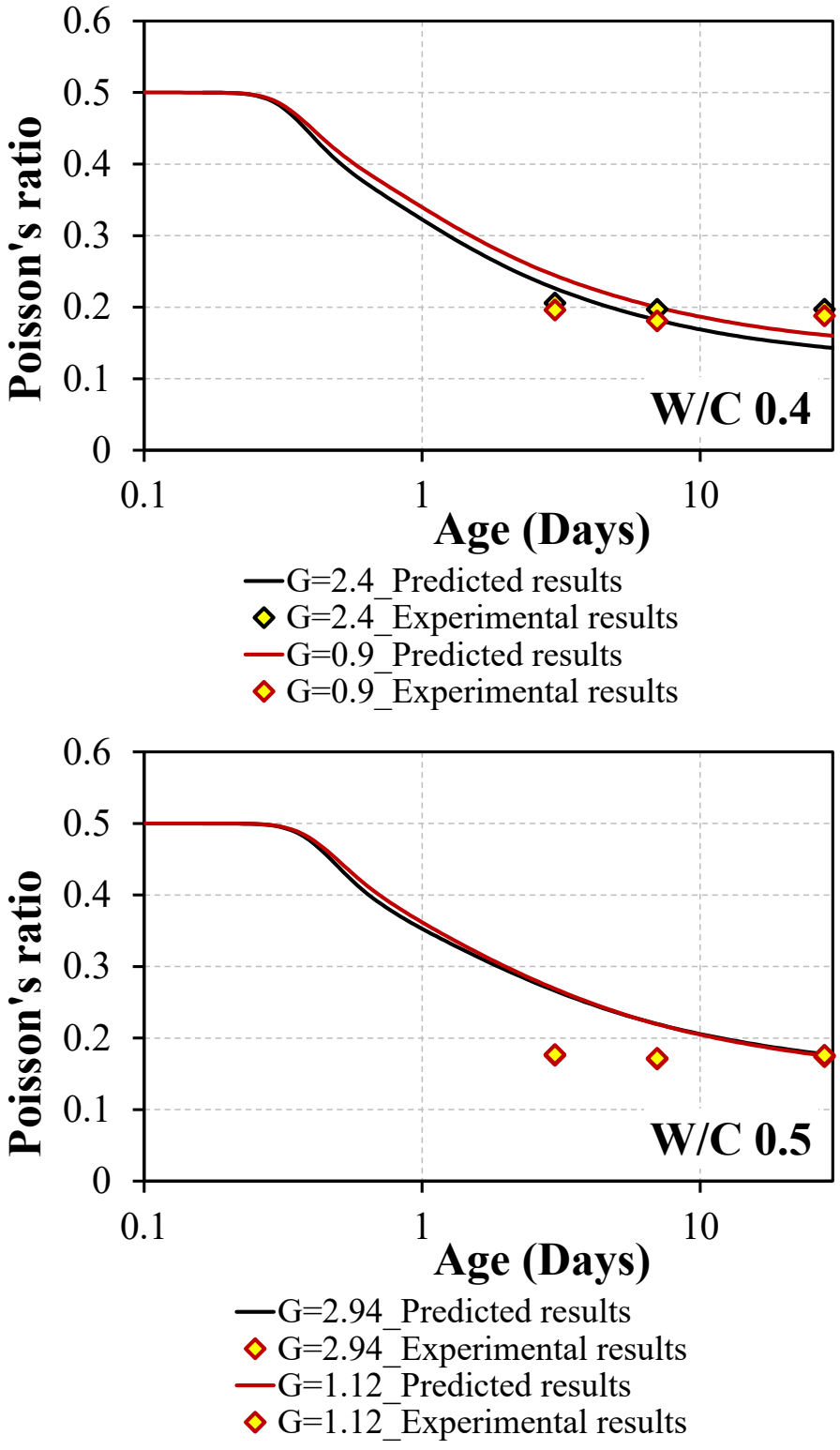

Figure 4.16: Validation of Poisson's ratio with hydration period for w/c ratio of 0.4 and 0.5 (G stands for weight ratio coarse aggregate/cement)

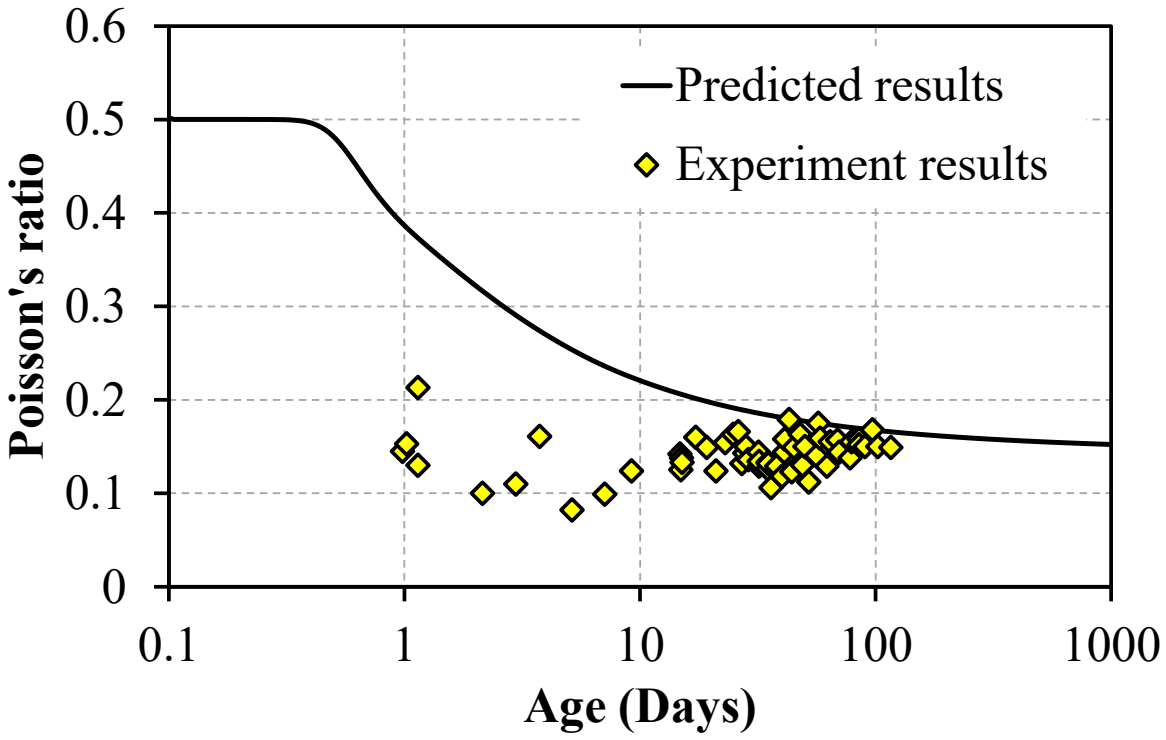

Figure 4.17: Validation of Poisson's ratio of concrete with hydration period (the experimental data were obtained from ref. (Allos and Martin, 1981))

4.3.6 Effect of ITZ on Young's modulus and Poisson's ratio of mortar and concrete

The Young's moduli of mortar and concrete computed with and without considering the ITZ are compared in **Figure 4.188** for different w/c ratios. The considered fine aggregate volume fraction for mortar is 0.6 and cement: fine aggregate: coarse aggregate weight ratio for concrete is 1: 1.5: 3.2. It is evident that the model overestimates the modulus when the effect of ITZ is neglected for both mortar and concrete **Figure 4.188(a)** and **Figure 4.188(b)**, respectively). Besides, the variation of Young's modulus between the cases of with and without ITZ decreases with increasing hydration period. As mentioned earlier, ITZ can also be considered as a distinct cement paste with low amount of clinker and high amount of water (Crumbie, 1994; Nadeau, 2002; Zheng, Zhou and Jin, 2012; Sharma and Bishnoi, 2020b). At

the early age, the ITZ remains the weakest region with very high amount of porosity. However, during the hydration process, the ITZ becomes hardened cement paste with increased mechanical properties. Owing to the above reason, the variation in later age appeared to be decreasing. Relatively a similar tendency can be observed for all the w/c ratios (**Figure 4.188**). However, the deviation observed for concrete (**Figure 4.188(b)**) is higher compared to the mortar results (**Figure 4.188(a)**), which is mainly due to the higher ITZ effect in concrete (attributing to fine aggregate and coarse aggregate). For instance, after one day of w/c for 0.4 mortar, the modulus of without-ITZ case is approximately 40 % higher than that of with-ITZ case, whereas the variation after 28 days is reduced to around 10 % (see **Figure 4.188(a)**). For the w/c 0.4 of concrete, after one day, the modulus of without-ITZ case is approximately 60 % higher than that of with-ITZ case, while the variation after 28 days is reduced to around 20 % (in **Figure 4.188(b)**).

The difference between with ITZ and without ITZ cases is observed to increase with w/c ratio for both the mortar and concrete. This could be due to the high migration of free water to the surface of aggregates for high w/c matrix. In fact, the rate of migration is higher for the paste with higher w/c ratios; as the result, there would be a higher w/c ratio in ITZ, while the remaining paste would have a lower ratio. Since the elastic properties of the matrix and the ITZ are directly related to the water content and their porous structure, greater migration process of the water (at higher w/c ratio) led to more negative effect on Young's modulus. Similar observation was reported by Simeonov and Ahmad (1995).

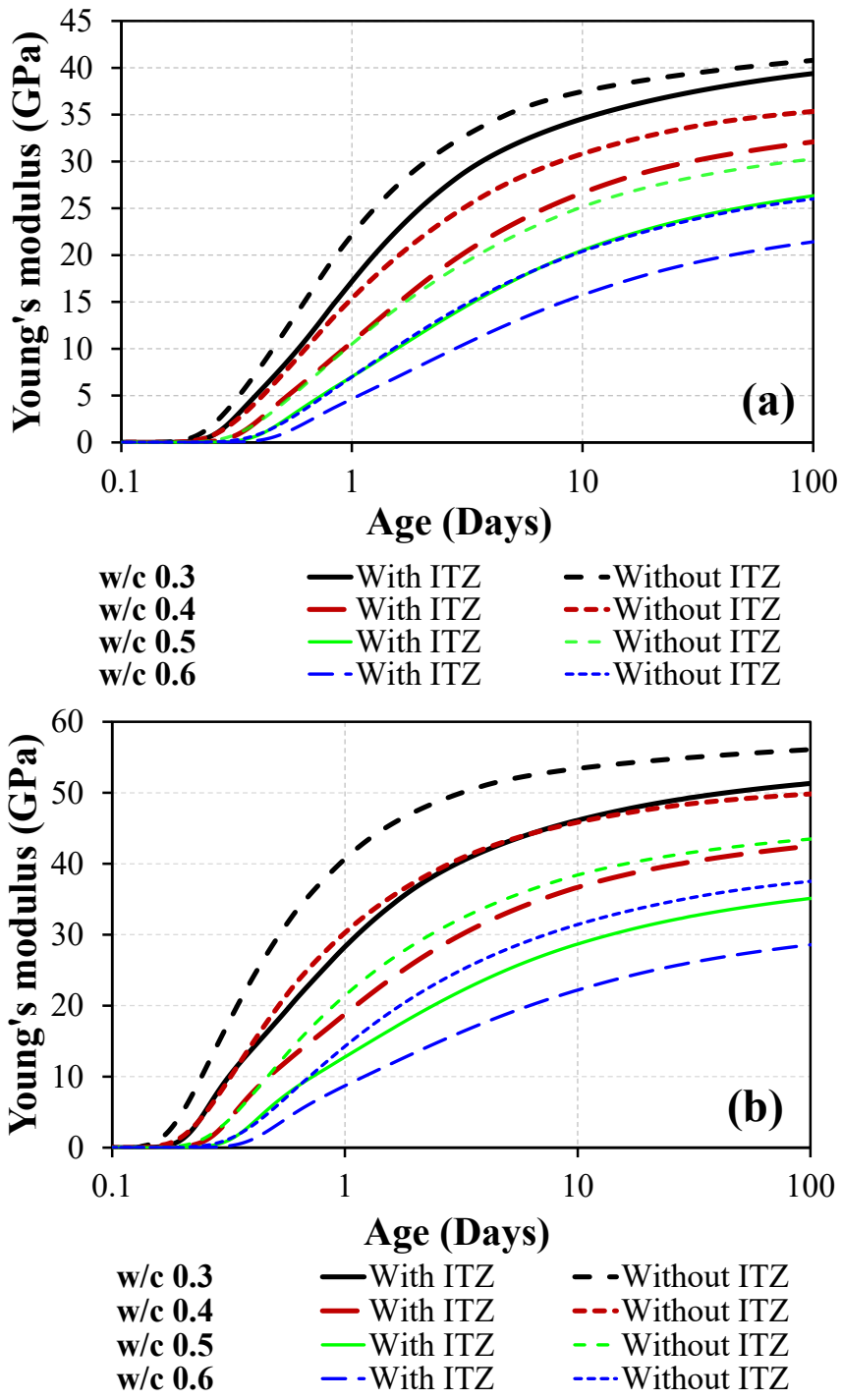

Figure 4.18: Comparison of predicted Young's modulus of (a) mortar and (b) concrete for the cases of with and without ITZ for w/c 0.3-0.6

The comparison of predicted Poisson's ratio of mortar and concrete for the cases with and

without ITZ is depicted in **Figure 4.199**. The results presented herein are corresponding to the w/c ratio of 0.3-0.6 and to the fine aggregate volume fraction of 0.6 for mortar whereas cement: fine aggregate: coarse aggregate weight ratio for concrete is 1: 1.5: 3.2. It can be seen that in the predicted results of both cases, the Poisson's ratio increases with increase in w/c ratio, which is in consistent with the tendency reported by Stefan et al. (2010). If the mortar and concrete is considered as two-phase matrix by neglecting ITZ, the effective Poisson's ratio is stiffer than that predicted for with-ITZ case for all w/c ratios as reflected in **Figure 4.199**. Moreover, the variation between the predicted results from both cases reduce with hydration period, which is probably because the mortar and concrete matrix become hardened solid including ITZ due to the hydration process of clinker. Nevertheless, the deviation observed for concrete (**Figure 4.199(b)**) is higher compared to the mortar results (**Figure 4.199(a)**), which is mainly due to the higher ITZ effect in concrete (attributing to fine aggregate and coarse aggregate). For instance, after one day of w/c for 0.4 mortar, the Poisson's ratio of without-ITZ case is approximately 10 % lower than that of with-ITZ case, whereas the variation after 28 days is reduced to around 2 % (see Figure 4.19(a)). For the w/c 0.4 of concrete, after one day, the Poisson's ratio of without-ITZ case is approximately 20 % lower than that of with-ITZ case, while the variation after 28 days is reduced to around 15 % (in **Figure 4.199(b)**). Moreover, similar to that observed in Young's modulus (refer to **Figure 4.188**), the variation between with and without ITZ cases increase with w/c ratio for both mortar and concrete.

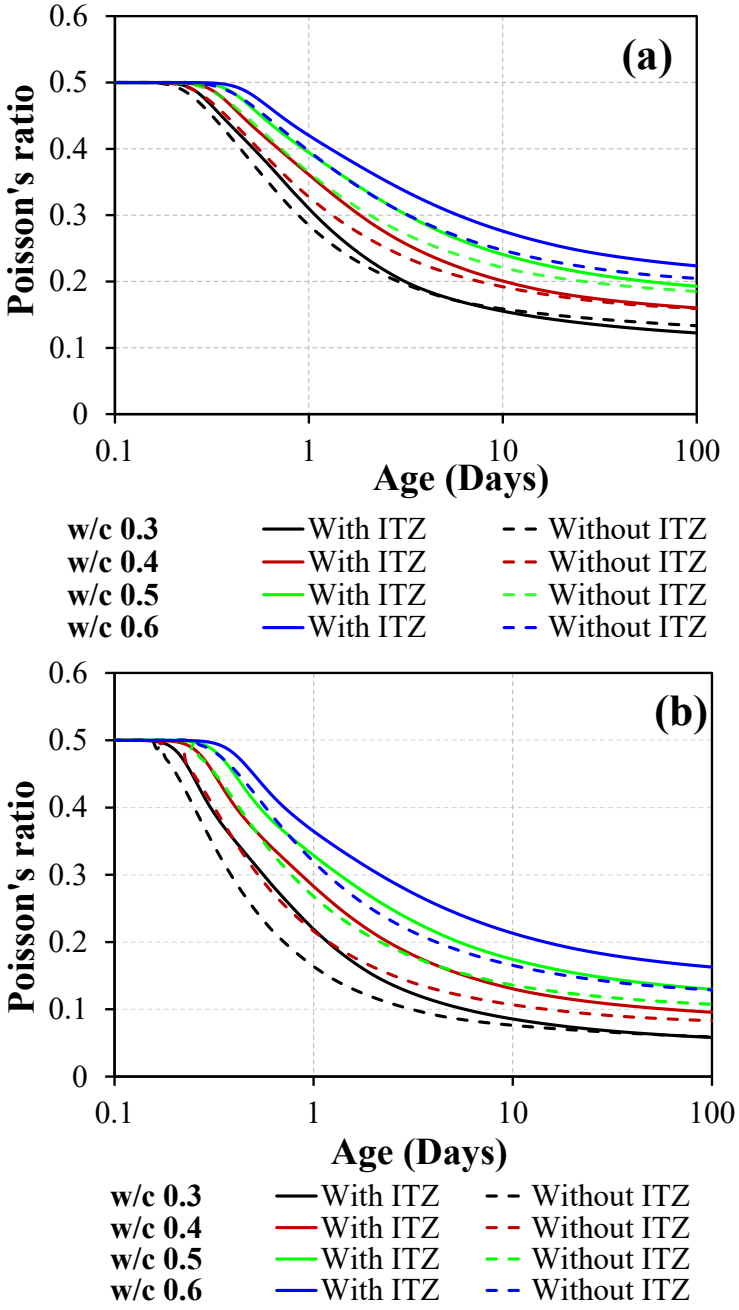

Figure 4.19: Comparison of predicted Poisson's ratio of (a) mortar and (b) concrete for the cases of with and without ITZ for w/c 0.3-0.6

4.4 Conclusions

In this research work, the mechanical properties such as Young's modulus and Poisson's ratio

of mortar and concrete were reliably predicted using the developed multi-scale model and homogenization method. The mortars and concretes were assumed as three-phase composites, and the ITZ for both coarse and fine aggregate were reliably considered as cement paste with high water content. The mechanical properties of ITZ and bulk paste were based on the detailed microstructure of hydrates during hydration reaction. The proposed models for mortar and concrete were validated with experiment results for wide range of aggregate contents and w/c ratios.

The predicted Young's modulus excellently captured the realistic behaviour for the w/c ratios ranging from 0.3 to 0.6 and aggregate content from 0.2 to 0.6. The computation of Poisson's ratio showed relatively good agreement with the experimental data for mortar and concrete. However, the model slightly overpredicted the Poisson's ratio at early stage (before 10 days) for concrete; thus, further validations are recommended with more independent experimental results to generalize the Poisson's ratio model of concrete. Moreover, the effect of ITZ on Young's modulus and Poisson's ratio were demonstrated using the proposed model for mortar and concrete. At the same time, the results predicted via typical way, i.e., two-phase model, was shown to reveal a stiffer material compared to that of both experiment results and three-phase model for both mortar and concrete. The effect of ITZ was higher for concrete compared to mortar due to the high amount of aggregates content.

Overall, the proposed novel three-phase models for mortar and concrete can be used to accurately predict the mechanical properties. One of the marked merits of this model is, if the chemical composition is known, the Young's modulus and Poisson's ratio can be computed, which would reduce the waste of time, cost, material and manpower compared to typical approaches.

CHAPTER 5

MODEL FOR MULTI-IONIC TRANSPORT PROPERTIES OF CEMENT PASTE DURING THE CHLORIDE INGRESSION AND CARBONATION

5.1 Introduction

Assessing the durability performance of both new and existing concrete structures remains one of the most significant challenges, particularly while considering the effective longevity of the structure. This is in turn dictated by the capability of the concrete structures for a large extent to resist numerous deterioration processes such as transportation of ions, gas (mainly carbon dioxide) and moisture, alkali-aggregate reactions and frost damage (Hatanaka et al., 2003; Gasch, Eriksson and Ansell, 2019). Worth to note that among the varying processes, chloride ingression and carbonation are most serious degradation processes in reinforced concrete structures, specifically for those exposed to such environments as air-bone chlorides in marine regions, and deicing salts in cold regions (Chindaprasirt, Rukzon and Sirivivatnanon, 2008; Q. F. Liu et al., 2014; Xie, Dangla and Li, 2021). Under these environments, the processes occur concurrently, thus leading to increase the risk of reinforcement corrosion. The transport of ions further involves chemical reactions between hydration products and pore solution, causing dissolution and precipitation in the hydrated matrix.

The diffusion of chloride ion into the hydrated matrix is mainly influenced by internal factors

such as pore structure and the hydration products which are determined by the type of cement (physical and chemical properties), water to cement ratio (w/c), curing method such as sealed curing, water curing ant etc., curing temperature, hydration period, exposure period and additives (Hosokawa, Yamada and Takahashi, 2012), and the concentration of the exposure solution is the major external factor. After entering of the chloride ion in pore network, due to the binding mechanism such as physical binding and chemical binding, the amount of free chloride in the pore solution suddenly decreases. Chemical binding refers the reaction of chloride ion with AFm phases. Generally, the reaction of gypsum with aluminate (C3A) produces ettringite, and further reaction of C3A with ettringite forms monosulfate which is the commonly available AFm phase in the OPC (Tennis and Jennings, 2000b; Krishnya, Yoda and Elakneswaran, 2021). The sulfate ions in the monosulfate phase exchange with chloride ions at their presence, and the formed phase is referred to as Friedel's salt (Jones et al., 2003; Sui et al., 2019) Moreover, the physical binding of chloride ion is the best known that is by the surface of the C-S-H as it is the main hydration products in OPC and having high specific surface area (Elakneswaran, Nawa and Kurumisawa, 2009; Florea and Brouwers, 2012; Guo et al., 2018). The bound chloride by precipitation of Friedel's salt or adsorbed by C-S-H has no effect on the corrosion of steel bars. On the other hand, the free chloride in the pore solution causes the reinforcement corrosion in the concrete structure (Maruya et al., 2003; Hirao et al., 2005). The free chloride ions destroy the thin protective passive film covered on the rebar due to the penetration of chloride ions into the pore solution which exceeds the threshold level after a certain exposure period, and finally, this leads to the initiation of corrosion in the reinforced structure (Hirao et al., 2005; Elakneswaran, Nawa and Kurumisawa, 2009; Guo et al., 2021). Therefore, it is truly significant to consider the chloride binding mechanism (physical and chemical) while developing a chloride ion transport model.

Carbonation of cement-based material is another complex process, altering the microstructural properties and performance of material underneath atmospheric conditions. The CO_2 gas reaction with hydrated matrix followed by the diffusion of CO2 gas via the pore network is generally referred to as the carbonation process. Almost all the concrete structures need to tolerate a certain level of carbonation reaction during their lifetime owing to the existence of CO_2 gas in the earth. However, this is a slow process, generally being considered as a part of prolonged degradation of concrete. Most of the hydration products (mainly portlandite (CH) and C-S-H) are consumed by the carbonation process and transformed to carbonate phases such as calcite, monocarboaluminate, hemicarboalumitae, amorphous silica gel, amorphous alumina gel and gypsum (Šavija and Luković, 2016; von Greve-Dierfeld et al., 2020; You et al., 2022). Moreover, decreasing of pH in carbonation is the utmost significant effect in the hydrated matrix, as the corrosion of reinforcement is accelerated by low pH due to the dissolution of thin oxide passive layer protecting the steel bars at lower alkaline conditions (Phung et al., 2016). Alternatively, carbonation shows positive effects in cement-basted material. During the carbonation process, the deposition of carbonation products (mainly calcite and silica gel) occurs in pores, benefitting to matrix densification and contributing to the development of mechanical properties and to the decrease of the transportation of hazardous ions (Phung et al., 2016; Song et al., 2021).

Coupling the transport processes and reactions between the transport of ions and solid phases for simulating the realistic changes of the porous matrix have gained a great deal of interest among researchers (Bary and Sellier, 2004; Elakneswaran et al., 2010; Azad et al., 2016; Phung et al., 2016; Guo et al., 2018; Shen et al., 2019; Omikrine Metalssi, Aït-Mokhtar and Turcry, 2020; Xie, Dangla and Li, 2021). Once, Elakneswaran et al.,(2010) developed a multi-

ionic transport model using the PHREEQC for transportation and phase assemblage calculations by considering the phase equilibrium module, surface complexation module and multi-component diffusion module. Afterwards, the finite element software called COMSOL Multiphysics was combined with geochemical program (PHREEQC or GEMS) to compute the transport and reaction calculation using computer languages such as Java and MATLAB (Azad et al., 2016; Guo et al., 2018). The transportation of carbon dioxide gas was modelled by several researchers to understand the solid phases and porosity changes in the hydrated matrix by using the simple numerical and empirical modelling approach (Bary and Sellier, 2004; Phung et al., 2016; Omikrine Metalssi, Aït-Mokhtar and Turcry, 2020). For another instance, the combined effect of transportation of both carbon dioxide and chloride ion on the phase assemblage, porosity and content of free chloride ion was analytically investigated by considering different aspects such as relative humidity, temperature and concentration of carbon dioxide gas (Shen et al., 2019; Xie, Dangla and Li, 2021).

For modelling the transport properties, incorporation of hydration process, chemical reaction, transportation process and appropriate coupling among them are essential. However, due the complexity of the coupling process, most of the previously developed models did not consider the hydration reaction simultaneously with transportation process (Bary and Sellier, 2004; Phung et al., 2016; Guo et al., 2018; Shen et al., 2019; Omikrine Metalssi, Aït-Mokhtar and Turcry, 2020; Xie, Dangla and Li, 2021). In most of them, hydrated matrix was assumed to be fully saturated, and gas phase was assumed to be nil in the pore solution (Guo et al., 2018) (Phung et al., 2016). The models did not consider the detail chemical reaction occurring inside the hardened cement matrix, instead C-S-H and portlandite were assumed as hydration products and calcite was as carbonate phase (Phung et al., 2016; Shen et al., 2019; Xie, Dangla

and Li, 2021). Yet, in reality, there are several other hydration products including C-S-H, portlandite, ettringite, monosulfate, silicious hydrogarnet, Friedel's salt (from as chloride phase), calcite, carboaluminate phases (mono carboaluminate and hemicarboaluminate), silica gel and alumina gel forming during the reaction of carbon dioxide with hydration products. Their progression influences the pore structure of the matrix and the ion concentration in pore solution. Therefore, addressing the limitations found in the beforehand models, a new model named as HyMeC-COMSOL is proposed here to predict the (i) transportation of chloride ion and carbon dioxide gas and (ii) phase assemblage due to the transportation process.

A modeling platform, HyMeC (Hydration and Mechanical properties of Cement based material) is coupled with COMSOL Multiphysics to enable the simulation of complex process simultaneously i.e., the hydration and transportation reaction. The HyMeC model consists of cement hydration model, thermodynamic model (PHREEQC), volume fraction model and multi-scale model to predict the hydration products and mechanical properties of cement paste. The proposed model considers the two types of C-S-H (low density C-S-H and high density C-S-H) and detail calculation of chemical shrinkage for the realistic prediction of porosity which is the significant factor for predicting the mechanical and transport properties. The finite element package, COMSOL Multiphysics is integrated with HyMeC model to solve the transportation calculation effectively under the saturated and partially saturated condition of the hydrated matrix. Phase assemblage and porosity after the transportation calculation is used to predict the mechanical properties of the cement paste with hydration period and distance from the exposure surface. The proposed model is validated with experimental results reported in the previous studies. Moreover, the effect of coupled

hydration reaction with reaction due to the transport of ion and gas are also discussed.

5.2 Methodology

A new multi-species reactive transport model is developed by combining cement hydration model, thermodynamic model, volume fraction of hydrates and transport model to predict the intrinsic properties of hydrated cement paste during the exposure of different environmental conditions such as sea water. The details and the flow of the proposed coupled transport model is illustrated in **Figure 5.1**. The necessary input parameters for the hydration model are clinker composition and physical properties of cement, mixing proportions and boundary conditions, whereas ionic concentration in the exposed environment, beginning of transport reaction relative to hydration time step and duration of the transport reaction are required for the transportation model as depicted in **Figure 5.1**. The adopted approach used herein to predict the hydration products and transport properties of hydrated cement matrix is widely described below.

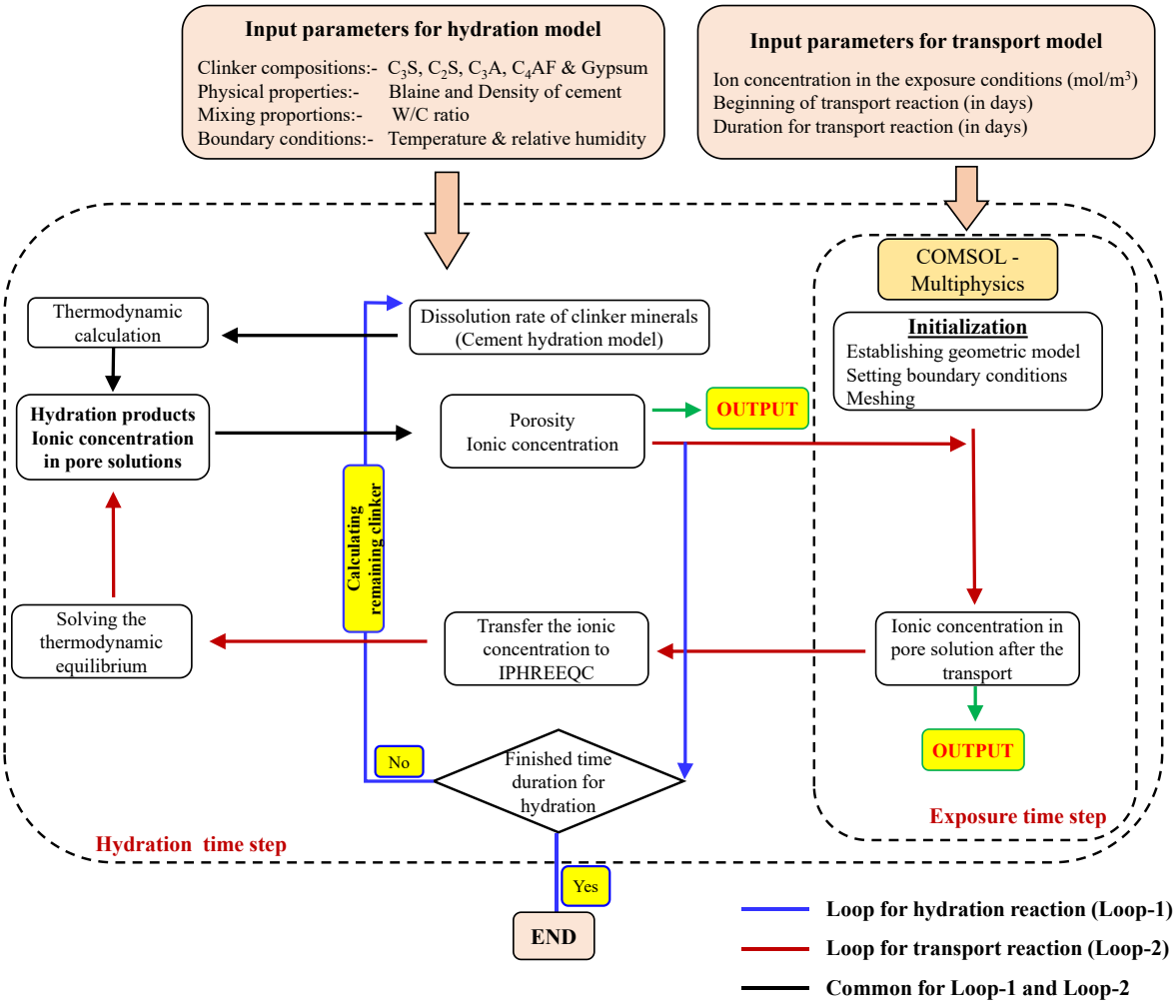

Figure 5.1: Structure of developed transport model

5.2.1 Cement hydration model

The cement hydration model (L.J. Parrot and Killoh, 1984), verified in several studies reported in the previous works (Lothenbach, Matschei, et al., 2008; Feng, Miao and Bullard, 2014; Lavergne et al., 2018), is used herein to compute the dissolution rate of each clinker minerals in the cement such as C_3S, C_2S, C_3A and C_4AF as a function of time. The detail of the cement hydration model is described in our previous work (Krishnya, Yoda and Elakneswaran, 2021). Based on the calculated reaction degree of each mineral (α_{C_3S}, α_{C_2S},

α_{C_3A} and α_{C_4AF}), total degree of hydration (α_f) for a specific time step is calculated as described in Eq. (5.1).

$$\alpha_f = \frac{\alpha_{C_3S}.W_{C_3S} + \alpha_{C_2S}.W_{C_2S} + \alpha_{C_3A}.W_{C_3A} + \alpha_{C_4AF}.W_{C_4AF}}{W_{C_3S} + W_{C_2S} + W_{C_3A} + W_{C_4AF}} \quad (5.1)$$

where, W_{C_3S}, W_{C_2S}, W_{C_3A} and W_{C_4AF} are mass fraction of each clinker phases.

The dissolved clinker phases calculated based on cement hydration model release Ca, Si, O, Al and Fe ions into the pore solution. Minor component in the clinker such as Na_2O, K_2O and MgO dissolve as the function of total degree of hydration (α_f) for a specific time step and release Na, K, Mg and O ions into the pore solution.

5.2.2 Thermodynamic model

Thermodynamic calculations, which are linked with the precise thermodynamic database of Cemdata18 (Lothenbach et al., 2019) and PHREEQC default thermodynamic database (Parkhurst and Appelo, 1999), are performed using the Geochemical software called PHREEQC. Mainly, phase equilibrium module and surface complexation module are used to predict the solid phases and ions concentration in the pore solutions based on the results of reaction module. The computed dissolved clinker phases and minor components are inputted in the reaction module for every time step. The phase equilibrium module is basically used to estimate the amount of phases which react reversibly with pore solution to achieve equilibrium condition. In PHREEQC, the reaction of equilibrium phases are based on law of mass action (Elakneswaran et al., 2010; Krishnya, Yoda and Elakneswaran, 2021). C-S-H, portlandite, gypsum, ettringite, monosulfate, calcite, hemicarbonate, monocarbonate, hydrotalcite, brucite, stralingite, Fe-Al-silicieous hydrogarnet, Friedel's salt, amorphous

silica and amorphous alumina gel are considered equilibrium phases in the proposed model.

The surface complexation reactions are used to compute the ionic adsorption on the surface of C-S-H. This surface complexation reaction is computed via mole-balance equations, charge-potential relations for surfaces and law of mass action in PHREEQC (Elakneswaran et al., 2010). Among the two types of surface sites in C-S-H such as silanol site ($\equiv SiOH$) and silandiol ($= Si(OH)_2$), silanol site reacts with ions in the pore solution as per the previous studies (Elakneswaran et al., 2010; Guo et al., 2018). The site reactions on silanol site and the equilibrium constants are shown in Table 5.1.

Table 5.1: C-S-H surface site reactions and equilibrium constants

Site reactions	$\mathbf{LogK_p}$
$\equiv \boldsymbol{SiOH} + \boldsymbol{OH^-} \leftrightarrow \equiv \boldsymbol{SiO^-} + \boldsymbol{H_2O}$	-12.7
$\equiv \boldsymbol{SiOH} + \boldsymbol{Ca^{+2}} \leftrightarrow \equiv \boldsymbol{SiOCa^+} + \boldsymbol{H^+}$	-9.4
$\equiv \boldsymbol{SiOH} + \boldsymbol{Ca^{+2}} + \boldsymbol{Cl^-} \leftrightarrow \equiv \boldsymbol{SiOCaCl} + \boldsymbol{H^+}$	-8.9
$\equiv \boldsymbol{SiOH} + \boldsymbol{Na^+} \leftrightarrow \equiv \boldsymbol{SiONa} + \boldsymbol{H^+}$	-13.64
$\equiv \boldsymbol{SiOH} + \boldsymbol{K^+} \leftrightarrow \equiv \boldsymbol{SiOK} + \boldsymbol{H^+}$	-13.64

Kinetic model for C-S-H

During the diffusion of carbon dioxide, the dissolutions of portlandite and C-S-H occur simultaneously, even though the portlandite has the priority than the C-S-H carbonation from thermodynamics perspective (Morandeau, Thiéry and Dangla, 2014). Therefore, a kinetic model is adopted herein for computing the dissolution rate of C-S-H ($rate$) with portlandite as shown in Eq. 5.2.

$$rate = R_1.\ \exp(\gamma_{CO2}\ .\ R_W)\ .\ M_{CSH}.\ M_{CO2} \quad (5.2)$$

where,

$$R_W = \frac{W_{carb\ CSH}}{W_{tot\ CSH}} \quad (5.3)$$

R_1 = 0.0005, γ_{CO2} = 0.2

$W_{carb\ CSH}$, $W_{tot\ CSH}$, M_{CSH}, and M_{CO2} are weight of carbonated C-S-H, Weight of initial C-S-H, mol of C-S-H and mol of CO_2 respectively.

5.2.3 Volume fraction of hydration products

The total weight of C–S–H matrix predicted from the thermodynamic model was further distinguished as LD C–S–H and HD C–S–H using the relationship proposed by Tennis and Jennings (2000). The average densities of both C–S–H were obtained from the literature (Jennings et al., 2007), 2000 kg/m^3 and 1700 kg/m^3 for HD and LD C–S–H respectively. Due to molar volume difference of the hydration products and clinker minerals, there is a reduction in the sum of reaction products compared to reactants during the hydration process, and this difference can be defined as chemical shrinkage. The detail chemical shrinkage calculation for each reacted clinker phases was carried out based on the chemical shrinkage coefficients of each phases proposed by Bentz, Lura and Roberts, (2005). The volume of all the other hydration products was computed by using their molar volumes. Finally, the capillary porosity of the cement matrix was estimated as balance of the system, obtained from the difference between initial volume and final volume of hydration products, chemical shrinkage and unreacted clinker minerals as described in Eq. (5.4).

$$\emptyset_{Cap} = V_i - (V_{UC} + V_{HP} + V_{CS}) \quad (5.4)$$

where, $\emptyset_{Cap}$ is volume of capillary porosity, V_{CS} is chemical shrinkage, V_i is initial volume of cement paste, V_{UC} is volume of unreacted clinker and V_{HP} is volume of hydration products.

5.2.4 Transport model

The governing equation used in COMSOL Multiphysics for variably saturated flow is described in equations from Eq. (5.5) to Eq. (5.9).

$$\frac{\partial(\theta_l C_{l,i})}{\partial t} + \frac{\partial(\theta_g C_{g,i})}{\partial t} + \nabla . J_i = Q_i \tag{5.5}$$

$$\theta_l = \emptyset . S \tag{5.6}$$

$$\theta_g = \emptyset(1 - S) \tag{5.7}$$

$$C_{g,i} = k_i . C_i \tag{5.8}$$

$$\frac{\partial(\theta_g C_{g,i})}{\partial t} = \theta_g k_i . \frac{\partial(C_i)}{\partial t} + k_i C_i . \frac{\partial(\theta_g)}{\partial t} \tag{5.9}$$

where, J, C_l, C_g, C and Q are ionic flux (mol/m^2/s), concentration of species in the liquid phases (mol/m^3), concentration of species in the gas phase (mol/m^3), total concentration (mol/m^3) and sink term (mol/m^3/s) of the ion i respectively. $\emptyset$, S and k are porosity, saturation degree and volatilization factors correspondingly. The total flux in the porous media can be defined by Eq. (5.10)

$$J = J_{l,i} + J_{g,i} \tag{5.10}$$

The ionic flux in liquid phase ($J_{l,i}$) can be expressed using Nernst-Planck equation as shown

in Eq. (5.11).

$$J_{l,i} = -D_{e,l,i}.\nabla C_{l,i} - D_{e,l,i}C_{l,i}.\frac{Z_i F}{RT}.\nabla\varphi \quad (5.11)$$

The flux in gas phase ($J_{g,i}$) is illustrated in Eq. (5.12)

$$J_{g,i} = -D_{e,g,i}.\nabla C_{g,i} \quad (5.12)$$

where, $D_{e,l}$, $D_{e,g}$, Z, F, R, T and φ are respectively the effective diffusion coefficient in liquid (m^2/s), effective diffusion coefficient in gas (m^2/s), electric charge number, the Faraday constant, the universal gas constant, absolute temperature and electrical potential (V). The effective diffusion coefficient in liquid ($D_{e,l}$) can be defined by Archie's law (Eq. 5.13) (Appelo and Postma, 2004).

$$D_{e,l,i} = D_{f,i}(\emptyset S)^{\varepsilon} \quad (5.13)$$

where $D_{f,i}$ is the diffusion coefficient in water, and the considered values are tabulated in **Table 5.2:** Diffusion Coefficient of ions in free water at 20 °C.

Table 5.2: Diffusion Coefficient of ions in free water at 20 °C

Ion	Diffusion coefficient x 10^{-9} (m^2/s)
Na^+	1.33
Cl^-	2.03
K^+	1.96
Ca^{+2}	0.793
Mg^{+2}	0.705
$SO4^{-2}$	1.07
OH^-	5.27

The effective diffusion coefficient in gas phase ($D_{e,g}$) can be defined as revealed in Eq. (5.14).

$$D_{e,g,i} = D_{g,i}\emptyset^{\varepsilon}(1-S)^{n} \quad (5.14)$$

where, D_g and ε are diffusion coefficient in air and tortuosity. The tortuosity is normally between 2.4 to 3 for cement-based materials and *n* is assumed as 4.2 based on the previous studies (You *et al.*, 2022).

During the ion diffusion process in liquid, the electrical current in the cement-based material is zero, and which therefore implies,

$$\sum_i Z_i j_i = 0 \quad (5.15)$$

By combining Eq. (5.5), (5.10) and (5.15), the concentration profile of each ion with distance from the exposure surface is calculated in this work. The relation between the relative humidity (RH) and the saturation degree (S) is given by the inversion of the desorption isotherm expression based on previous studies as shown in Eq. (5.16) (Bary and Sellier, 2004).

$$S_r = \alpha RH^3 + \beta RH^2 + \gamma RH + \delta \quad (5.16)$$

where, $\alpha = 6.43,\ \beta = -15.46,\ \gamma = 12.52,\ \delta = -2.5$

5.2.5 Coupling approach

This proposed model is developed in MATLAB language, and the required input parameters can be updated through excel file which is convenient to user. The following steps involve in the coupling process.

Step 1: - After entering all the required parameters, the model starts the calculation by reading

the input parameters from the specific excel file and calculate the dissolution rate of each clinker phases and minor phases using cement hydration model (refer section 5.2.1).

Step 2: - The calculated dissolved minerals are transferred to thermodynamic calculation to compute the amount of hydration products and ion concentration in the pore solution by using the phase equilibrium module in PHREEQC (see section 5.2.2).

Step 3: - The capillary porosity of the matrix is computed based on the two types of C-S-H, other hydration products, unreacted clinker and chemical shrinkage of the reacted clinker (section 5.2.3). These three steps repeat until the beginning of the exposure condition which can be defined by the user (see input parameters for transport calculation in **Figure 5.1**).

Step 4: - The calculated ions concentration in pore solution and porosity at the beginning of the exposure are used as the initial conditions for the transport calculation, and they are transferred to COMSOL Multiphysics via LiveLink™ for MATLAB® feature available in COMSOL. Based on the defined exposure condition and time step, the ions concentration profiles are predicted using the relationship explained in section 5.2.4 in COMSOL.

Step 5: - Afterwards, the predicted ionic concentration with exposure distance is updated to the thermodynamic calculation to compute the amount products and ion concentration using phase equilibrium and surface complexation module, in order to maintain the thermodynamic equilibrium.

Step 6: - As the next step of this model, the outcome of the thermodynamic calculation due to the transport of ion are used to react with dissolved clinker minerals for continuing the hydration reaction using the PHREEQC package.

Step 7: - The predicted products are then converted to volume fraction for calculating the capillary porosity at that time step (similar to Step 3)

Step 8: - The ion concentration after the hydration reaction (outcome of Step 6) is input to COMSOL Multiphysics as the initial parameters for next time step (similar to Step 4).

These whole procedures are repeated until reach the final time step which is defined by the user. In this research work, Na^{+}, K^{+}, Ca^{+2}, $H2SiO4^{-2}$, $SO4^{-2}$, Cl^{-} and OH^{-} are mainly considered ions in the pore solution for participating in the transportation process.

5.3 Results and Discussion

5.3.1 Model validation with PHREEQC transport model

Figure 5.2 and **Figure 5.3** depict validation of the proposed transport model (HyMeC-COMSOL) with transport model developed in PHREEQC (Elakneswaran et al., 2010). The Ordinary Portland cement (clinker composition: C_3S 62.2%, C_2S 18.3%, C_3A 5.6% C_4AF 9.8% and Gypsum 3%, density: 3.16 g/cm^3, Blaine: 311 m^2/kg) with w/c of 0.4 and temperature of 20 °C are used as the initial condition for the hydration model. The cement paste was exposed to 500 mol/m^3 of NaCl solution after the 28 days of hydration for 30 days (input parameter for transport model). As shown in **Figure 5.2** and **Figure 5.3,** the predicted results from the proposed model exhibit a very good agreement with the results from the PHREEQC model. However, the ion concentration profile for Ca^{+2} ion shows slight deviation only up to 2.5 mm from the exposed surface, and with further increase, it coincides with the results from the PHREEQC model. The reason could be that the concentration of exposure solution is not constant during the transportation process due to the leaching and diffusion of

ions. However, in the proposed model, the specified exposure solution by user is updated for every time step in order to simulate the actual condition like sea water exposure. Therefore, the concentration of leaching ions including Ca^{+2} does not accumulate in the exposure solution, while Ca^{+2} concentration accumulates in previous PHREEQC model.

The concentration of Na^{+} and Cl^{-} are approximately 500 mol/m^3 at the exposed surface due to the high concentration of exposure solution (500 mol/m^3 of NaCl), and then the concentrations of both ions gradually decrease with the distance from the exposed surface as shown in **Figure 5.2**. However, after 30 mm from the exposed surface, the Cl^{-} concentration becomes 0. This could possibly be attributed to the fact that the normal Portland cement does not contain Cl^{-}, and Na^{+} concentration is approximately 180 mol/m^3 which is the initial concentration of Na^{+} from the 28 days of hydration reaction before the diffusion process. The concentration profile of K^{+} shows an increasing tendency with distance up to 30 mm, followed by a constant value of 225 mol/m^3 which is same as before the transport reaction from the hydration reaction. The K^{+} ion is not available in the exposure solution. Therefore, the K^{+} leaches from the pore solution to exposure solution through diffusion process due to the concentration gradient between the exposure solution and pore solution (in cement matrix). Similar tendency in the experimental results was also reported by Elakneswaran et al., (2010). Hence, the concentration of K^{+} ions decreases near to the exposed surface.

Moreover, the pH of the exposure solution and pore solution are about 7.0 and 13.5 respectively. Similar to the leaching of K^{+}, the OH^{-} ion also leaches to the exposure solution due to the concentration gradient. Therefore, pH near to the exposed surface is lower compared to that away from the exposed surface (refer **Figure 5.2**). Furthermore, the Ca^{+2} concentration profile increases to 5.5 mol/m^3 till 2.5 mm (due to the leaching of Ca^{+2}),

decrease to 1.5 mol/m^3 and then unchanged. The peak of the Ca^{+2} profile is due to the dissolution of portlandite (CH) which gives more Ca^{+2} ions in the pore solution as shown in **Figure 5.2** and **Figure 5.3**. It can be noticed that the portlandite mainly dissolves near to the exposed surface due to the leaching of Ca^{+2} in the pore solution and low pH.

The penetrated Cl^- ion is possible to substitute the sulfate ions in AFm type products like monosulfate to forms chloride containing phases like Friedel's salt as described in Eq. (5.15). In addition, SO_4^{-2} from the Friedel's salt reaction released form dissolution of monosulfate reacts with existing monosulfate to form the secondary ettringite close to the exposed surface (see Eq. 5.16). As the results, Friedel's salt and considerably high amount of ettringite can be found near to the exposed surface, where monosulfate does not appear in the presence of Cl^- ion. As illustrated in **Figure 5.3**, the formation of Friedel's salt and slightly higher amount of ettringite could be seen up to only 15 mm, and afterwards, monosulfate exists. Similar observations were also reported in the several previous studies (Hirao et al., 2005; Elakneswaran et al., 2010; Florea and Brouwers, 2012; Guo et al., 2018).

$$C_3A.CaSO_4.12H_2O + Cl^- \rightarrow C_3A.CaCl_2.10H_2O + SO_4^{-2} \quad (5.15)$$

$$C_3A.CaSO_4.12H_2O + Ca^{+2} + SO_4^{-2} \rightarrow C_3A.3CaSO_4.32H_2O \quad (5.16)$$

As depicted in **Figure 5.3**, at the exposed surface, the porosity is very high, approximately 27%, due to the high dissolution of portlandite up to the point where portlandite dissolves. Afterwards, the porosity remains slightly lower due to the formation of secondary ettringite up to 15 mm, where the high amount of ettringite exists. The porosity value of 19.4% is in the hydrated matrix away from the degraded area. The amount of C-S-H, Fe-siliceous hydrogarnet and hydrotalcite do not show either dissolution or precipitation during the 30

days of transport of ion reactions, revealing constant values as 0.24 mol, 0.023 mol and 0.008 mol for the whole length of specimens respectively.

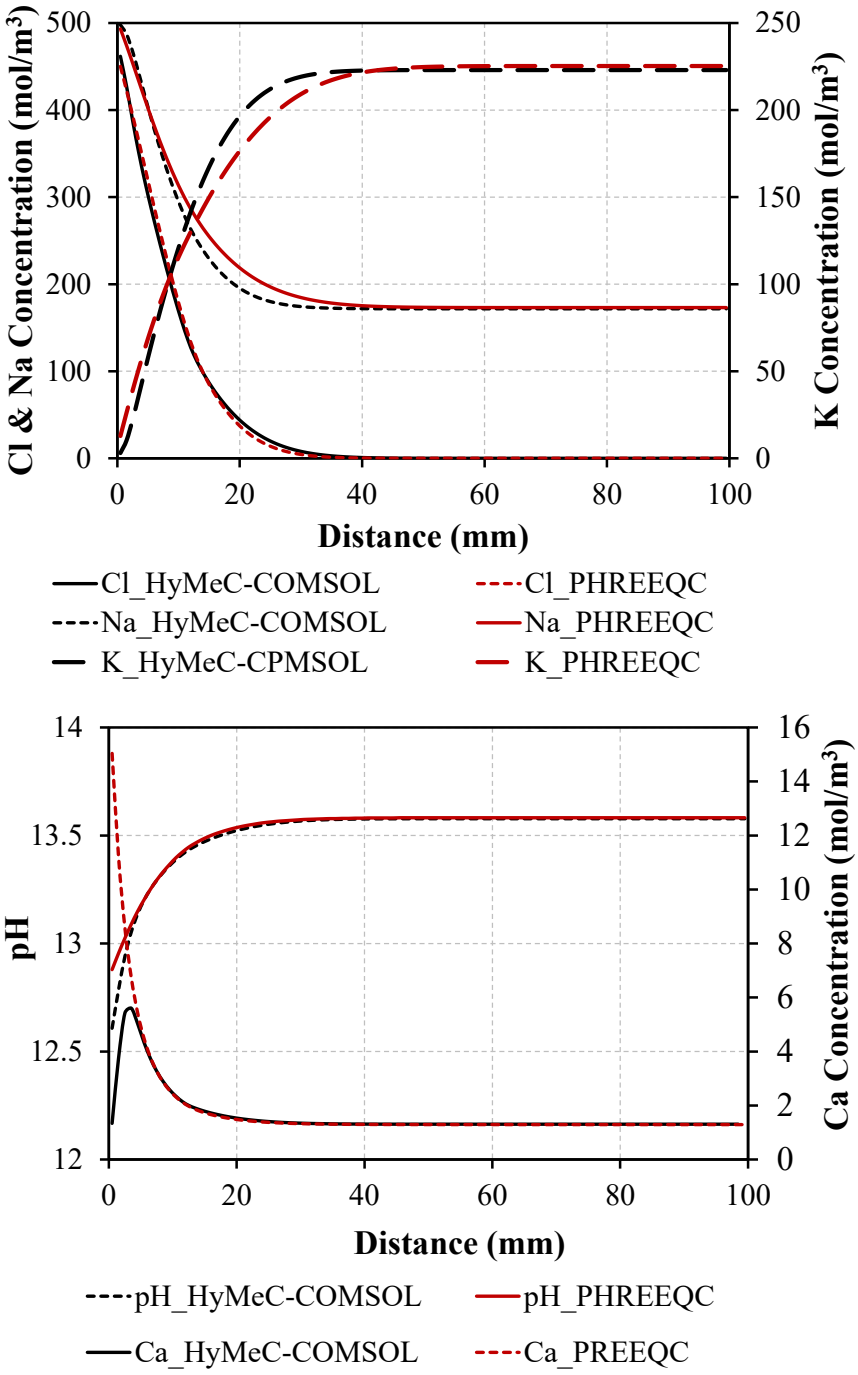

Figure 5.2: Validation of ionic concentration in the pore solution with PHREEQC model

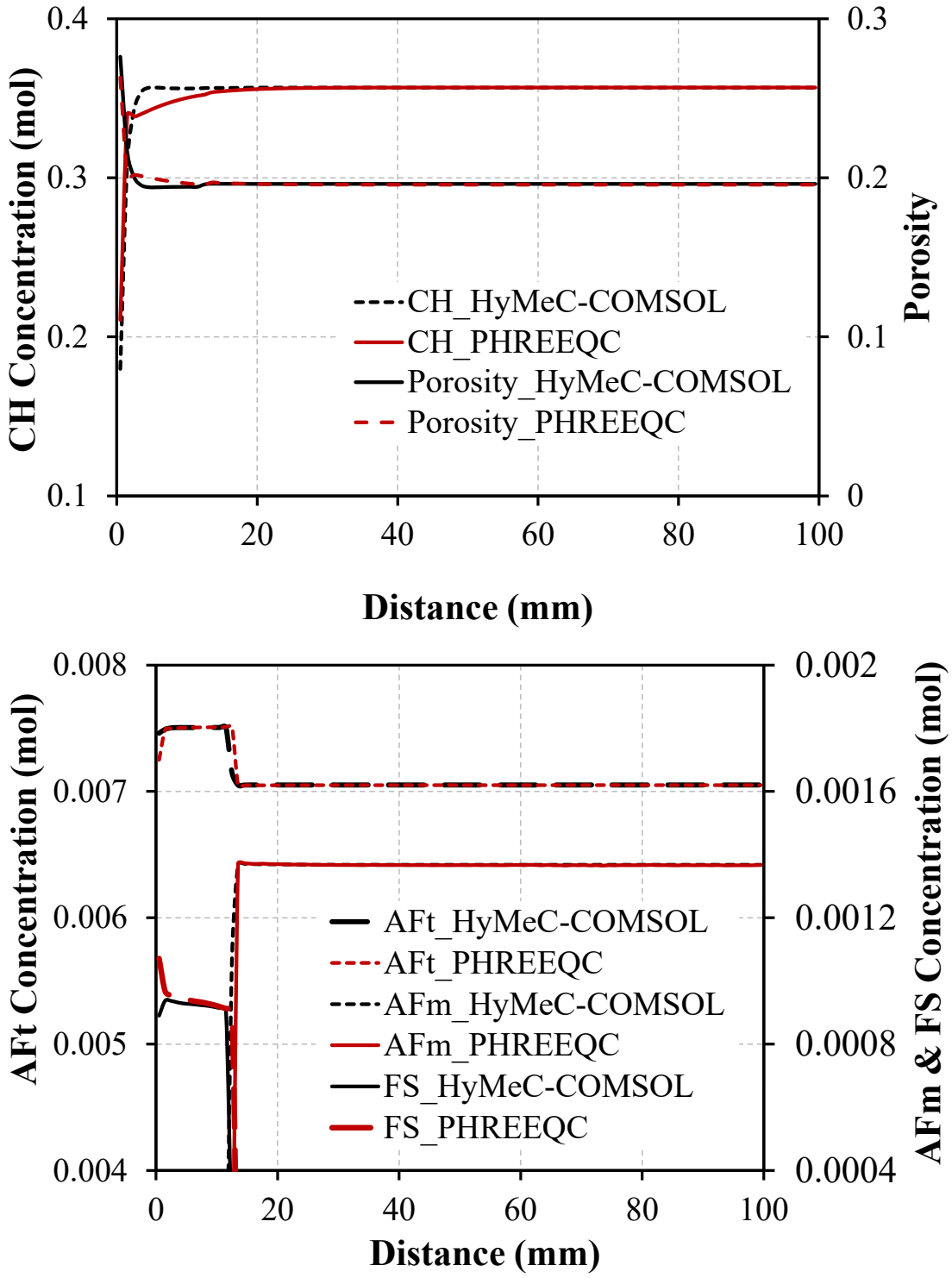

Figure 5.3: Validation of hydration products with PHREEQC model (CH, AFt, AFm and F-S stand portlandite, ettringite, monosulfate and Friedel's salt respectively)

5.3.2 Verification of chloride profile with experimental results

To verify the predictability of the proposed model, the predicted results of total amount of chloride ion profile is compared with experimental results for w/c of 0.3, 0.4 and 0.5 which has been taken from the study of Mori et al., (2006). The chemical composition of the clinker used for the simulation is C_3S 65%, C_2S 11%, C_3A 9% C_4AF 9% and Gypsum 4% (density: 3.16 g/cm^3, Blaine: 323 m^2/kg and temperature 20 °C). Similar experimental condition that after the 28 days of hydration samples were kept in 3% of NaCl solution for 91 days, was used in the proposed model to predict the chloride ion diffusion in the hydrated matrix. As detailed in **Figure 5.4**, the proposed model shows excellent prediction for w/c ranging from 0.3-0.5. However, the proposed model slightly underestimates in some places like 11-15 mm for w/c 0.5, 9-11 mm for w/c 0.4 and 6-7 mm for w/c 0.3. This is mainly due to the formation of Friedel's salt, leading to the sudden drop in the predicted profile. But there is no such rapid drop in the experimental results. In fact, the formation of Friedel's salt is controlled by clinker phases such as C_3A, C_4AF and gypsum. Due to the unavailability of the clinker composition in the reported study, the ordinary Portland cement (normally used in Japan) is considered for predictions, and which might possibly be the reason for underestimated results at some points. The penetration of chloride ion in the hydrated matrix increases with w/c as shown in **Figure 5.4**. Similar behavior was also reported by Hosokawa, Yamada and Takahashi, (2012) Mori et al., (2006) and Han, (2007) for different w/c of concrete and paste. For instance, the penetration depth for w/c 0.3 is approximately 10 mm, while it is about 30 mm for w/c 0.5. This finding can be explained by **Figure 5.5**, **Figure 5.6** and **Figure 5.7**.

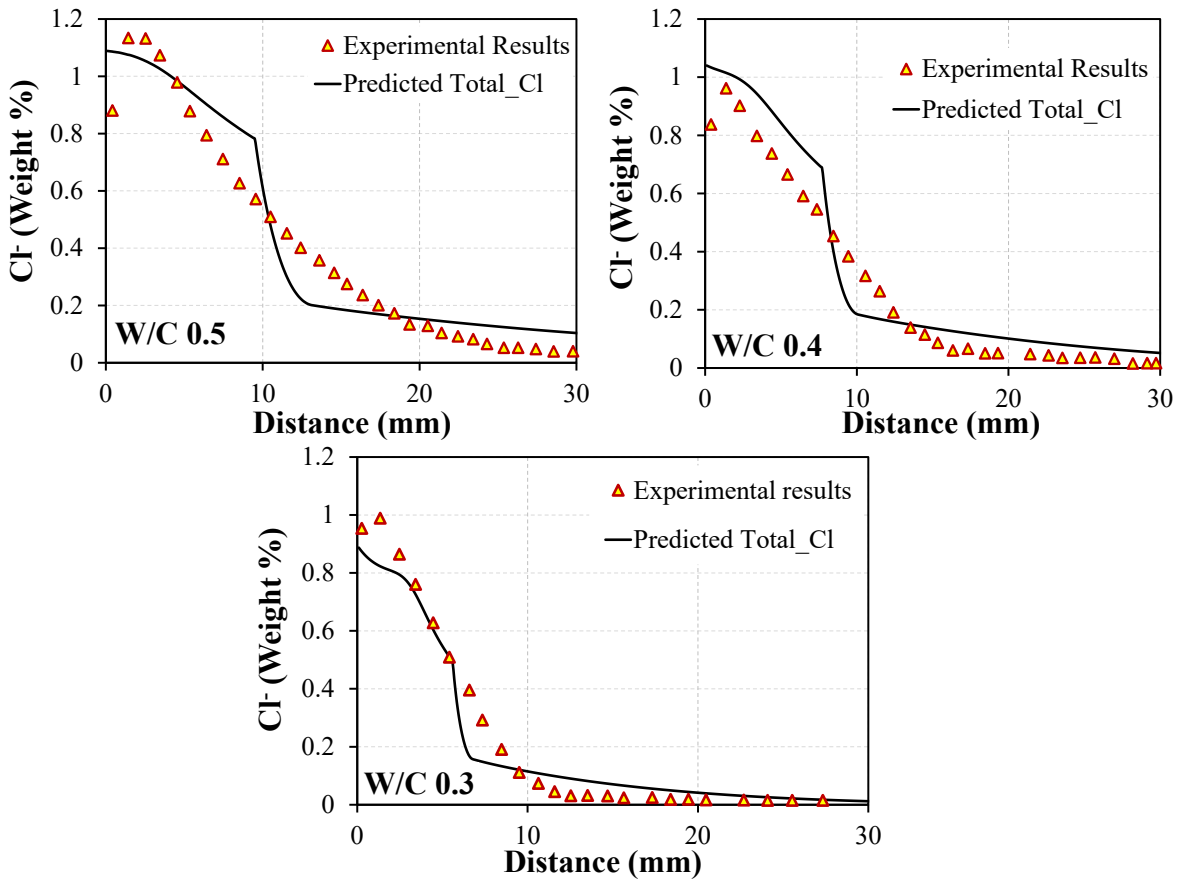

Figure 5.4: Comparison of predicted chloride ion profile with experimental results for w/c of 0.3, 0.4 and 0.5 (experimental results obtained from Mori et al., (2006))

When the chloride ions diffuse in the hydrated matrix form the external environments, they react with hydration products, and some are bound by the surface of the hydrates, while the rest remain free ions in the pore solution. Therefore, the total amount of chloride ion in the hydrated matrix can mainly exist as free chloride ion in the pore solution, chemical reaction of chloride ion with AFm phases like monosulfate to form Friedel's salt (see Eq. 5.15) and physical adsorption of chloride ion by C-S-H surface during the diffusion of chloride ion into the hydrated matrix (Florea and Brouwers, 2012; Aguayo et al., 2014). It is possible to predict the above three types of chloride ion in the matrix from the proposed model, shown in **Figure**

5.5. The results suggest that the above three types of chloride ion profile increase with w/c. The total amount of transported chloride ion in the hydrated matrix is primarily influenced by the concentration of exposure solution, ions in pore solution, hydration products and porosity. In order to investigate the effect of w/c on the chloride ion transport for the same exposure condition and same clinker, capillary porosity is the key factor. This porosity directly relates with the effective diffusion coefficient of the chloride ion in the matrix (Eq. 5.11). The effective diffusion coefficient and capillary porosity with distance from the exposure surface are respectively shown in **Figure 5.6(a)** and **(b).** The porosity of the hydrated matrix increases with w/c due to the high amount of space employed by water (Krishnya, Yoda and Elakneswaran, 2021). For example, porosity of the w/c 0.5 paste is approximately 0.18, whereas it is only 0.05 for w/c 0.3 at distances away from the exposed surface after the hydration of around 120 days. It should be noted that the capillary porosity and the hydration products during the hydration period have already been validated in our previous works (Elakneswaran et al., 2016; Krishnya, Yoda and Elakneswaran, 2021). Due to the 91 days of exposure of NaCl solution, the capillary porosity increases for all w/c ratio paste. Similar tendency is also observed in effective diffusion coefficient with distance from the exposed area which is expected due to the changes in capillary porosity (Guo et al., 2021). As the results of dissolution of hydration products due to the different exposure environment, the effective diffusion coefficient also tends to increase with w/c, similar to that of porosity. Similar observations have also been documented in previous studies (Haga et al., 2005; Kamali, Moranville and Leclercq, 2008; Zhang and Ye, 2010; Wan, Li and Sun, 2013). After the 91 days of exposure in the NaCl solution, diffusion coefficient at the exposure surface is 13.5 x 10-12 m^2/s for w/c 0.5, while 6.5 x 10-12 m^2/s is for w/c 0.3. Even though the leaching depth of the hydrated matrix decreases with w/c as shown in **Figure 5.6** which is similar to

the outcome of the previous studies (Kamali, Moranville and Leclercq, 2008; Wan, Li and Sun, 2013), the dissolution rate of portlandite increases with decreasing w/c as illustrated in **Figure 5.6(c)**. The leaching depth for w/c 0.3, 0.4 and 0.5 are approximately 7mm, 9mm and 12 mm respectively. Due to the high dissolution rate of portlandite in low w/c paste, the incremental rate of porosity is also high. The reason for the high dissolution rate of portlandite in low w/c paste is might be due to the low pH near to the exposed surface, and it decreases with increasing w/c. Typically, the pH increases with decreasing w/c because of the hydration reaction, and it can be well seen in **Figure 5.6(d)** at the distance away from the exposed surface (i.e., after 10 mm). In order to maintain the ionic equilibrium in the pore solution due to the diffusion of Cl^- and Na^+ and leaching of ions in the pore solution such as K^+, Ca^{+2} and SO_4^{-2}, OH^- leach from the solution, which leads to the decrease in pH near to the exposed surface. Similar decrease near to the exposed surface with increasing w/c was also once reported by Haga et al., (2005) for w/c ratio ranging from 0.4 to 1, in the case of leaching. The existence of low amount of portlandite near to the degraded area has been disclosed for low w/c paste by Kamali, Moranville and Leclercq, (2008) using the experimental results.

The weight % of chloride ion in the liquid phase of the total transported chloride ion is depicted in **Figure 5.5(a)**, and as expected, it shows an increasing tendency with w/c ratio. This could be due to the exisitance of high pore volume (porosity) in high w/c paste as illustrated in **Figure 5.6(b)**. At the same time, the free chloride ion % decreases with increasing distance from the external environment due to low amount of total chloride ion and low porosity. The similar pattern was also reported by Han, (2007). Another form for chloride ion to exist in the hydrated matrix is the Friedel's salt due to the chemical reaction of monosulfate with diffused chloride ion (see Eq. 5.15). The weigh % of chloride ion in the

Friedel's salt with distance from the exposed part for w/c of 0.3, 0.4 and 0.5 is shown in **Figure 5.5(b)**. The chloride ion in the formation of Friedel's salt is also increasing with w/c similar to the tendency of free chloride ion. The formation of Friedel's salt (see **Figure 5.7(a)**) is mainly controlled by the amount of transported chloride ion and the formation of monosulfate. As explained earlier, the transported chloride ion increases with w/c. And normally, the high amount monosulfate also form in high w/c paste due to the hydration reaction as detailed in **Figure 5.7(b)** (i.e., away from the exposed surface without transport reaction). Initially, C_3A reacts with gypsum ($C\bar{S}H_2$) and forms as ettringite ($C_6A\bar{S}_3H_{32}$) as shown in Eq. 5.17. Besides, the additional aluminate (C_3A) reacts with ettringite to produce monosulfate ($C_4A\bar{S}H_{12}$) after the running out of the gypsum (see Eq. 5.18).

$$C_3A + C\bar{S}H_2 + H \rightarrow C_6A\bar{S}_3H_{32} \quad (5.17)$$

$$C_3A + C_6A\bar{S}_3H_{32} + H \rightarrow C_4A\bar{S}H_{12} \quad (5.18)$$

It is therefore clear that the formation of monosulfate mainly depends on the reaction of C_3A and gypsum. For a specific cement, the amount of gypsum is constant. Almost a constant maximum amount of ettringite can be formed even with different w/c ratio (refer **Figure 5.7(c)**). It is a well-known fact that the reaction degree of hydration (which include reaction rate of C_3A) increases with increasing w/c (Florea and Brouwers, 2012). Therefore, the high amount of ettringite can be potentially dissolved and converted as monosulfate in high w/c paste. As the result, high amount of ettringite presents in low w/c paste, whereas high amount of monosulfate forms in high w/c paste as shown in **Figure 5.7(b)** and **(c)**. Considerably high amount of Friedel's salt precipitates in the presence of chloride ion in high w/c paste, which can also clearly be seen form the **Figure 5.7(a)**. This leads to the high amount of chloride ion

binding in Friedel's salt in high w/c paste (**Figure 5.5(b**)). This whole phenomenon is realistically captured in the proposed integrated model. Moreover, as explained in **Eq. 5.16**, the secondary ettringite forms near to the exposed area due to the reaction of existing monosulfate with available sulfate ion. This leads to significantly high amount of ettringite in the exposed area compared to that away from the exposed surface (see the illustration in **Figure 5.7(c)**). As the result of additionally formed ettringite, the porosity of the matrix close to the exposed surface is even considerably lower than undegraded matrix i.e., away from the exposed surface as demonstrated in **Figure 5.6(b)**. For example, the porosity decreases up to 0.03 for w/c of 0.3 from 2.5 mm to 7 mm from the exposed surface, whereas it reduces to 0.16 for w/c 0.5 from 3 to 12 mm, which is exactly the same location as up to the formation of secondary ettringite (**Figure 5.7(c)**).

As demonstrated in several studies, adsorption of chloride ion by C-S-H surface due to the large specific surface area and surface complexation module in IPHREEQC was used to predict the adsorbed ions (Elakneswaran, Nawa and Kurumisawa, 2009; Elakneswaran et al., 2010; Guo et al., 2018; Chang et al., 2019). In this research work, the surface complexation model developed by Elakneswaran et al., (2010) is used to predict the adsorbed amount of chloride by C-S-H surface, and the predicted results with different w/c are shown in **Figure 5.5(c)**. The predicted results indicates that adsorbed chloride ion increase with w/c and above the distance of around 5 mm from the exposed surface. This is because, the amount of C-S-H is highly formed in high w/c paste due to the high reaction rate of clinker (**Figure 5.7(d)**). However, adjacent to the exposed surface, the adsorbed chloride ion is higher for w/c of 0.3 and 0.4 compared to w/c 0.5 paste. The reason might be due to the high amount of dissolution of portlandite in low w/c paste. As detailed in **Table 5.1**, to adsorb the chloride ion by C-S-H,

it is required additional Ca^{+2} ion in this proposed model. Therefore, in low w/c paste, high amount of Ca^{+2} ions are freely available due to high dissolution rate of portlandite close to the exposed surface as aforementioned. Therefore, it is possible to adsorb considerably high amount of chloride ion in low w/c pastes.

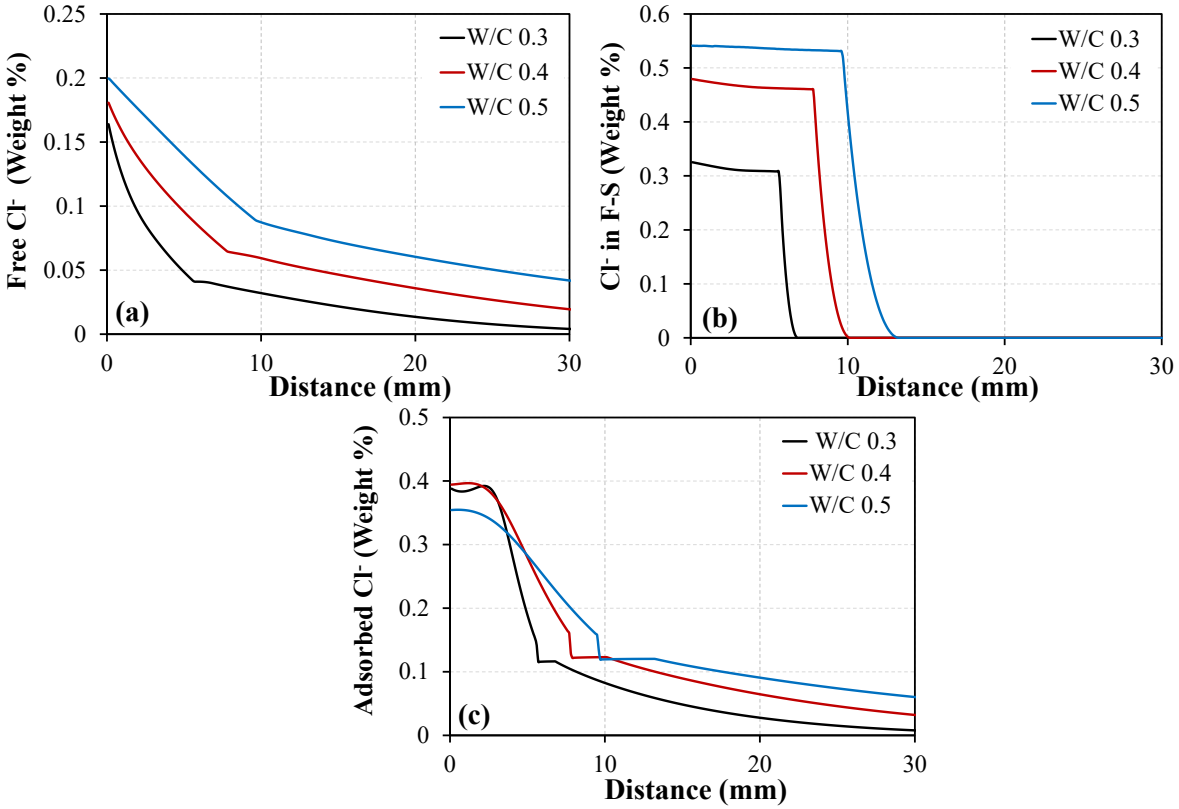

Figure 5.5: Three types of chloride ion exist in the hydrated cement matrix for w/c from 0.3-0.5 (a) Free Cl- in pore solution, (b) Cl- in F-S and (c) Adsorbed Cl- by C-S-H (F-S stands for Friedel's salt)

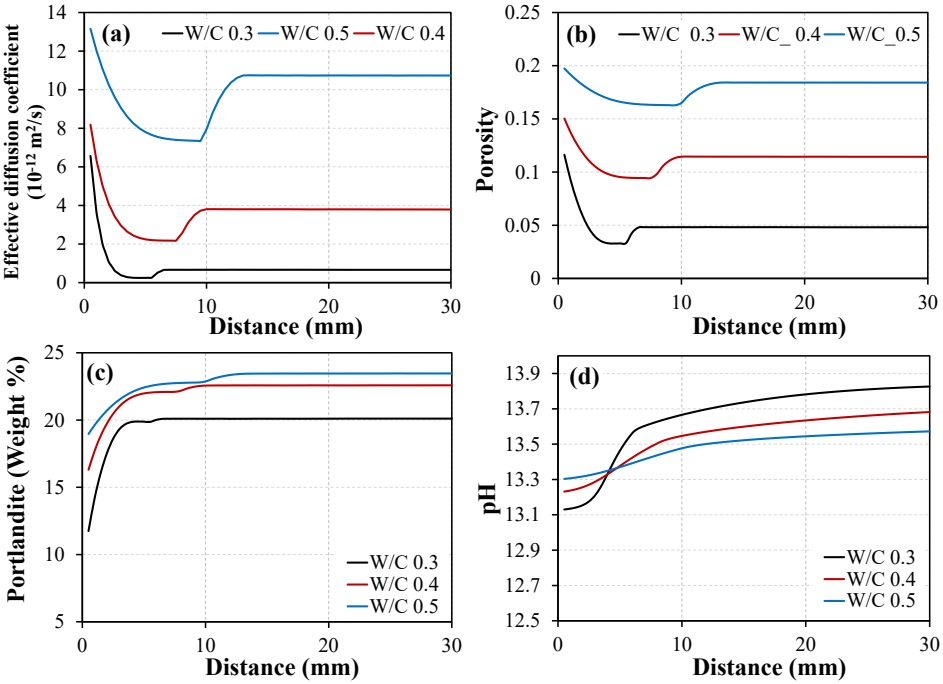

Figure 5.6: Variation of (a) effective diffusion coefficient, (b) porosity, (c) weight % of portlandite and (d) pH for w/c of 0.3, 0.4 and 0.5 with distance from the exposed surface

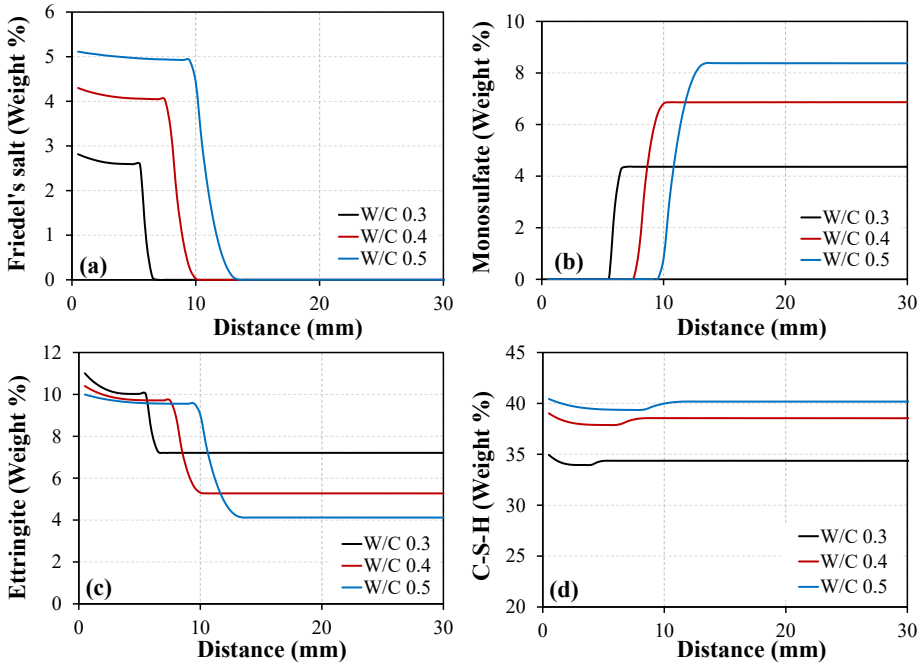

Figure 5.7: Variation of weight % of (a) Friedel's salt, (b) Monosulfate, (c) Ettringitre and (d) C-S-H for w/c of 0.3, 0.4 and 0.5

5.3.3 Verification of carbon dioxide diffusion

To verify the predictability of the proposed model on carbon dioxide diffusion, the computed results of the weight percentage of portlandite are compared with experimental results of Suda *et al.*, (2021) for the cement paste of w/c 0.55 and CO_2 concentration 3 % (of the air volume). Based on the proposed model combined with kinetic model for C-S-H dissolution rate, the predicted results of portlandite show good agreement with experimental results as shown in **Figure 5.8**. During the carbonation, portlandite dissolves due to the decrease of pH and forms as calcite. Therefore, the total weight percentage of portlandite decreases with carbonation time. However, the parameters used in Eq 5.2 need further validations for different w/c and different carbonation period.

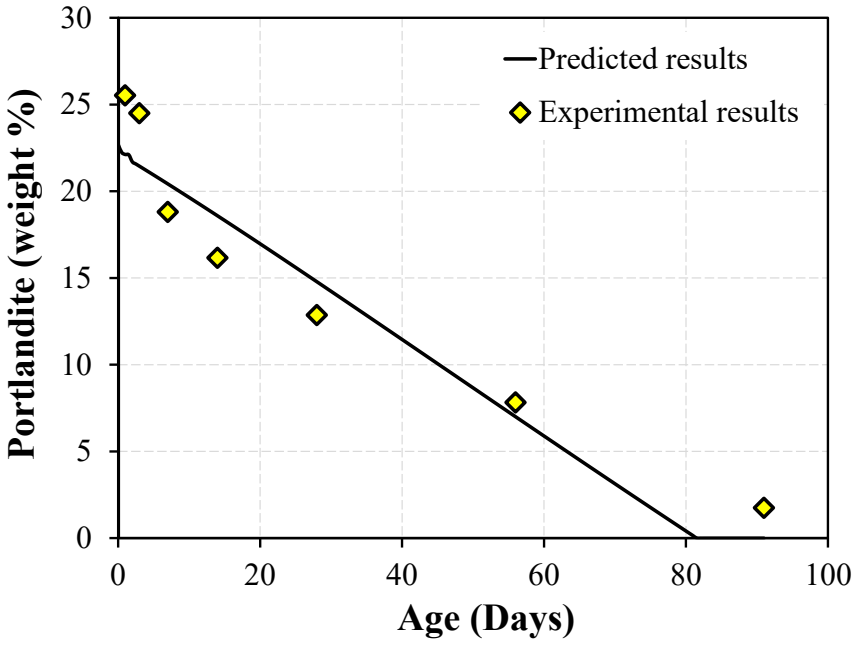

Figure 5.8: Variation of weight percentage of porlandite with carbonation period

Figure 5.9 illustrates the phase assemblage of hydration products **(a)** prior to the exposure time (i.e., after 28 days of hydration) and **(b)** after three years of 10 % (v/v) CO_2 exposure for

w/c of 0.3 cement paste. It can be observed that the carbonation depth of this sample is not observed even after 3 years of carbonation due to the low porosity of the hydrated matrix. All the hydration products except hydrotalcite generally dissolve and form considerable calcite, silica gel, alumina gel and gypsum and low amount of starlight, monocarbonate and hemicarbonate. As per **Figure 5.9(b),** the porosity of the hydrated matrix decrease adjacent to the exposed area due to the carbonation reaction.

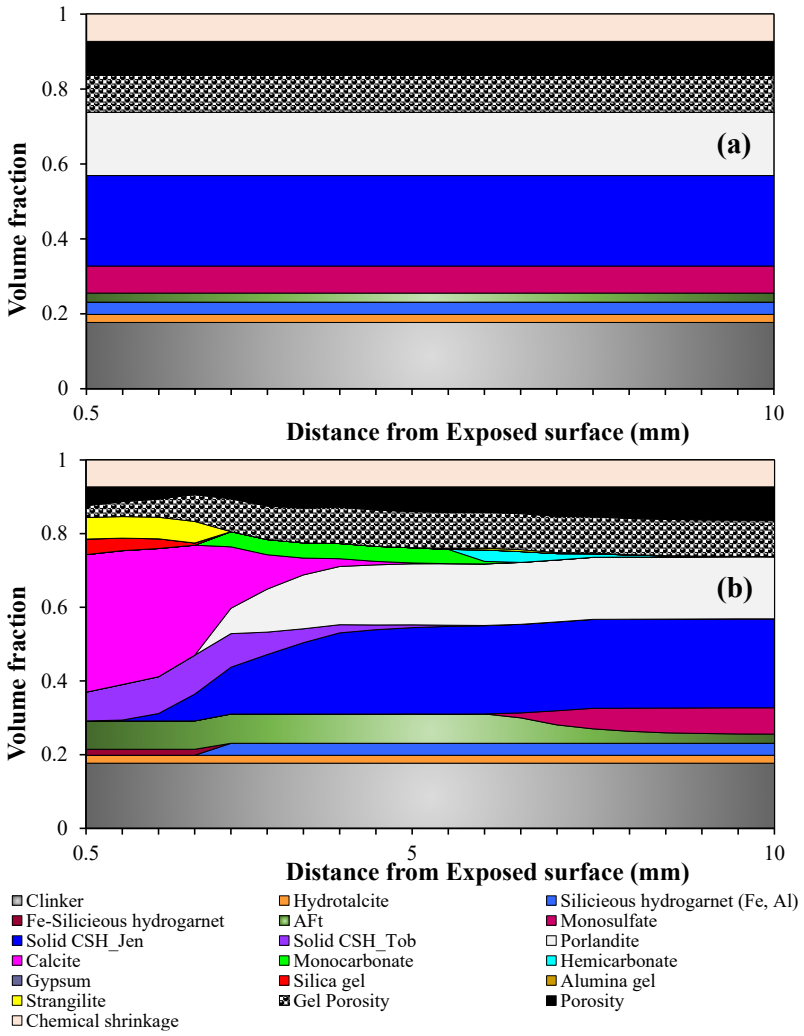

Figure 5.9: Variation of volume fraction of hydration products with distance from the exposure surface (a) before carbonation and (b) after 3 years of carbonation

5.4 Conclusion

A new model developed in MATLAB, HyMeC integrated with COMSOL Multiphysics (HyMeC-COMSOL) is proposed to predict the changes on the microstructure of the pores matrix due to transport of ions and gases. The proposal involves cement hydration model to compute the dissolution rate of clinker, thermodynamic model to perform the chemical reaction and COMSOL Multiphysics to determine the transport of ions and gas. With several succeeding conclusions, the model reveals a high potential for predicting transport properties. The model for the chloride ion transportation through the hydrated cement paste under the fully saturated condition have been verified with previously developed model, PHREEQC and experimental results for different w/c as well. The model for the transport of ions excellently captures the realistic behavior of the transportation process and chemical reaction. Moreover, the proposed transport model for carbon dioxide diffusion combined with kinetic model for the dissolution of C-S-H has been verified with experimental results of dissolution of portlandite, showing good agreement. However, the proposed kinetic model needs further validation for different w/c and different exposure conditions.

CHAPTER 6

CONCLUSIONS AND RECOMMENDATIONS

6.1 Introduction

This dissertation presents the analysis of the newly proposed model for predicting the mechanical and durability properties of cement-based materials. The objective of the research is to develop a new model, capable of determining the mechanical and transport properties of cementitious material from its evolution of microstructure with less assumption. From the perspective of Material Engineering, yet significant effort has been given on understanding microstructural responses, mechanical responses and durability responses by considering different factors such as different type of cement (clinker composition), w/c, aggregate content, hydration, exposure period and etc.

The research work consists of the following major components: (i) an overview on cement hydration and microstructure in cement paste, mortar and concrete (described in Chapter 2), (ii) an overview on the transportation of ion and gas into the cement based material (described in Chapter 2), (iii) developing a new model for predicting the mechanical properties of cement paste from hydration products and porosity of the matrix (described in Chapter 3), (iv) extending the cement paste model to predict the mechanical properties of mortar and concrete by considering as three phase material (aggregates, ITZ and cement paste) (described in Chapter 4) and (v) proposing an integrated model consist of cement hydration and transportation of ion and gas to predict the durability characteristic of cement paste (described in Chapter 5).

6.2 Summary of conclusions

6.2.1 A new model for predicting the mechanical properties of cement paste (HyMeC)

In this part, a two-stage model (called HyMeC) has been proposed to predict the mechanical properties of OPC paste such as compressive strength, Young's modulus and Poisson's ratio from the development of microstructure during the hydration process. In Stage-1, the volume fraction of hydrates has been predicted by integrating (i) relative humidity model (ii) thermodynamic model, (iii) cement hydration model and (iv) model for volumetric prediction. The multi-scale model (3 levels from C-S-H matrix to cement paste) has been developed in Stage-2 for predicting the above mechanical properties using the volume hydrates obtained from Stage-1. From the analysis of the successfully developed model, the following conclusions are drawn.

The behaviour of the relative humidity during the hydration process have been realistically reflected through the proposed relationships as a function of w/c ratio and hydration period, and the predicted results exhibit a fairly good agreement with experimental results for w/c of 0.2-0.5. The microstructure and porosity of the hydrated cement paste, in terms of volume fraction, have been predicted using the integrated Stage-1 model, which comprehensively expresses the variation of phase assemblage with hydration process for long periods. The predicted chemical shrinkage and capillary porosity shows a very good agreement with reported experimental results of w/c 0.4 and 0.55 in Stage-1 analysis. The proposed multi-scale model (Stage-2) demonstrates accurate predictability of the mechanical properties of cement paste. The predicted compressive strength excellently captures the realistic values for the w/c ratios ranging from 0.3 – 0.6, and similarly, the Young's modulus is predicted. The

computation of Poisson's ratio also shows relatively good agreement with the available experimental data of two w/c (0.4 and 0.55). However, the model slightly overpredicts the Poisson's ratio at early stage (before 10 days); thus, further validations are required with more independent experimental results to generalize the Poisson's ratio model.

6.2.2 A three-phase model for simulating the mechanical properties of mortar and concrete

In this chapter, the mechanical properties such as Young's modulus and Poisson's ratio of mortar and concrete were reliably predicted using the developed multi-scale model and homogenization method. The mortars and concretes were assumed as three-phase composites, and the ITZ for both coarse and fine aggregate were reliably considered as cement paste with high water content. The mechanical properties of ITZ and bulk paste were based on the detailed microstructure of hydrates during hydration reaction. The proposed models for mortar and concrete were validated with experiment results for wide range of aggregate contents and w/c ratios.

The predicted Young's modulus excellently captured the realistic behaviour for the w/c ratios ranging from 0.3 to 0.6 and aggregate content from 0.2 to 0.6. The computation of Poisson's ratio showed relatively good agreement with the experimental data for mortar and concrete. However, the model slightly overpredicted the Poisson's ratio at early stage (before 10 days) for concrete; thus, further validations are recommended with more independent experimental results to generalize the Poisson's ratio model of concrete. Moreover, the effect of ITZ on Young's modulus and Poisson's ratio were demonstrated using the proposed model for mortar and concrete. At the same time, the results predicted via typical way, i.e., two-phase model,

was shown to reveal a stiffer material compared to that of both experiment results and three-phase model for both mortar and concrete. The effect of ITZ was higher for concrete compared to mortar due to the high amount of aggregates content.

Overall, the proposed novel three-phase models for mortar and concrete can be used to accurately predict the mechanical properties. One of the marked merits of this model is, if the chemical composition is known, the Young's modulus and Poisson's ratio can be computed, which would reduce the waste of time, cost, material and manpower compared to typical approaches.

6.2.3 An integrated model (HyMeC-COMSOL) to perform the durability and mechanical properties of cement past due to the transport of ion and gas

A new model developed in MATLAB, HyMeC integrated with COMSOL Multiphysics (HyMeC-COMSOL) is proposed to predict the changes on the microstructure and mechanical properties of the pores matrix due to transport of ions and gases. The proposal involves cement hydration model to compute the dissolution rate of clinker, thermodynamic model to perform the chemical reaction and COMSOL Multiphysics to determine the transport of ions and gas. With several succeeding conclusions, the model reveals a high potential for predicting transport properties. The model for the chloride ion transportation through the hydrated cement paste under the fully saturated condition have been verified with previously developed model, PHREEQC and experimental results for different w/c as well. The model for the transport of ions excellently captures the realistic behavior of the transportation process and chemical reaction. Moreover, for carbon dioxide diffusion, the proposed transport model combined with kinetic model (relating the dissolution of C-S-H) is well verified with

experimental results of the dissolution of portlandite.

6.3 Suggestions for future works

The following considerations open for interesting research opportunities:

The proposed model for predicting the mechanical properties of cement paste from the development of hydration products (Chapter 3) needs further elaboration to predict the mechanical properties of blended cement which consist of fly ash, slag, silica fume and etc. Moreover, the C-S-H distribution factor used in the multi-scale model to predict the mechanical properties of cement paste is needed further investigation based on experimental evaluation on how it varies with w/c and cement replacement ratio for blended cement as well.

The model for mechanical properties such as elastic modulus and Poisson's ratio of mortar and concrete considered as three phase material (aggregate, ITZ and cement paste) has been proposed using the homogenization method based on the development of hydration products in ITZ and cement paste (Chapter 4). The extension of this homogenization method to predict the compressive strength of mortar and concrete can be performed. Moreover, in the proposed model, ITZ is considered as single shell with uniform properties for a specific time to reduce the complexity of the calculation. However, based on the experimental results (Nadeau, 2002; Scrivener, Lyon and Laugesen, 2004a; Gao et al., 2014) show varying clinker content and w/c with distance from the aggregate surface. Therefore, it will be more realistic, if the ITZ would be considered as a greater number of layers. Moreover, the aggregate is considered as inert and no reaction with cement. But depends on the chemical composition of aggregate types (mainly silica) react with cement and the properties of ITZ also can be affected by aggregate reaction (Multon and Sellier, 2016). Therefore, the proposed model needs further

modification to consider the aggregates reaction with cement paste.

The coupled HyMeC-COMSOL model has been developed to simulate the durability characteristic of cement paste. It can be extended to perform the durability properties of mortar and concrete. Moreover, in the COMSOL Multiphysics model, the activity coefficient was not considered for the calculation of transportation process. It will be better if the model modified to consider the activity of ions during the transportation process.

REFERENCES

Aguayo, M. *et al.* (2014) 'Electrically driven chloride ion transport in blended binder concretes: Insights from experiments and numerical simulations', *Cement and Concrete Research*. Elsevier Ltd, 66, pp. 1–10.

Al-Ostaz, A. *et al.* (2010) 'A molecular dynamics and microporomechanics study on the mechanical properties of major constituents of hydrated cement', *Composites Part B: Engineering*, 41(7), pp. 543–549.

Allos, A. E. and Martin, L. H. (1981) 'Factors affecting Poisson's ratio for concrete', *Building and Environment*. Pergamon, 16(1), pp. 1–9.

Aouissi, F. *et al.* (2016) 'Study of the influence of the interfacial transition zone on the elastic modulus of concrete using a triphasic model', *Journal of Adhesion Science and Technology*. Taylor and Francis Ltd., 30(9), pp. 994–1005.

Appelo, C. and Postma, D. (2004) *Geochemistry, groundwater and pollution*.

Azad, V. J. *et al.* (2016) 'A COMSOL-GEMS interface for modeling coupled reactive-transport geochemical processes', *Computers and Geosciences*. Elsevier Ltd, 92, pp. 79–89.

Bahafid, S. *et al.* (2018) 'Effect of the hydration temperature on the pore structure of cement paste: Experimental investigation and micromechanical modelling', *Cement and Concrete Research*. Elsevier, 111(June), pp. 1–14.

Bary, B. and Sellier, A. (2004) 'Coupled moisture - Carbon dioxide-calcium transfer model for carbonation of concrete', *Cement and Concrete Research*, 34(10), pp. 1859–1872.

Bauchy, M. *et al.* (2015) 'Fracture toughness of calcium-silicate-hydrate from molecular dynamics simulations', *Journal of Non-Crystalline Solids*. Elsevier, 419, pp. 58–64.

Bažant, Z. P. and Planas, J. (1998) *Fracture and Size Effect in Concrete and Other Quasibrittle Materials, CRC Press*.

Di Bella, C. *et al.* (2015) 'Application of microstructurally-designed mortars for studying early-age properties: Microstructure and mechanical properties', *Cement and Concrete Research*. Elsevier Ltd, 78, pp. 234–244.

Bentz, B. Y. D. P., Lura, P. and Roberts, J. W. (2005) 'Mixture proportioning for internal curing', *Concrete International*, (February), pp. 35–40.

Bentz, D. P. (1999) 'CEMHYD3D: A Three-Dimensional Cement Hydration and Microstructure Development Modeling Package', *Automation in construction*, 8(April 2000), pp. 227–235.

Bentz, D. P. (2006) 'Influence of water-to-cement ratio on hydration kinetics: Simple models based on spatial considerations', *Cement and Concrete Research*. Pergamon, 36(2), pp. 238–244.

Bernard, F. and Kamali-Bernard, S. (2015) 'Numerical study of ITZ contribution on mechanical behavior and diffusivity of mortars', *Computational Materials Science*. Elsevier, 102, pp. 250–257.

Bernard, O., Ulm, F.-J. and Lemarchand, E. (2003) 'A multiscale micromechanics-hydration model for the early-age elastic properties of cement-based materials', *Cement and Concrete Research*. Pergamon, 33(9), pp. 1293–1309.

van Breugel, K. (1995a) 'Numerical simulation of hydration and microstructural development in hardening cement-based materials (I) theory', *Cement and Concrete Research*. Pergamon, 25(2), pp. 319–331.

van Breugel, K. (1995b) 'Numerical simulation of hydration and microstructural development in hardening cement-based materials (I) theory', *Cement and Concrete Research*, 25(2), pp. 319–331.

Brown, L., Allison, P. G. and Sanchez, F. (2018) 'Use of nanoindentation phase characterization and homogenization to estimate the elastic modulus of heterogeneously decalcified cement pastes', *Materials and Design*. Elsevier Ltd, 142, pp. 308–318.

Bullard, J. W. *et al.* (2017) 'Coupling thermodynamics and digital image models to simulate hydration and microstructure development of portland cement pastes'. doi: 10.1557/jmr.2010.41.

Chang, H. *et al.* (2019) 'A novel method for assessing C-S-H chloride adsorption in cement pastes', *Construction and Building Materials*. Elsevier, 225, pp. 324–331.

Chen, H. *et al.* (2013) 'Prediction of self-desiccation in low water-to-cement ratio pastes based on pore structure evolution', *Cement and Concrete Research*. Pergamon, 49, pp. 38–47.

Chen, Q. *et al.* (2016) 'A multiphase micromechanical model for hybrid fiber reinforced concrete considering the aggregate and ITZ effects', *Construction and Building Materials*. Elsevier Ltd, 114, pp. 839–850.

Chindaprasirt, P., Rukzon, S. and Sirivivatnanon, V. (2008) 'Effect of carbon dioxide on chloride penetration and chloride ion diffusion coefficient of blended Portland cement mortar', *Construction and Building Materials*. Elsevier, 22(8), pp. 1701–1707.

Christensen, R. M. and Lo, K. N. (1979) 'Solutions for Effective Shear Properties in', *Journal of the Mechanics and Physics of Solids*, 27(4), pp. 315–330.

Colangelo, F., Messina, F. and Cioffi, R. (2015) 'Recycling of MSWI fly ash by means of cementitious double step cold bonding pelletization: Technological assessment for the production of lightweight artificial aggregates', *Journal of Hazardous Materials*. Elsevier, 299, pp. 181–191.

Constantinides, G. and Ulm, F.-J. (2004) 'The effect of two types of C-S-H on the elasticity of cement-based materials: Results from nanoindentation and micromechanical modeling', *Cement and Concrete Research*, 34(1), pp. 67–80.

Constantinides, G. and Ulm, F.-J. (2007) 'The nanogranular nature of C–S–H', *Journal of the Mechanics and Physics of Solids*. Pergamon, 55(1), pp. 64–90.

Corinaldesi, V. and Moriconi, G. (2009) 'Influence of mineral additions on the performance of 100% recycled aggregate concrete', *Construction and Building Materials*. Elsevier, 23(8), pp. 2869–2876.

Crumbie, A. K. (1994) 'Characerisation of the microstructure of concrete', *PhD Dissertation*, (May).

Das, S., Maroli, A. and Neithalath, N. (2016) 'Finite element-based micromechanical modeling of the influence of phase properties on the elastic response of cementitious mortars', *Construction and Building Materials*. Elsevier Ltd, 127, pp. 153–166.

Deschner, F. *et al.* (2012) 'Hydration of Portland cement with high replacement by siliceous fly ash', *Cement and Concrete Research*. Pergamon, 42(10), pp. 1389–1400.

Dridi, W. (2013) 'Analysis of effective diffusivity of cement based materials by multi-scale modelling', *Materials and Structures/Materiaux et Constructions*, 46(1–2), pp. 313–326.

Duplan, F. *et al.* (2014) 'Prediction of modulus of elasticity based on micromechanics theory and application to low-strength mortars', *Construction and Building Materials*. Elsevier, 50, pp. 437–447.

Elakneswaran, Y. *et al.* (2010) 'Ion-cement hydrate interactions govern multi-ionic transport model for cementitious materials', *Cement and Concrete Research*, 40(12), pp. 1756–1765.

Elakneswaran, Y. *et al.* (2016) 'Hydration study of slag-blended cement based on thermodynamic considerations', *Construction and Building Materials*. Elsevier, 124, pp. 615–625.

Elakneswaran, Y. *et al.* (2019) 'Characteristics of Ferrite-Rich Portland Cement: Comparison With Ordinary Portland Cement', *Frontiers in Materials*, 6(May), pp. 1–11.

Elakneswaran, Y., Nawa, T. and Kurumisawa, K. (2009) 'Electrokinetic potential of hydrated cement in relation to adsorption of chlorides', *Cement and Concrete Research*. Pergamon, 39(4), pp. 340–344.

Elsharief, A., Cohen, M. D. and Olek, J. (2003) 'Influence of aggregate size, water cement ratio and age on the microstructure of the interfacial transition zone', *Cement and Concrete Research*. Pergamon, 33(11), pp. 1837–1849.

Erdem, S., Dawson, A. R. and Thom, N. H. (2012) 'Influence of the micro- and nanoscale local mechanical properties of the interfacial transition zone on impact behavior of concrete made with different aggregates', *Cement and Concrete Research*, 42(2), pp. 447–458.

Feng, P., Miao, C. and Bullard, J. W. (2014) 'A model of phase stability, microstructure and properties during leaching of portland cement binders', *Cement and Concrete Composites*. Elsevier, 49, pp. 9–19.

Ferraro, A. *et al.* (2020) 'Cold-bonding process for treatment and reuse of waste materials: Technical designs and applications of pelletized products', *Critical Reviews in Environmental Science and Technology*, pp. 1–35.

Florea, M. V. A. and Brouwers, H. J. H. (2012) 'Chloride binding related to hydration products: Part I: Ordinary Portland Cement', *Cement and Concrete Research*. Elsevier Ltd, 42(2), pp. 282–290.

Gal, E. and Kryvoruk, R. (2011) 'Meso-scale analysis of FRC using a two-step homogenization approach', in *Computers and Structures*. Pergamon, pp. 921–929.

Gao, Y. *et al.* (2013) 'Characterization of ITZ in ternary blended cementitious composites: Experiment and simulation', *Construction and Building Materials*, 41, pp. 742–750. d

Gao, Y. *et al.* (2014) 'The ITZ microstructure, thickness and porosity in blended cementitious composite: Effects of curing age, water to binder ratio and aggregate content', *Composites Part B: Engineering*. Elsevier, 60, pp. 1–13.

Gao, Y. *et al.* (2018) 'Characterisation of the interfacial transition zone in mortars by nanoindentation

and scanning electron microscope', *Magazine of Concrete Research*, 70(18).

Garboczi, E. J. and Bentz, D. P. (1997) 'Analytical formulas for interfacial transition zone properties', *Advanced Cement Based Materials*. Elsevier Science Inc, 6(3–4), pp. 99–108.

Garboczi, E. J. and Bentz, D. P. (1998) 'Multiscale Analytical/Numerical Theory of the Diffusivity of Concrete', *Advanced Cement Based Materials*. Elsevier, 8(2), pp. 77–88.

Gasch, T., Eriksson, D. and Ansell, A. (2019) 'On the behaviour of concrete at early-ages: A multiphase description of hygro-thermo-chemo-mechanical properties', *Cement and Concrete Research*, 116, pp. 202–216.

Gesoğlu, M., Özturan, T. and Güneyisi, E. (2006) 'Effects of cold-bonded fly ash aggregate properties on the shrinkage cracking of lightweight concretes', *Cement and Concrete Composites*. Elsevier, 28(7), pp. 598–605.

von Greve-Dierfeld, S. *et al.* (2020) *Understanding the carbonation of concrete with supplementary cementitious materials: a critical review by RILEM TC 281-CCC*, *Materials and Structures/Materiaux et Constructions*.

Griffith, A. (1924) 'Theory of rupture', in *In : C. Biezeno, J. Burgers (Eds.), First International Congress for Applied Mechanics, Delft*, pp. 55–63.

Gunning, P. J., Hills, C. D. and Carey, P. J. (2009) 'Production of lightweight aggregate from industrial waste and carbon dioxide', *Waste Management*. Pergamon, 29(10), pp. 2722–2728.

Guo, B. *et al.* (2018) 'A COMSOL-PHREEQC interface for modeling the multi-species transport of saturated cement-based materials', *Construction and Building Materials*. Elsevier Ltd, 187, pp. 839–853.

Guo, Y. *et al.* (2021) 'Evaluating the chloride diffusion coefficient of cement mortars based on the tortuosity of pore structurally-designed cement pastes', *Microporous and Mesoporous Materials*. Elsevier B.V., 317, p. 111018.

Haecker, C. J. *et al.* (2005) 'Modeling the linear elastic properties of Portland cement paste', *Cement and Concrete Research*. Pergamon, 35(10), pp. 1948–1960.

Haga, K. *et al.* (2005) 'Effects of porosity on leaching of Ca from hardened ordinary Portland cement paste', *Cement and Concrete Research*. Pergamon, 35(9), pp. 1764–1775.

Haile, B. F. *et al.* (2019) 'Multi-level homogenization for the prediction of the mechanical properties of ultra-high-performance concrete', *Construction and Building Materials*. Elsevier Ltd, 229, p. 116797.

Han, S. H. (2007) 'Influence of diffusion coefficient on chloride ion penetration of concrete structure', *Construction and Building Materials*. Elsevier, 21(2), pp. 370–378.

Han, S. H. and Kim, J. K. (2004) 'Effect of temperature and age on the relationship between dynamic and static elastic modulus of concrete', *Cement and Concrete Research*. Pergamon, 34(7), pp. 1219–1227.

Hashin, Z. and Monteiro, P. J. M. (2002) 'An inverse method to determine the elastic properties of the interphase between the aggregate and the cement paste', *Cement and Concrete Research*. Pergamon, 32(8), pp. 1291–1300.

Hatanaka, A. *et al.* (2003) 'The Impact of Tortuosity on Chloride Ion Diffusion in Slag-Blended Cementitious Materials Multi-scale Modeling of Concrete Performance-Integrated Material and Structural Effect of the key mixture parameters on tortuosity and permeability of concrete Enhan', *Journal of Advanced Concrete Technology*, 15(1), pp. 426–439.

Hirao, H. *et al.* (2005) 'Chloride Binding of Cement Estimated by Binding Isotherms of Hydrates', *Journal of Advanced Concrete Technology*, 3(1), pp. 77–84.

Hlobil, M., Šmilauer, V. and Chanvillard, G. (2016) 'Micromechanical multiscale fracture model for compressive strength of blended cement pastes', *Cement and Concrete Research*, 83, pp. 188–202.

Hosokawa, Y., Yamada, K. and Takahashi, H. (2012) 'Time dependency of Cl diffusion coefficients in concretes with varied phase compositions and pore structures under different environmental conditions', *Journal of Advanced Concrete Technology*, 10(11), pp. 363–374.

Hu, C. *et al.* (2014) 'Property investigation of calcium–silicate–hydrate (C–S–H) gel in cementitious composites', *Materials Characterization*. Elsevier, 95, pp. 129–139.

Hu, Z. *et al.* (2018) 'A novel method to predict internal relative humidity in cementitious materials by 1H NMR', *Cement and Concrete Research*. Elsevier Ltd, 104, pp. 80–93.

Huang, H. *et al.* (2019) 'Microstructure investigation of the interface between lightweight concrete and normal-weight concrete', *Materials Today Communications*. Elsevier Ltd, 21, p. 100640.

Igarashi, G. and Maruyama, I. (2011) 'Relationship between mechanical properties and phase composition of hardened cement phase (In Japanes)', *J.Struct. Constr. Eng.*, 76(660), pp. 213–222.

Jebli, M. *et al.* (2018) 'Experimental characterization of mechanical properties of the cement-aggregate interface in concrete', *Construction and Building Materials*. Elsevier, 161, pp. 16–25.

Jennings, H. M. *et al.* (2005) 'Nanostructure of CSH gel in cement paste as a function of curing conditions and relative humidity Nanostructure of C-S-H gel in cement paste as a function of curing conditions and relative humidity', in *Proceeding of Concreep*, pp. 19–37.

Jennings, H. M. *et al.* (2007a) 'A multi-technique investigation of the nanoporosity of cement paste', *Cement and Concrete Research*. Pergamon, 37(3), pp. 329–336.

Jennings, H. M. *et al.* (2007b) 'A multi-technique investigation of the nanoporosity of cement paste', *Cement and Concrete Research*, 37(3), pp. 329–336.

Jiang, Y., Ling, T. C. and Shi, M. (2020) 'Strength enhancement of artificial aggregate prepared with waste concrete powder and its impact on concrete properties', *Journal of Cleaner Production*. Elsevier Ltd, 257, p. 120515.

Jiang, Z. *et al.* (2016) 'Experimental Study of Diffusivity of the Interfacial Transition Zone between Cement Paste and Aggregate'.

Jiang, Z., Sun, Z. and Wang, P. (2006) 'Internal relative humidity distribution in high-performance cement paste due to moisture diffusion and self-desiccation', *Cement and Concrete Research*. Pergamon, 36(2), pp. 320–325.

Jirásek, M. and Rolshoven, S. (2009) 'Localization properties of strain-softening gradient plasticity models. Part I: Strain-gradient theories', *International Journal of Solids and Structures*. Pergamon, 46(11–12), pp. 2225–2238.

Jones, M. R. *et al.* (2003) 'Studies using 27Al MAS NMR of AFm and AFt phases and the formation of Friedel's salt', *Cement and Concrete Research*. Pergamon, 33(2), pp. 177–182.

Kamali, S., Moranville, M. and Leclercq, S. (2008) 'Material and environmental parameter effects on the leaching of cement pastes: Experiments and modelling', *Cement and Concrete Research*. Pergamon, 38(4), pp. 575–585.

Kim, S. M. and Abu Al-Rub, R. K. (2011) 'Meso-scale computational modeling of the plastic-damage

response of cementitious composites', *Cement and Concrete Research*. Pergamon, 41(3), pp. 339–358.

Klein, N. S., Lenz, L. A. and Mazer, W. (2020) 'Influence of the granular skeleton packing density on the static elastic modulus of conventional concretes', *Construction and Building Materials*. Elsevier Ltd, 242, p. 118086.

Königsberger, M. *et al.* (2018) 'Hydrate failure in ITZ governs concrete strength: A micro-to-macro validated engineering mechanics model', *Cement and Concrete Research*, 103, pp. 77–94.

Krishnya, S., Elakneswaran, Y. and Yoda, Y. (2021) 'Proposing a three-phase model for predicting the mechanical properties of mortar and concrete', *Materials Today Communications*. Elsevier, 29, p. 102858.

Krishnya, S., Yoda, Y. and Elakneswaran, Y. (2021) 'A two-stage model for the prediction of mechanical properties of cement paste', *Cement and Concrete Composites*. Elsevier, 115, p. 103853.

Lam, L., Wong, Y. . and Poon, C. . (2000) 'Degree of hydration and gel/space ratio of high-volume fly ash/cement systems', *Cement and Concrete Research*. Pergamon, 30(5), pp. 747–756.

Lavergne, F. *et al.* (2018) 'Estimating the mechanical properties of hydrating blended cementitious materials: An investigation based on micromechanics', *Cement and Concrete Research*. Pergamon, 104, pp. 37–60.

Lawrence, F. V. J. and Young, J. . (1973) 'Studies on the hydration of tricalcium silicate pastes: I. Scanning electron microscopic examination of microstructural features', *Cement and Concrete Research*, 3(2), p. 149±161.

Li, G. *et al.* (1999) 'Effective Young's modulus estimation of concrete', *Cement and Concrete Research*. Elsevier Science Ltd, 29(9), pp. 1455–1462.

Li, G., Zhao, Y. and Pang, S. S. (1999) 'Four-phase sphere modeling of effective bulk modulus of concrete', *Cement and Concrete Research*. Elsevier Science Ltd, 29(6), pp. 839–845.

Li, Yaqiang, Li, Yue and Wang, R. (2019) 'Quantitative evaluation of elastic modulus of concrete with nanoidentation and homogenization method', *Construction and Building Materials*. Elsevier Ltd, 212, pp. 295–303.

Li, Yue and Li, Yaqiang (2019) 'Evaluation of elastic properties of fiber reinforced concrete with

homogenization theory and finite element simulation', *Construction and Building Materials*. Elsevier Ltd, 200, pp. 301–309.

Liu, L. *et al.* (2019) 'Influence of decalcification on structural and mechanical properties of synthetic calcium silicate hydrate (C-S-H)', *Cement and Concrete Research*. Pergamon, 123, p. 105793.

Liu, Q. F. *et al.* (2014) 'Three-phase modelling of electrochemical chloride removal from corroded steel-reinforced concrete', *Construction and Building Materials*. Elsevier Ltd, 70, pp. 410–427.

Liu, Z. *et al.* (2014) 'Solid Phases Percolation and Capillary Pores Depercolation in Hydrating Cement Pastes'.

Lothenbach, B., Le Saout, G., *et al.* (2008) 'Influence of limestone on the hydration of Portland cements', *Cement and Concrete Research*. Pergamon, 38(6), pp. 848–860.

Lothenbach, B., Matschei, T., *et al.* (2008) 'Thermodynamic modelling of the effect of temperature on the hydration and porosity of Portland cement', *Cement and Concrete Research*, 38(1), pp. 1–18.

Lothenbach, B. *et al.* (2019) 'Cemdata18: A chemical thermodynamic database for hydrated Portland cements and alkali-activated materials', *Cement and Concrete Research*, 115, pp. 472–506.

Lothenbach, B. and Zajac, M. (2019) 'Application of thermodynamic modelling to hydrated cements', *Cement and Concrete Research*. Pergamon, 123, p. 105779.

Lu, B. and Torquato, S. (1992) 'Nearest-surface distribution functions for polydispersed particle systems', *Physical Review A*, 45(8), pp. 5530–5544.

Lutz, M. P., Monteiro, P. J. M. and Zimmerman, R. W. (1997) 'Inhomogeneous interfacial transition zone model for the bulk modulus of mortar', *Cement and Concrete Research*. Elsevier Ltd, 27(7), pp. 1113–1122.

Ma, H. and Li, Z. (2014) 'Multi-aggregate approach for modeling interfacial transition zone in concrete', *ACI Materials Journal*, 111(2), pp. 189–200.

Maekawa, K., Ishida, T. and Kishi, T. (2009) *Multi- scale modeling of structural concrete*.

Maekawa, Koichi, Ishida, T. and Kishi, T. (2009) *Multi-scale modeling of structural concrete*. Taylor & Francis.

Maghsoodi, V. (2018) 'W/C Ratio Profile in ITZ of Mortar', *Arabian Journal for Science and*

Engineering. Springer Berlin Heidelberg, 43(4), pp. 1817–1824.

Manzano, H. *et al.* (2007) 'Mechanical properties of crystalline calcium-silicate-hydrates: Comparison with cementitious C-S-H gels', *Physica Status Solidi (A) Applications and Materials Science*, 204(6), pp. 1775–1780.

Maruya, T. *et al.* (2003) 'Numerical Modeling of Steel Corrosion in Concrete Structures due to Chloride Ion, Oxygen and Water Movement', *Journal of Advanced Concrete Technology*, 1(2), pp. 147–160.

Maruyama, I. and Igarashi, G. (2014) 'Cement Reaction and Resultant Physical Properties of Cement Paste', *Journal of Advanced Concrete Technology*, 12(6), pp. 200–213.

Mazaheripour, H. *et al.* (2018) 'Microstructure-based prediction of the elastic behaviour of hydrating cement pastes', *Applied Sciences (Switzerland)*, 8(3).

Morandeau, A., Thiéry, M. and Dangla, P. (2014) 'Investigation of the carbonation mechanism of CH and C-S-H in terms of kinetics, microstructure changes and moisture properties', *Cement and Concrete Research*. Pergamon, 56, pp. 153–170.

Mori, D. *et al.* (2006) 'Applications of electron probe microanalyzer for measurement of Cl concentration profile in concrete', *Journal of Advanced Concrete Technology*, 4(3), pp. 369–383.

Mori, T. and Tanaka, K. (1973) 'Average stress in matrix and average elastic energy of materials with misfitting inclusions', *Acta Metallurgica*, 21(5), pp. 571–574.

Multon, S. and Sellier, A. (2016) 'Multi-scale analysis of alkali-silica reaction (ASR): Impact of alkali leaching on scale effects affecting expansion tests', *Cement and Concrete Research*. Elsevier Ltd, 81, pp. 122–133.

Nadeau, J. C. (2002) 'Water-cement ratio gradients in mortars and corresponding effective elastic properties', *Cement and Concrete Research*. Pergamon, 32(3), pp. 481–490.

Nadeau, J. C. (2003) 'A multiscale model for effective moduli of concrete incorporating ITZ water–cement ratio gradients, aggregate size distributions, and entrapped voids', *Cement and Concrete Research*. Pergamon, 33(1), pp. 103–113.

Narayan Swamy, R. (1971) 'Dynamic Poisson's ratio of portland cement paste, mortar and concrete', *Cement and Concrete Research*. Pergamon, 1(5), pp. 559–583.

Nemecek, J. *et al.* (2018) 'Fracture properties of cement hydrates determined from microbending tests and multiscale modeling', in *Computational modelling of concrete structures : proceedings of the Conference on Computational Modelling of Concrete and Concrete Structures (EURO-C 2018), 26 February 26 - 1 March, 2018,*

Nilsen, U. A. and Monteiro, P. J. M. (1993) 'Concrete: A three phase material', *Cement and Concrete Research*, 23(1), pp. 147–151.

Noguchi, N. *et al.* (2021) 'Hydration of ferrite-rich Portland cement: Evaluation of Fe-hydrates and Fe uptake in calcium-silicate-hydrates', *Construction and Building Materials*. Elsevier, 288, p. 123142.

Omikrine Metalssi, O., Aït-Mokhtar, A. and Turcry, P. (2020) 'A proposed modelling of coupling carbonation-porosity-moisture transfer in concrete based on mass balance equilibrium', *Construction and Building Materials*. Elsevier, 230, p. 116997.

Papatzani, S., Paine, K. and Calabria-Holley, J. (2015a) 'A comprehensive review of the models on the nanostructure of calcium silicate hydrates', *Construction and Building Materials*. Elsevier, 74, pp. 219–234.

Papatzani, S., Paine, K. and Calabria-Holley, J. (2015b) 'A comprehensive review of the models on the nanostructure of calcium silicate hydrates', *Construction and Building Materials*. Elsevier Ltd, 74(March 2019), pp. 219–234.

Parkhurst, D. L. and Appelo, C. A. J. (1999) 'A computer program for speciation, batch- reaction, one-dimensional transport and inverse geochemical calculations', *USGS Report*.

Parrot, L. J. and Killoh, D. C. (1984) 'Prediction of Cement Hydration.', in *British Ceramic Proceedings*, pp. 41–53.

Parrot, L.J. and Killoh, D. C. (1984) 'Prediction of cement hydration', in *British Ceramic Proceedings*, pp. 35, 41–53.

Phung, Q. T. *et al.* (2016) 'Modelling the carbonation of cement pastes under a CO2 pressure gradient considering both diffusive and convective transport', *Construction and Building Materials*. Elsevier Ltd, 114, pp. 333–351.

Pichler, B. *et al.* (2013) 'Effect of gel–space ratio and microstructure on strength of hydrating cementitious materials: An engineering micromechanics approach', *Cement and Concrete Research*.

Pergamon, 45, pp. 55–68.

Ramesh, G., Sotelino, E. D. and Chen, W. F. (1996) 'Effect of transition zone on elastic moduli of concrete materials', *Cement and Concrete Research*. Elsevier Ltd, 26(4), pp. 611–622.

Rupasinghe, M. *et al.* (2017) 'Compressive strength prediction of nano-silica incorporated cement systems based on a multiscale approach', *Materials and Design*. Elsevier Ltd, 115, pp. 379–392.

S˘milauer, V. and Bittnar, Z. (2006) 'Microstructure-based micromechanical prediction of elastic properties in hydrating cement paste', *Cement and Concrete Research*. Pergamon, 36(9), pp. 1708–1718.

Sant, G., Bentz, D. and Weiss, J. (2011) 'Capillary porosity depercolation in cement-based materials: Measurement techniques and factors which influence their interpretation', *Cement and Concrete Research*. Pergamon, 41(8), pp. 854–864.

Le Saoût, G. *et al.* (2013) 'Hydration of Portland cement with additions of calcium sulfoaluminates', *Cement and Concrete Research*. Pergamon, 43, pp. 81–94.

Šavija, B. and Luković, M. (2016) 'Carbonation of cement paste: Understanding, challenges, and opportunities', *Construction and Building Materials*. Elsevier, 117, pp. 285–301.

Scrivener, K. L., Lyon, A. K. C. and Laugesen, F. P. (2004a) 'The Interfacial Transition Zone (ITZ) Between Cement Paste and Aggregate in Concrete', *INTERFACE SCIENCE*, 12, pp. 411–421.

Scrivener, K. L., Lyon, A. K. C. and Laugesen, F. P. (2004b) *The Interfacial Transition Zone (ITZ) Between Cement Paste and Aggregate in Concrete*, *INTERFACE SCIENCE*.

Sharma, M. and Bishnoi, S. (2020a) 'Influence of properties of interfacial transition zone on elastic modulus of concrete: Evidence from micromechanical modelling', *Construction and Building Materials*. Elsevier Ltd, 246.

Sharma, M. and Bishnoi, S. (2020b) 'Influence of properties of interfacial transition zone on elastic modulus of concrete: Evidence from micromechanical modelling', *Construction and Building Materials*. Elsevier Ltd, 246, p. 118381.

Shen, X. han *et al.* (2019) 'Combine ingress of chloride and carbonation in marine-exposed concrete under unsaturated environment: A numerical study', *Ocean Engineering*. Pergamon, 189, p. 106350.

Simeonov, P. and Ahmad, S. (1995) ‘Effect of transition zone on the elastic behavior of cement-based composites’, *Cement and Concrete Research*. Pergamon, 25(1), pp. 165–176.

Singh, L. P. *et al.* (2015) ‘Hydration studies of cementitious material using silica nanoparticles Preparation of size controlled silica nano particles and its functional role in cementitious system Hydration Studies of Cementitious Material using Silica Nanoparticles’, *Journal of Advanced Concrete Technology*, 13, pp. 345–354.

Šmilauer, V., Hlobil, M. and Hlaváček, P. (2017) ‘ENGINEERING MICROSTRUCTURES OF SLAG-BLENDED CEMENTS AND ALKALI-ACTIVATED FOAMS-EXPERIMENTS AND MODELLING’, in *5th International Slag Valorisation Symposium, Leuven*, pp. 411–424.

Song, B. *et al.* (2021) ‘Effect of early CO2 curing on the chloride transport and binding behaviors of fly ash-blended Portland cement’, *Construction and Building Materials*. Elsevier, 288, p. 123113.

Stefan, L. *et al.* (2010a) ‘Prediction of elastic properties of cement pastes at early ages’, *Computational Materials Science*. Elsevier, 47(3), pp. 775–784.

Stefan, L. *et al.* (2010b) ‘Prediction of elastic properties of cement pastes at early ages’, *Computational Materials Science*. Elsevier, 47(3), pp. 775–784.

Suda, Y. *et al.* (2021) ‘Phase Assemblage, Microstructure and Shrinkage of Cement Paste during Carbonation at Different Relative Humidities’, *Journal of Advanced Concrete Technology*, 19, pp. 687–699.

Sugiyama, T., Ritthichauy, W. and Tsuji, Y. (2003) *Simultaneous Transport of Chloride and Calcium Ions in Hydrated Cement Systems*, *Journal of Advanced Concrete Technology*.

Sui, S. *et al.* (2019) ‘Quantification methods for chloride binding in Portland cement and limestone systems’, *Cement and Concrete Research*. Pergamon, 125, p. 105864.

Sun, D. *et al.* (2021) ‘C−S−H gel structure and water molecules behaviors under different chemical environments in a range of temperatures’, *Materials Today Communications*. Elsevier Ltd, 26, p. 101866.

Takahashi, T. *et al.* (1997) ‘Relationship Between Compressive Strength and Pore Structure of Hardened Cement Pastes’, *Advancces in cement research*, 9(33), pp. 25–30.

Tennis, P. D. and Jennings, H. M. (2000a) ‘A model for two types of calcium silicate hydrate in the

microstructure of Portland cement pastes', *Cement and Concrete Research*. Pergamon, 30(6), pp. 855–863.

Tennis, P. D. and Jennings, H. M. (2000b) 'A model for two types of calcium silicate hydrate in the microstructure of Portland cement pastes', *Cement and Concrete Research*. Pergamon, 30(6), pp. 855–863.

Teramoto, A., Igarashi, G. and Maruyama, I. (2011) 'Study on the effect of aggrgate volume fraction on dynamic elasticity in hardening process', *Cement Science and Concrete Technology*, (65), pp. 132–139.

Termkhajornkit, P. *et al.* (2014) 'Dependence of compressive strength on phase assemblage in cement pastes: Beyond gel–space ratio — Experimental evidence and micromechanical modeling', *Cement and Concrete Research*. Pergamon, 56, pp. 1–11.

Thomas, J. J. and Jennings, H. M. (2006) 'A colloidal interpretation of chemical aging of the C-S-H gel and its effects on the properties of cement paste', *Cement and Concrete Research*. Pergamon, 36(1), pp. 30–38.

Thomas, J. J., Jennings, H. M. and Allen, A. J. (2010) 'Relationships between composition and density of tobermorite, jennite, and nanoscale CaO-SiO2-H2O', *Journal of Physical Chemistry C*, 114(17), pp. 7594–7601.

Toghroli, A., Sajedi, F. and Ibrahim, Z. (2018) 'A review on pavement porous concrete using recycled waste materials an evaluation on accessibility to urban rail transit system in klang valley, malaysia view project development of stone mastic asphalt pavement design with wastes as aggregate replacement View project Mahdi Shariati', *Smart Structures and Systems*, 22(4), pp. 433–440.

TSUKAHARA, E., KATO, Y. and UOMOTO, T. (2000) 'Estimation Method of Young's Modulus of Mortar Including Transition Zone at Aggregate Cement Paste Interface (in Japanese)', 研 究 速 報. 東京大学生産技術研究所, 52(8), pp. 333–336.

Varas, M. J., De Buergo, M. A. and Fort, R. (2005) 'Natural cement as the precursor of Portland cement: Methodology for its identification', *Cement and Concrete Research*. Pergamon, 35(11), pp. 2055–2065.

Velez, K. *et al.* (2001) 'Determination by nanoindentation of elastic modulus and hardness of pure constituents of Portland cement clinker', *Cement and Concrete Research*. Pergamon, 31(4), pp. 555–561.

Vorel, J., Šmilauer, V. and Bittnar, Z. (2012) 'Multiscale simulations of concrete mechanical tests', in *Journal of Computational and Applied Mathematics*, pp. 4882–4892.

Wan, K., Li, Y. and Sun, W. (2013) 'Experimental and modelling research of the accelerated calcium leaching of cement paste in ammonium nitrate solution', *Construction and Building Materials*. Elsevier, 40, pp. 832–846.

Wang, X. and Subramaniam, K. V. (2011) 'Ultrasonic monitoring of capillary porosity and elastic properties in hydrating cement paste', *Cement and Concrete Composites*. Elsevier, 33(3), pp. 389–401.

Wriggers, P. and Moftah, S. O. (2006) 'Mesoscale models for concrete: Homogenisation and damage behaviour', *Finite Elements in Analysis and Design*. Elsevier, 42(7 SPEC. ISS.), pp. 623–636.

Wu, W. *et al.* (2012) 'Concrete as a Hierarchical Structural Composite Material', *International Journal for Multiscale Computational Engineering*, 8(6), pp. 585–595.

Wyrzykowski, M. and Lura, P. (2016) 'Effect of relative humidity decrease due to self-desiccation on the hydration kinetics of cement', *Cement and Concrete Research*. Elsevier Ltd, 85, pp. 75–81.

Xie, M., Dangla, P. and Li, K. (2021) 'Reactive transport modelling of concurrent chloride ingress and carbonation in concrete', *Materials and Structures/Materiaux et Constructions*, 54(5).

Ye, G., Van Breugel, K. and Fraaij, A. L. A. (2003) 'Three-dimensional microstructure analysis of numerically simulated cementitious materials', in *Cement and Concrete Research*, pp. 215–222.

Yoda, Y. *et al.* (2018) 'Estimation method of compressive strength of composition, water to binder ratio and curing blended ce-ment paste with different binder temperature by conduction calorimeter (In Japanese)', *Cement science and concrete technology*, 71, pp. 1–21.

You, X. *et al.* (2022) 'A review on the modelling of carbonation of hardened and fresh cement-based materials', *Cement and Concrete Composites*. Elsevier, 125, p. 104315.

Zajac, M. *et al.* (2018) 'Impact of microstructure on the performance of composite cements: Why higher total porosity can result in higher strength', *Cement and Concrete Composites*. Elsevier, 90, pp.

178–192.

Zhang, M. and Ye, G. (2010) ‘Modelling of time dependency of chloride diffusion coefficient in cement paste’, *Journal of Wuhan University of Technology-Mater. Sci. Ed.*, 25(4), pp. 687–691.

Zhang, T. *et al.* (2017) ‘Hydration behavior of magnesium potassium phosphate cement and stability analysis of its hydration products through thermodynamic modeling’, *Cement and Concrete Research*. Elsevier Ltd, 98, pp. 101–110.

Zheng, J. *et al.* (2010) ‘Simple Three-Step Analytical Scheme for Prediction of Elastic Moduli of Hardened Cement Paste’, *Journal of Materials in Civil Engineering*, 22(11), pp. 1191–1194.

Zheng, J., Wong, H. S. and Buenfeld, N. R. (2009) ‘Assessing the influence of ITZ on the steady-state chloride diffusivity of concrete using a numerical model’, *Cement and Concrete Research*, 39(9), pp. 805–813.

Zheng, J., Zhou, X. and Jin, X. (2012) ‘An n-layered spherical inclusion model for predicting the elastic moduli of concrete with inhomogeneous ITZ’, *Cement and Concrete Composites*. Elsevier, 34(5), pp. 716–723.

Zhu, X. *et al.* (2017) ‘Identification of interfacial transition zone in asphalt concrete based on nano-scale metrology techniques’, *Materials and Design*. Elsevier Ltd, 129, pp. 91–102.

Zhu, X. *et al.* (2018) ‘Effect of interfacial transition zone on the Young’s modulus of carbon nanofiber reinforced cement concrete’, *Cement and Concrete Research*. Elsevier Ltd, 107, pp. 49–63.

Zhu, Z., Provis, J. L. and Chen, H. (2018) ‘Quantification of the influences of aggregate shape and sampling method on the overestimation of ITZ thickness in cementitious materials’, *Powder Technology*. Elsevier B.V., 326, pp. 168–180.

Zhutovsky, S. and Kovler, K. (2009) ‘Effect of water to cement ratio and degree of hydration on chemical shrinkage of cement pastes’, *Concrete Durability and Service Life Planning*, (April 2016), pp. 47–54.

H. Kawakami, The relationship between elastic modulus and age of mortar (In Japanese), Concrete Engineering Annual Proceedings. 27 (2005).

H. Kawakami, A Study on the Relationship between Elastic Modulus and Compressive Strength of Concrete (In Japanese), Concrete Engineering Annual Proceedings. 28 (2006).

Appendix A: Material and Experimental Methodology

Material

The cement used for experimental works of mortar was ordinary Portland cement (OPC). The chemical composition and physical properties of the cement are detailed in Table A1. Fine aggregates used were natural mountain sand with specific gravity of 2.57 g/cm^3, obtained from Kakegawa city in Shizuoka prefecture of Japan and coarse aggregates used were crushed stone with specific gravity of 2.68 g/cm^3 produced from Ibaraki prefecture of Japan.

Table A1. Chemical composition and physical properties of cement

Chemical composition (%)	SiO2	20.89
	Al2O3	5.44
	Fe2O3	2.94
	Cao	65.11
	MgO	1.54
	SO3	2.08
	Na2O	0.27
	K2O	0.53
	TiO2	0.26
	P2O5	0.14
	MnO	0.05
	LOI	0.71
Physical properties	Blaine (cm^2/g)	3450
	Density (g/cm^3)	3.16

Mix design

The experiments were carried out for mortar and concrete at three different w/c: 0.3, 0.4 and

0.5 and two different sand contents (in total volume fraction): 0.3 and 0.6 for mortar and two different coarse aggregate content: 1000 kg and 500 kg for concrete. The mix proportions for each of these mixes are stated in Table A2 and Table A3.

Table A2. Mixing proportion of mortar

Water (g)	Cement (g)	Sand (g)	w/c	Volume fraction of sand
1023	3408	2322	0.3	0.3
585	1947	4644		0.6
1173	2931	2322	0.4	0.3
669	1674	4644		0.6
1287	2571	2322	0.5	0.3
735	1470	4644		0.6

Table A3. Mixing proportion of concrete

Water	Cement	Sand	Coarse aggregate	w/c
		(kg/m^3 of concrete)		
170	567	681	1000	0.3
222	740	891	500	
170	425	797	1000	0.4
222	554	1042	500	
170	340	864	1000	0.5
222	446	1130	500	

Sample preparation

According to mix proportion, φ50 x 100 mm cylinder samples for mortar and φ100 x 200 mm for concrete were prepared. After demolding, the samples were sealed and cured in an environment of 20 °C for 3, 7 and 28 days.

Compressive strength test

The compressive strength was tested in accordance with JIS A 1108. The compressive strength was the average value of test results of three samples.

Young's modulus test

The Young's modulus was tested in accordance with JIS A 1149. The Young's modulus was the average value of test results of three samples.

Poisson's ratio test

The Poisson's ratio experiment was carried out in accordance with JHS 307, and the Poisson's ratio value was the average value of three samples.

Experiment results

The experiment results of compressive strength, Young's modulus and Poisson's ratio are shown in Table A4 and Table A5 for three sets of w/c and two sets of aggregates content for mortar and concrete.

Table A4. Mechanical properties of mortar

W/C	Sand (volume %)	Time (Days)	Compressive strength (N/mm^2)	Young's modulus (kN/mm^2)	Poisson's ratio
0.3	30	3	52.3	20.7	0.218
		7	61.8	23.9	0.209
		28	77.1	25.2	0.203
	60	3	48.9	23.5	0.206
		7	66.8	27.1	0.183
		28	80.9	29.3	0.192
0.4	30	3	29.5	15.6	0.206
		7	42.7	18.7	0.197
		28	60.9	26.4	0.192
	60	3	31.2	20.0	0.216
		7	44.4	23.4	0.187
		28	59.5	25.5	0.186
0.5	30	3	12.4	9.56	0.179
		7	23.6	13.9	0.189
		28	43	16.6	0.212
	60	3	20.6	17.0	0.170
		7	30.2	21.1	0.176
		28	44.6	23.2	0.174

Table A5. Mechanical properties of concrete

W/C	Coarse aggregate (Kg)	Time (Days)	Compressive strength (N/mm^2)	Young's modulus (kN/mm^2)	Poisson's ratio
0.3	1000	3	60.1	30.6	0.186
		7	78.4	33.9	0.187
		28	93.4	36.7	0.208
	500	3	54.4	27.0	0.186
		7	67.6	30.5	0.195
		28	84.2	33.4	0.207
0.4	1000	3	36.9	27	0.191
		7	52.5	30.7	0.181
		28	68.3	33	0.197
	500	3	35.3	23.3	0.196
		7	49.4	27.9	0.181
		28	65.1	30.5	0.188
0.5	1000	3	24.6	23.7	0.176
		7	36.9	27.3	0.171
		28	53.1	31.2	0.174
	500	3	22.6	20.5	0.177
		7	34.4	24.8	0.172
		28	50.1	28.3	0.176